Dose tracking assessment for image-guided radiotherapy of the cervical cancer treatment using a hybrid deformable image registration (DIR) method

Tam Thi Thu Tran

Thesis submitted for the degree of

Master in Biophysics and Medical Physics

60 credits

Department of Physics

Faculty of mathematics and natural sciences

UNIVERSITY OF OSLO

Spring 2021

Dose tracking assessment for image-guided radiotherapy of the cervical cancer treatment using a hybrid deformable image registration (DIR) method

Tam Thi Thu Tran

Dose tracking assessment for image-guided radiotherapy of the cervical cancer treatment using a hybrid deformable image registration (DIR) method

http://www.duo.uio.no/

Printed: University of Oslo

Abstract

Background and Purpose: Organ motion, and deformation caused by physiological changes, such as bladder and rectum filling may result in variations in the position of the clinical target volume during radiation therapy of cervical cancer patients. Consequently, it may impact on the actual dose delivered to the target and organ at risks, i.e., this may lead to discrepancies between planned and actual delivered dose during the course of treatment. The aims of this study were to assess the volume of bladder on daily cone beam computed tomography (CBCT), to validate the possibility of deformable image registration (DIR) in estimating the accumulated delivered dose distributions, and to perform dose tracking, i.e., comparing accumulated delivered dose with the initial plan.

Materials and methods: The clinical data from eight patients with locally advanced cervical cancer that underwent volumetric modulated arc therapy (VMAT) were retrospectively analysed. The low risk target, CTV_T_LR and the bladder were delineated on all the 25 CBCTs for all the patients. The hybrid DIR algorithm on the RayStation treatment planning system (RaySearch version 9.0, RaySearch Laboratories AB, Sweden) was used for registering the daily CBCT image set to planning CT image set. Qualitative evaluation of DIR was performed through visual inspection using validation tools in RayStation, based on overlaps between delineated structures. Quantitative evaluation of DIR used the Dice Similarity Coefficient (DSC) metric. Reasonable DIRs were applied to deform daily dose distributions to the initial treatment plan for accumulating dose distribution. In addition, accumulated delivered dose calculated by simple DVH parameter addition-based method was investigated. The accumulated delivered dose was compared with the planning dose by evaluating the differences in DVH metrics such as D98 for the CTV_T_LR, and Dmean, D50, and D2 for the bladder. Two treatment plan scenarios were: large margin (individualised ITV margins) and small margin (ITV margin of 10 mm).

Results: One patient with bad CBCT image quality was excluded from the investigation. The bladder volumes reduced during treatment. Qualitative and quantitative validations of DIR showed reasonable results for the deform dose. For individual patient, the mean DSCs overall the fractions for the CTV_T_LR and the bladder were greater than 0.95 and 0.9, respectively. It was proved that ROIs assisted the hybrid DIR algorithm to improve DIR. Also in some case, POIs were required in addition to ROIs. According to clinical objectives for CTV_T_LR and bladder, dose tracking results showed no clinically significant difference between accumulated delivered dose from accumulated planned dose for both margin plans. Moreover, dosimetric parameters results showed no statistically significant differences between two methods for estimating accumulated dose.

Conclusions: Although all patients were instructed with bladder filling, their bladder volumes varied during the course of radiotherapy.

Even with limitations of DIR accuracy, it is feasible to use DIR-based dose accumulation method to compare the cumulative delivered dose of the target and the bladder and to planned dose for cervical cancer radiotherapy.

Even though the results in this work showed no significant differences between planned and delivered dose for small and large margin, further investigations using this method on a large number of patients are needed.

Preface

This master project was conducted in the Department of Medical Physics, Oslo University Hospital, in cooperation with section of Biophysics and Medical Physics, Department of Physics, University of Oslo. This thesis has been performed from August 2020 to May 2021, and accounts for 60 credits.

Acknowledgements

Foremost, I would like to express my special thanks and sincere gratitude to my primary supervisor, Assoc. Prof. Taran Paulsen Hellebust, for her expertise, precious guidance, support, encouragement, and inspiring enthusiasm throughout the completion of this project.

I am deeply grateful to my second supervisor, Prof. Eirik Malinen, and a program coordinator, Assoc. Prof. Nina Fredrik J Edin, for their passions who provided me advice, proposed direction, and gave follow-up during my study and project.

I would like to express my deep appreciation to Prof. Eli Olaug Hole for her kind support and encouragement who provided me with the opportunity to study in a friendly environment.

I indeed appreciate generous support from a doctor, Silje Skjelsvik Os for her guidance in delineation of target volume and organ-at-risk. Valuable assistant from a medical physicist, Francisca Belen Correas Viduarre for her help with RayStation treatment planning system is very much acknowledged.

Finally, I would like to thank my family, my classmates and my friends for their love, continuous support, and encouragement throughout my study and project work.

List of Abbreviations

ART	.....	Adaptive Radiotherapy
CT	.....	Computed Tomography
CBCT	.....	Cone Beam Computed Tomography
CTV	.....	Clinical Target Volume
DICOM	.....	Degital Imaging and COmmunication in Medicine
DIR	.....	Deformable Image Registration
DSC	.....	Dice Similarity Coefficient
DVH	.....	Dose Volume Histogram
FOV	.....	Field Of View
Gy	.....	Gray(J/kg)
GTV	.....	Gross Tumour Volume
HU	.....	Hounsfield Unit
IAEA	.....	International Atomic Energy Agency
ICRU	.....	International Commission of Radiation Units
IMRT	.....	Intensity Modulated Radiation Therapy
IGRT	.....	Image Guided Radiation Therapy
MLC	.....	Multi Leaf Collimator
MRI	.....	Magnetic Resonance Imaging
MU	.....	Monitor Units
NTCP	.....	Normal Tissue Complication Probability
OAR	.....	Organ At Risk
pCT	.....	planning CT
PDF	.....	Probability Distribution Function
PET	.....	Positron Emission Tomography
PRV	.....	Planning organ at Risk Volume
PTV	.....	Planning Target Volume
QUANTEC	.....	Quantitative Analyses of Normal Tissue Effects in the Clinic
ROI	.....	Region Of Interest
RT	.....	Radiation Therapy
SD	.....	Standard Deviation
TCP	.....	Tumour Control Probability
TPS	.....	Treatment Planning System
TV	.....	Target Volume
VMAT	.....	Volumetric Modulated Arc Therapy
VOI	.....	Volume Of Interest

Contents

List of Tables

List of Figures

Chapter 1

Introduction

Cervical cancer is the fourth most common cancer in women. It has been estimated an annual number of 570 000 women diagnosed with and about 311 000 women died from cervical cancer (according to WHO statistics, 2018 [2]). However, it is one of the most successful treatable cancer sites if it is diagnosed early and managed effectively.

Locally advanced cervical cancer has been treated using combination of radiotherapy and chemotherapy (radiochemotherapy). Recently, the most sophisticated radiation delivery methods for locally advanced cervical cancer radiotherapy is Intensity-Modulated Radiation Therapy (IMRT) and Volumetric-Modulated Arc Therapy (VMAT). These techniques have advantages of higher dose conformity, ability to escalate dose to cancer targets, and to spare normal tissues. Several studies reported that patients treated with IMRT showed dosimetric and clinical benefits, with reduction in acute gastrointestinal and hematologic toxicity [36, 80].

Nonetheless, the target and organ motion and deformation in pelvis are unpredictable and therefore are challenging during high-precision external beam radiation therapy for cervical cancer treatment. It has been well documented by number of studies that the inter-fractional changes in target shape and position are influenced by bladder inter-fraction volume variations [10, 17, 37, 49, 56, 66, 79]. Consequently, bladder volume changes may significantly change the dose to target and Organ-At-Risk (OARs), resulting in discrepancies between actual delivered dose to the planned dose [14, 32, 48, 83]. The straightforward positional correction is often not possible. To compensate for these geometrical uncertainties, large safety margins around the target volume have to be applied [7, 10]. However, these margins may result in high dose to surrounding healthy tissue and target underdose [15, 32].

Image-guided radiation therapy (IGRT) aims to safeguard the delivery of the planned dose to

the patient. Recently, in many clinics, cone beam computed tomography (CBCT)-based IMRT is a technology used for reducing positional set-up errors in RT. CBCT scan may achieve 3D volume imaging of organs, with adequate soft tissue contrast in the images. Based on CBCT scans, the target motion, and OARs motions (bladder, rectum, and vaginal motion) may be observed. Therefore, this technique may facilitate dosimetric treatment evaluation [27, 34]. Alongside dosimetric knowledge, it is possible to perform the dose tracking, i.e., to compare accumulated delivered dose with accumulated planned dose to determine if the target is underdosed or if the healthy organs are receiving more dose than the constraint planned dose. It would be then possible to re-plan based on dose tracking process, as well as systematic anatomy changes. The detection of new adaptive radiation therapy (ART) strategies are currently motivated researchers in the field of radiation therapy. Image-Guided Adaptive Radiotherapy is a potential methodology for cervical cancer treatment.

Image registration is image processing that defines spatial relationship between different volumetric image sets [30]. Two form of image registration, including rigid image registration (RR) and deformable image registration (DIR). Rigid image registration is image fusion by changing translation and rotation in three dimensions. On the other hand, DIR includes RR and use deformable vector field to match all the field of volumetric images. DIR method is capable of locally warping the moving image to align with reference image that can account for organ motions. Therefore, this method has been becoming useful tool in modern radiotherapy included Image-Guided Radiotherapy (IGRT) and Adaptive Radiotherapy (ART). The applications of DIR such as auto segmentation and dose accumulation were reviewed in literatures [4, 13, 23, 59, 84].

The aims of this study were to quantitatively assess the bladder volume inter-fractional variations for cervical cancer patients on daily CBCT images during the course of treatment, to validate the feasibility of DIR in estimating the accumulated delivered dose distributions in dose tracking process, also compare this DIR based-method with the simple DVH addition-based method, and to perform dose tracking for two treatment plan scenarios, i.e., large margin plan (individual margin for each patient) and small margin plan (10 mm ITV).

Chapter 2

Background

2.1 Cervix and Cervical cancer

2.1.1 Female Pelvis Anatomy

The Fig. 2·1 shows the female pelvis anatomy which includes: uterine (fallopian) tube, ovary, fundus of uterus, corpus (body) of uterus, cervix, vagina, symphysis pubis, clitoris, urethra, labium majora, and labium minora.

Cervix is the lower and narrow part of uterus (womb) that connects to vagina and located between the bladder and rectum. It is 2 to 3 cm long and in roughly cylindrical shape.

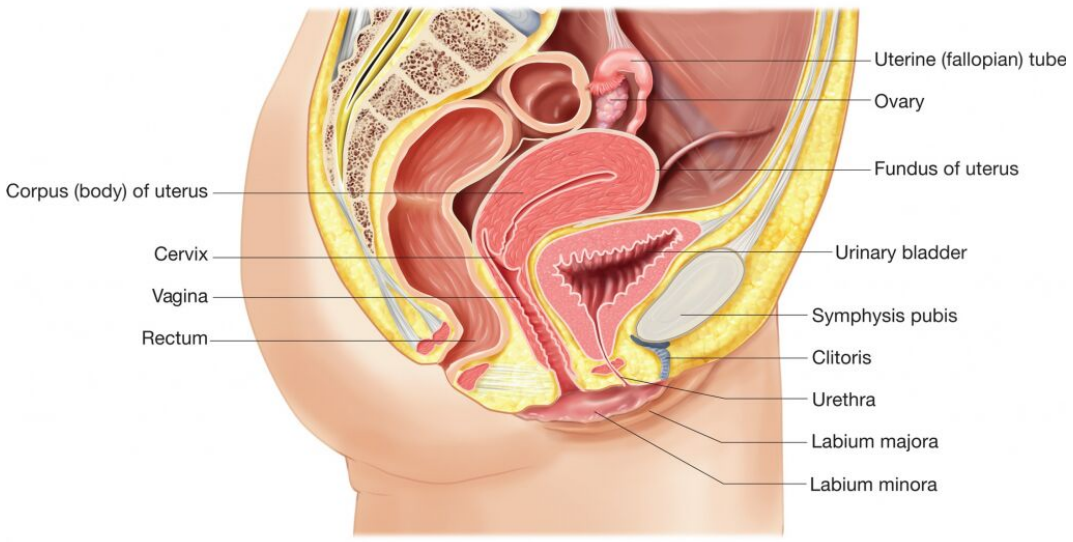

Figure 2·1: Female pelvis anatomy [1].

2.1.2 Cervical Cancer

Cancer

The human body is made up of the basic units - cells. They have specific functions and fixed lifetime. Cells grow and divide to make new cells, when needed in a controlled manner with a balance between new cells and cell death. Cancer is characterized by a disorderly proliferation of cells that can invade adjacent tissues and spread via the lymphatic system or blood vessels to other parts of the body [53]. Since cancers are growth and division of cells out of control, the cells do not perform their functions. Cancer cells can form a tumour, destroy the immune system and cause changes that inhibit the human body from functioning normally.

Cervical cancer and tumour staging

Cervical cancer is a type of cancer that occurs in the women's cervix. The highest risk factors for cervical cancer is the human papillomavirus (HPV) infection that causes abnormal cells.

Cervical cancer staging is the assessment of cervical cancer to decide how far the cancer has progressed. It is staged by the International Federation of Gynecology and Obstetrics (FIGO) staging system, based on clinical examination [50], as shown in Table 2.1.

Table 2.1: An explanation of the FIGO system is in the stage [50].

FIGO Stage	Description
IA	There is a very small amount of cancer, and it can be seen only under a microscope. It has not spread to nearby lymph nodes. It has not spread to distant sites.
IB	This includes stage I cancer that has spread deeper than 5 mm (about 1/5 inch) but is still limited to the cervix. It has not spread to nearby lymph nodes. It has not spread to distant sites.
IIA	The cancer has grown beyond the cervix and uterus but has not spread into the tissues next to the cervix (called the parametria). It has not spread to nearby lymph nodes. It has not spread to distant sites.
IIB	The cancer has grown beyond the cervix and uterus and has spread into the tissues next to the cervix (the parametria). It has not spread to nearby lymph nodes. It has not spread to distant sites.
IIIA	The cancer has spread to the lower part of the vagina but not the walls of the pelvis. It has not spread to nearby lymph nodes. It has not spread to distant sites.
IIIB	The cancer has grown into the walls of the pelvis and/or is blocking one or both ureters causing kidney problems (called hydronephrosis). It has not spread to nearby lymph nodes. It has not spread to distant sites.
IIIC	The cancer can be any size. Imaging tests or a biopsy show the cancer has spread to nearby pelvic lymph nodes (IIIC1) or para-aortic lymph nodes (IIIC2). It has not spread to distant sites.
IVA	The cancer has spread to the bladder or rectum or it is growing it is growing out of the pelvis.
IVB	The cancer has spread to distant organs outside the pelvic area, such as distant lymph nodes, lungs or bones.

2.1.3 Cervical Cancer Treatment

The standard curative treatment for the cervical cancer in the early stages (stage IA, IIA and small tumors in IB) is surgery.

Radiotherapy is another treatment method for some patients in early stages. This method can be combined with surgery or chemotherapy, or both.

For locally advanced cervical cancer (stage IIB, III and IVA) are usually treated using combination of radiotherapy and chemotherapy so called radiochemotherapy.

2.2 Basic Radiobiology

The theory below is based on IAEA publication (ISBN 92-0-107304-6) [53].
The aim of radiotherapy is to deliver enough radiation to eradicate the tumour without irradiating normal tissue to a dose that will lead to serious complications (morbidity).

2.2.1 Therapeutic Ratio

The therapeutic ratio (or "therapeutic index") of a particular radiation treatment is a measure of the damage to the tumour vs. the damage to critical normal structures.
Concept of the therapeutic ratio is used to represent the optimal radiotherapy treatment. As can be seen from the Fig. 2·2, high therapeutic ratio gives high probability of tumour control and low probability of normal tissue morbidity. In contrast, low therapeutic ratio gives low tumour control and high normal tissue morbidity.

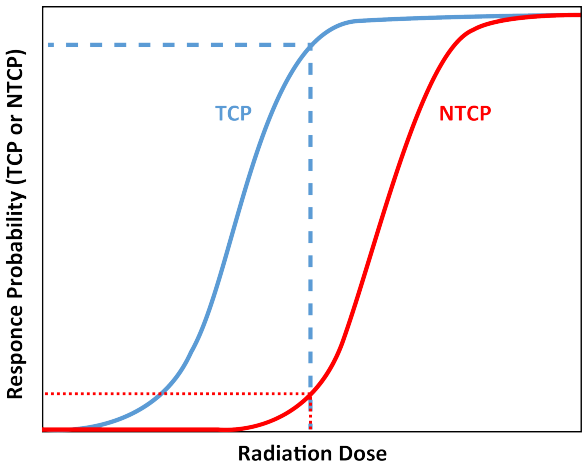

Figure 2·2: Therapeutic Index: is the ratio between the probablity of tumour control and normal tissue morbidity. TCP = Tumour control probability; NTCP = Normal tissue control probability.

2.2.2 Time, Dose, and Fractionation

The radiation treatments are scheduled by time, dose, and fractionation. Higher total dose increases the probability of tumour control, but it may cause late complications. Fractionation of dose can help to increase therapeutic ratio and to improve normal tissue tolerance in

radiotherapy [53].

Conventional fractionation is 5 daily (1.8 -2 Gy) treatments per week, delivered over several weeks. Other fractionation schemes are being studied with the aim of improving therapeutic ratio, such as [53]: **Hyperfractionation**(i.e., uses more than one fraction per day with a smaller dose per fraction (< 1.8 Gy) to reduce long term complications and to allow delivery of higher total tumour dose); **Accelerated fractionation** (i.e., reduces the overall treatment time, minimizing tumour cell re-population during the course of treatment); **Continuous hyperfrationated accelerated radiation therapy**(i.e., is an experimental programme used with three fractions per day for 12 continuous days); **Hypofractionation** (i.e., uses a large dose per fraction).

2.2.3 EQD2 Dose

The linear-quadratic (LQ) model is a mathematical modelling which can express the relationship between cell survival and delivered dose after fractioned irradiation:

$$S = e^{-(\alpha.d+\beta.d^2).n} \tag{2.1}$$

Biological effect, E is expressed as follows:

$$E = -logS \tag{2.2}$$

Thus,

$$E = (\alpha.d + \beta.d^2).n = (\alpha + \beta.d).n.d = (\alpha + \beta.d).D \tag{2.3}$$

Then,

$$\frac{E}{\beta} = (\frac{\alpha}{\beta} + d).D \tag{2.4}$$

Where: S = cell survival; E is biological effect; α and β are parameters describing cell's radiosensitivity; $\frac{\alpha}{\beta}$ = property of the irradiated tissue; D = total dose, given by $D = n.d$; n = number of fractions; d = dose per fraction.

In clinical practice, a plan with 2 Gy per fraction is usually used. Hence, a plan other than 2

Gy per fraction should be converted to 2 Gy equivalent dose, EQD2 as follows:

$$(\frac{\alpha}{\beta} + d).D = (\frac{\alpha}{\beta} + 2Gy).D_{2Gy} \tag{2.5}$$

Therefore,

$$EQD2 = D_{2Gy} = D.\frac{(d + \frac{\alpha}{\beta})}{2Gy + \frac{\alpha}{\beta}} \tag{2.6}$$

2.3 Target Volume, Organ At Risk and Margins

The theory below is based on the ICRU reports (50, 62, and 83 [46, 47, 74]).

2.3.1 Target Volume Definition

Fig. 2·3 shows the target volumes for the treatment in radiation therapy that are defined according to the International Commission on Radiation Units and Measurements (ICRU) in the reports 50 and 62 [46, 47].

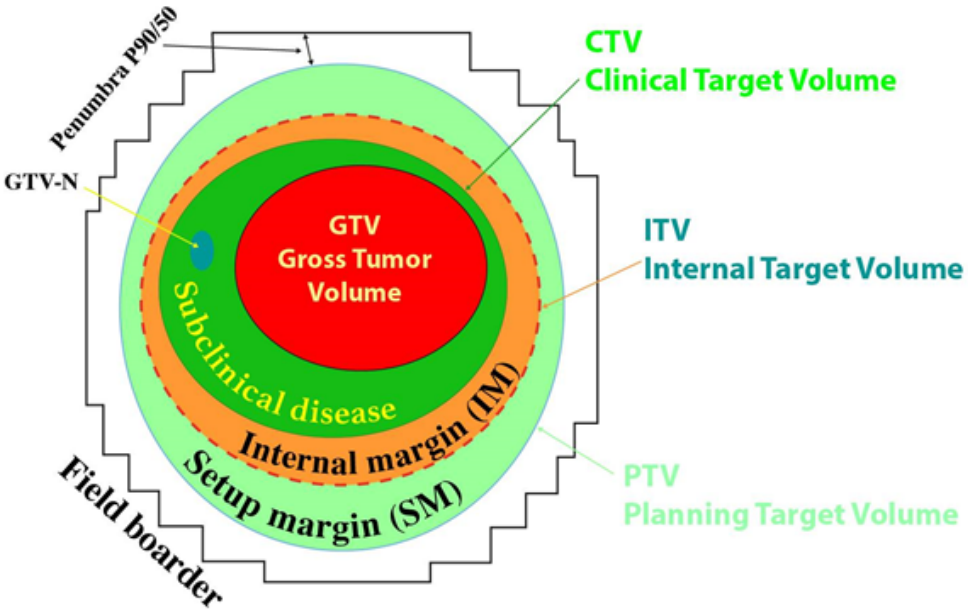

Figure 2·3: Prescription target volumes in radiotherapy [88].

- **Gross Tumour Volume (GTV):** is visible tumour and location of malignant growth. Delineation of GTV is based on different imaging modalities such as CT, MRI, PET, and ultrasound, etc. The GTV is divided into subtypes, GTV-T which presents for the primary tumour and GTV-N which represents for lymph note metastases (positive lymph node).

- **Clinical Target Volume (CTV):** is the volume which contains the GTV and/or sub-clinical microscopic malignant disease.

- **Internal Target Volume (ITV):** consists of the CTV and plus an internal margin (IM) (ITV = CTV + IM). The IM accounts for the variations in size and position of CTV relative to the patient's reference frame which is defined by the bony anatomy, i.e., variations due to organ motions such as bladder or rectum filling, breathing, etc.

- **Planning Target Volume (PTV):** is a geometrical concept. PTV consists of CTV with addition of margins including **internal margin (IM)** (accounts for organ motion) and **set-up margin (SM)**(accounts for any uncertainty in patient-set-up and beam alignment)

2.3.2 Organ At Risk and Planning Organ at Risk Volume

Organ at risk (OAR) is an organ which is sensitive to the radiation. During the treatment planning, the dose to OAR maybe significant compared to its constraint dose [46, 47].

Planning Organ at Risk Volume (PRV) consists of OAR with addition of margin that accounts for OAR motion during treatment [74].

2.3.3 Margins for Radiation Therapy

The Need for Margins in Radiotherapy

During radiation therapy, a safety margin is introduced in order to account for the errors/uncertainties (any deviation) between planning and executed treatment [45]. The margins are chosen so that the CTV receives the sufficient dose during the course of treatment [39].

Types of Set-up Errors in Radiotherapy

The theory of margins below is based on document written by B. Jane [85].

Margins comprise systematic errors and random errors.

Systematic errors

Systematic error ($\sum$) component of any error is a deviation that occurs in the same direction and is of a similar magnitude for each fraction throughout the treatment course. The term systematic error may referred to the individual patient or to the treatment population.

- **Individual** ($\sum_i$) - the systematic error for an individual patient is the mean error over the course of treatment.
- **Population** ($\sum_p$) - for the group of patients is the standard deviation of ($\sum_i$).

Systematic error may occur in each treatment fraction at localisation, planning or treatment delivery phases. Possible errors are: **target delineation error**, **target position and shape change** (possible causes of organ motion, e.g., bladder and rectum filling, breathing, or tumour regression or growth), **patient set-up error** (displacement of the target relative to skin set-up marks caused by the CT scan and treatment being performed on different couches), and **phantom transfer error** (the error that accumulates when transferring image data from initial localisation through the treatment planning system to the linear accelerator. Possible deviations in laser alignment between CT and linear accelerator, CT couch longitudinal position indication, isocenter position, field egde and multileaf collimator (MLC) position).

Systematic uncertainties are added quadratically:

$$\Sigma = (\Sigma^2_{set-up} + \Sigma^2_{organmotion} + \Sigma^2_{delineation})^{1/2} \tag{2.7}$$

Random errors

Random error (σ) is a deviation that can vary in direction and magnitude during the treatment. The term random error may referred to the individual patient or to the treatment population.

- **Individual** (σ_i) - the random error for an individual patient is the standard deviation of the measured errors over the course of treatment.
- **Population** (σ_p) - for the group of patients is the mean of (σ_i).

Random errors occurs at the treatment delivery phase. Therefore, they are referred to as treatment (or daily) execution errors. Possible errors are: **patient set-up error** (similar to systematic error), **target position and shape** (similar to the systematic errors but accounts for motion between fractions rather than from delineation to treatment), and **intra-fraction errors** (the change in the patient's position and internal anatomy movement during the delivery of a single fraction, for example, due to breathing).

Random uncertainties are added quadratically:

$$\sigma = (\sigma^2_{set-up} + \sigma^2_{organmotion})^{1/2} \tag{2.8}$$

Set-up Error and Treatment Margin

The systematic and random errors impact on dose distribution [85]. Random errors (delivered treatment) which vary from day to day lead to a blurring of the dose distribution around the CTV, whereas systematic errors could lead to under-dose to a portion of CTV. Therefore, a CTV-PTV margin is needed to ensure adequate coverage from various sources of systematic errors.

Quantifying the Errors for Margin Setup

Quantification and optimization of margins in radiation therapy have been investigated in many studies. Van Herk et al. suggested that the aim of adding margin is to ensure 90 % of patients must get a minimum CTV isodose of 95 %. Furthermore, they suggested that the PTV margin is found as follows [44]:

$$\text{PTV margin} = 2.5 \sum p + 0.7\sigma_p \tag{2.9}$$

Where:

$\sum_p$ is the systematic error for a group of patient.

σ_p is the random error for a group of patient.

According to report ICRU 62, the total margin (TM) can be calculated as following [46]:

$$TM = \sqrt{IM^2 + SM^2} \tag{2.10}$$

Where:
TM is total margin, IM is internal margin, and SM is set up margin.

2.4 Image Modalities in Radiation Therapy Planning

The theory below is based on the book Khan's treatment planning in Radiation Oncology [86].

The success of radiotherapy is dependent upon localizing a tumour and its microscopic extensions so that they are treated accurately with a right radiation dose. In modern radiotherapy, medical imaging tools has contributed to the potential of improving the cancer treatment. Imaging plays an essential role in tumour localization, treatment planning, guiding radiation delivery, and monitor the response. This section provides an overview of several imaging modalities used in radiation therapy. Each modality has its strengths and applications, and complements the strengths of other imaging techniques [86].

2.4.1 Computed Tomography

Computed tomography (CT) is based on the variable absorption x rays by different tissues. It measures the linear attenuation coefficient of each pixel in the transverse imaging plane. A fan beam of diagnostic energy x-rays passes through the patient body, and the transmitted radiation is measured. The x-ray source rotates around the patient and multiple projection views are acquired. From these projections, image reconstruction algorithms generate a transverse digital image. Each pixel value is a measurement of μ_x, the linear attenuation coefficient (relative to water μ_w at an effective diagnostic x-ray energy. Then, pixel values are quantified in Hounsfield units (HU):

$$\text{CT pixel value (HU)} = \frac{1000(\mu_x - \mu_w)}{\mu_w} \tag{2.11}$$

For a single energy scan, the HUs associated with various body components are: air (-1000 HU), water (0 HU), fat (~ -80 HU), muscle (~ 30 HU), and bone (variable up to or greater than 1000 HU) [86]. HUs of different tissues at diagnostic energies can be approximately extrapolated to electron density values used for dose calculations [68].

CT is a primary imaging modality which is typically used to construct detailed three dimensional anatomic and physical models of the patient. The volumetric CT scans are input into treatment planning, used for designing beam arrangements and shapes, calculating the dose delivered by these beams, and as a guide to position the patient for treatment.

2.4.2 Cone Beam Computed Tomography

Cone beam computed tomography (CBCT) is the most common implementation in use today in radiotherapy treatment room, involving adding tomographic imaging capability to the treatment machine. A x-ray tube and flat panel detector are mounted orthogonal to the treatment axis. The x-ray beams are divergent, forming a cone. During imaging, the CBCT scanner rotates around the patient and the projection images for reconstruction are acquired at multiple angles Fig. 2·4. Reconstruction algorithms optimized for CBCT are used to generate anatomical maps. CBCT provides views that can be presented as 3D volumes or 2D images for both diagnosis and advanced planning in RT. CBCT images provide clinically useful information even in the presence of motion during acquisition, radiation scatter, and mechanical isocenter wobble during scans [86].

Another approach to treatment room tomographic imaging is to use the MV treatment. The therapeutic beam serves as the radiation source and a flat panel radiation detector to acquire image projections [26]. Although, the soft tissues contrast on MV CBCT images is not as good as in the kv CBCT images, they provide adequate information for patient positioning and additional 3D information.

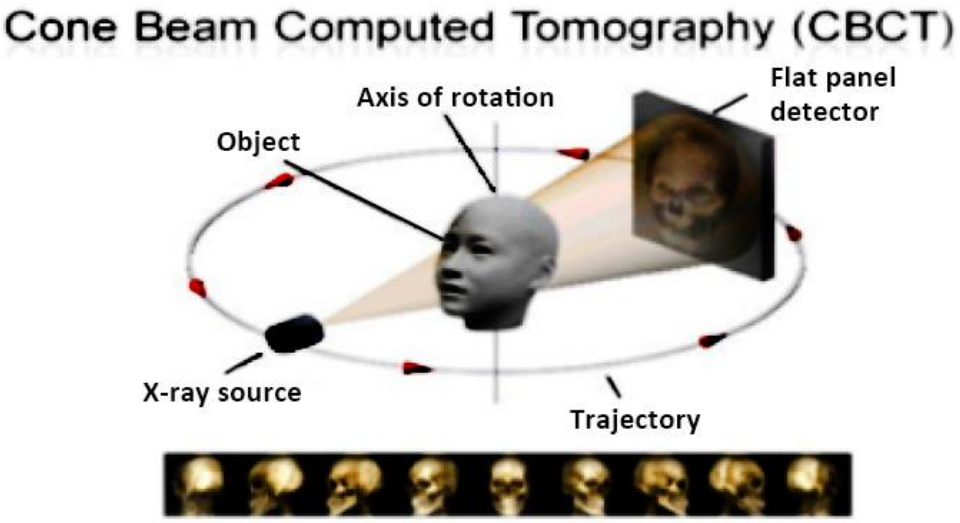

Figure 2·4: Cone Beam Computed Tomography (CBCT).

2.4.3 Magnetic Resonance Imaging

Magnetic resonance imaging (MRI) is medical imaging procedure for creating images of the internal structures of the body. MRI scanners use strong magnetic fields and radio wave (RF energy) for providing a spatial map of the bulk magnetization of the voxel. The signal in an MR image comes mainly from the protons in water molecules and fat in the body. Acquisition sequences can be tailored to vary image contrast and content. The most commonly acquired MRI scans are proton density, T1- and T2-weighted images. In which T1 and T2 refer to spin-lattice and spin-spin relaxation times, respectively. They are time constants associated with nuclear magnetic moment reorientation after excitation to an excited energy state. Factors that influence the image appearance are proton density within the voxel, relaxation times, blood flow, and magnetic susceptibility [11]. MRI images have better soft tissue contrast in comparison to CT images because spin density and relaxations times of soft tissues vary considerably depending on the micro-environment. A new approach IGRT is the integration of a diagnostic MRI and a linear accelerator [29].

2.4.4 Emission Tomography

Emission Tomography probes tumour biochemistry by measuring the biodistribution of biologically active radiolabelled pharmaceuticals. It is based on the detection of the γ-rays emitted

and the resulting visible light is amplified by photomultiplier tubes. Reconstruction of these signals provide the volumetric information in the 3D and 4D biodistribution of the administered radiopharmaceutical.

In positron emission tomography (PET), positron emitters are used. The positrons annihilate nearby electrons with emission of opposed γ-rays. PET is useful in defining the target volume and in staging disease. The application of PET in treatment planning have been studied [41]. The role of PET in radiation oncology has increased with the development of the PET/CT scanners [16].

2.5 Treatment Planning

The aim of radiation therapy treatment planning is to achieve a pre-defined dose distribution inside the target volume and a dose as low as possible in healthy tissues surrounding the target [91]. Nowadays, the computerized treatment planning system (TPS) are usually used in the clinics.

The process of treatment planning is described as in the Fig. 2·5.

Figure 2·5: Treatment planning process

.

2.5.1 Step 1: Patient Preparation and CT-Simulation

- **Internal anatomy:** The patient's internal anatomy is restricted or controlled, e.g, bladder or/and rectum filling is controlled.
- **Immobilization - External Anatomy:** Some "immobilization" devices such as masks, headrest, or form-fit body molds will be used to maintain the patient's body position the same during treatment. Sometimes, it is required tattoo mark on the patient's body.

- **CT-Simulation:** a CT-simulator is a diagnostic CT with flat table top and aligning system to "mimic" the conditions on a linac. The patient's computed tomography (CT) scans will be acquired. The information on CT scans will be translated into accurate treatment planning and dose calculation. It also results in better and more reproducible set-up on treatment machine.

2.5.2 Step 2: Contouring

In this step, the target volume and OAR will be delineated on CT images by the oncologist. Also other imaging, such as MR and PET images could be used to guide the contouring. These images are usually fused with CT images using image registration methods Section 2.7. The anatomical knowledge is vital. The accuracy and consistent of the contouring will impact the treatment plans and the outcome of RT.

2.5.3 Step 3: Treatment Planning

Inverse planning algorithm is the most frequently used method. In **inverse planning** technique, the planner defines the target volume(s) and organs at risk (OARs). Then, a planer provides required target doses, constraints to OARs and weight factors for each. After that, an optimization program used analytical methods and iterative methods to find the treatment plan that best matches all input criteria [69].

Energy choice: The energy choice is determined by the depth and surface sparing. It usually has access to several beam energies (e.g., 6 MV, 10 MV and 15 MV).

2.5.4 Step 4: Dose Calculation

3D calculations use CT images that acquired from the simulation. On the CT image, each pixel is assigned a numerical value (CT number) and is converted into relative electron densities to represent corresponding attenuated values, which are displayed using Hounsfield unit (HU) scale. The HU information is used to predict the delivered dose along the beam path by calculating the attenuation of X-ray beams. The different dose calculation algorithms are available in the TPS, such as pencil beam, collapse cone convolution and Monte Carlo with

accuracy and computation time being relevant trade-off [87].

2.5.5 Step 5: Plan Evaluation

The theory below is based on the ICRU reports (50, 62, and 83) [46, 47, 74].

The treatment plan should be evaluated comprehensively based on some criteria, such as quantitative analysis (by looking at Dose-volume Histogram (DVH)), dose statistics, and qualitative analysis (by looking at isodose distribution).

Quantitative analysis using dose-volume histogram (DVH)

In modern radiation therapy, with the help of precise dose calculation algorithms and advanced 3D imaging techniques, absorbed dose distribution is generated to characterize the delivery dose to relevant anatomic volumes rather than to single points in the conventional therapy [74]. Dose volume histograms (DVH) has become useful tool to evaluate treatment plan with complex dose distributions.

DVHs provide quantitative information relating absorbed radiation dose to specified tissue volumes [87]. With a modern TPS, DVHs are calculated and generated based on 3D reconstructed images [55]. It is a way to take complicated dose distribution into a single curve for each specific delineated structure of interest (ROI). Fig. 2·6 shows an example of DVHs. A differential DVH represents the percentage or absolute volume of interest that receives dose in the corresponding dose bin. A cumulative DVH represents the percentage or absolute volume of interest that receives a dose greater than or equal to the absorbed dose value in the corresponding dose bin. Each point on the curve of a cumulative DVH is expressed by the following [74]:

$$DVH_{\text{relative cumulative}}(D) = 1 - \frac{1}{V}\int_{0}^{D_{max}} \frac{dV(D)}{dD} dD, \tag{2.12}$$

Where V is volume of the structure of interest and D_{max} the maximum absorbed dose in the structure, and the differential DVH is defined as $dV(D)/dD$, which is the increment of volume per absorbed dose at absorbed dose, D (as shown in Fig. 2·6).

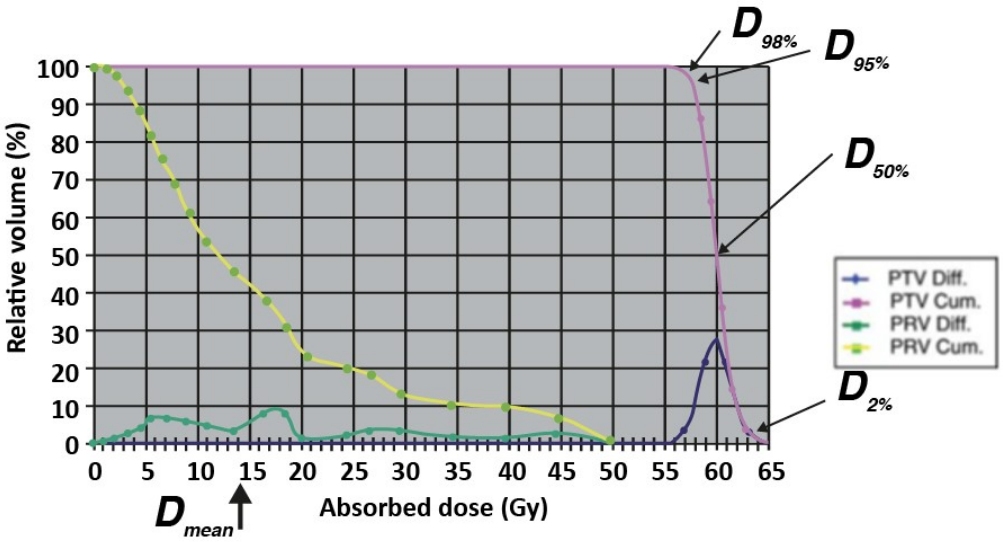

Figure 2·6: Example of differential DVHs and their corresponding cumulative DVHs including PTV (planning target volume) and PRV (Planning OAR volume) [74]. The dose volume metrics: $D_{98\%} = D_{near-min}$, $D_{95\%}$, $D_{50\%}$ (median), and $D_{2\%} = D_{near-max}$ received by PTV. For this example, the values of $D_{98\%}$, $D_{95\%}$, $D_{50\%}$ (median), and $D_{2\%}$ are 57 Gy, 57.5 Gy, 60 Gy, and 63 Gy, respectively. The D_{mean} received by PRV is also indicated. Notice that the mean absorbed dose for an OAR is different from its median absorbed dose, whereas the mean absorbed dose for the PTV is generally very close to its median absorbed dose.

Visual inspection of cumulative DVHs is commonly used in clinical practice since important features of an absorbed-dose distribution, such as the existence of regions of low or high dose can be provided. Therefore, the coverage of PTV by a specific absorbed dose can be evaluated and governed through optimized planning [74]. However, DVHs cannot visualize spatial information of absorbed dose, e.g., the location of low dose regions within the GTV, CTV, and PTV boundaries. Hence, the inspection of dose distribution (isodose curves) is always vital to ensure that the PTV is being adequately irradiated.

Qualitative analysis using isodose curves

Isodose curves (as shown in Fig. 2·7) are used for verifying the treatment plan in order to ensure that the target coverage is adequate and critical structures surrounding PTV are spared. The ICRU report 50 [46], ICRU report 62 [47], and ICRU report 83 [74] recommends a PTV uniformity within +7 % and -5 % relative to the dose delivered to a well defined prescription point within the target.

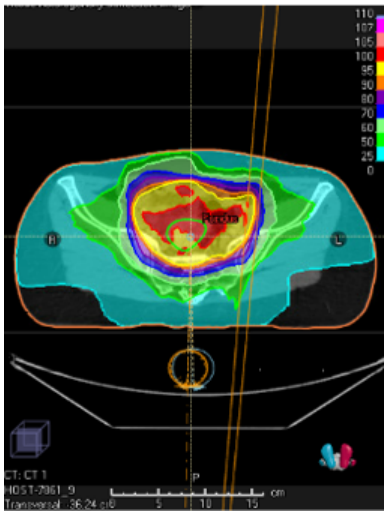

Figure 2·7: Isodose curves in transverse plane[***from RayStation TPS***].

Dose reporting, Recording and Prescriptions

Some concepts in dose statistics:

- $D_{x\%}$: $x\%$ of the volume receives this dose D (in Gy) or higher [93].
- V_y: the volume V (in %) that receives this y Gy [93].
- D_{max}: the highest dose to the volume. A volume is considered clinically meaningful if its minimum diameter exceeds 15 mm. However, if it occurs in a small organ (e.g., the eye, optic nerve, larynx), a dimension smaller than 15 mm has to be considered.
- D_2: is designated as $D_{near-max}$, i.e., near-maximum absorbed dose.
- D_{min}: the lowest dose to the volume. In contrast to maximum dose, no volume limit is recommended.
- D_{98}: is designated as $D_{near-min}$, i.e., near-minimum absorbed dose.
- D_{mean}: the average dose to the volume.
- D_{xcc}: this number describes the minimum dose given to x cm^3 of the most irradiated volume and gives an impression of "hot spot" radiation to organ.
- "hot spots": is a volume outside PTV which receives dose higher than 100 % of the specified PTV dose.

- "cold spots": is a volume outside PTV which receives dose lower than 100 % of the specified PTV dose.

2.5.6 Step 6: Delivery

The treatment is delivered in the number of days and given in the number of fractions. Prior to each fraction treatment, patients are positioned on the treatment couch and immobilization devices, and lasers (marked on the skin) are used to minimize set-up errors and to ensure accurate positioning. The patients' anatomies are changed during the treatment courses. These changes could be breathing, tumour changes in shapes and sizes, weight loss and gains. As time passes, the treatment plan may end up different from optimal. It could cause decreases the coverage of the tumour, and/or increases dose to the healthy tissues. Therefore, pre-treatment imaging is required for accurate dose delivery. Image-guided radiation therapy (IGRT) which takes images frequently, typical used CBCT or MRI when the patient is on the treatment couch. This image is then used to reposition the patient to ensure optimal the delivery according to the plan [5].
The treatment is delivered to patient in the treatment room with the linear accelerator (linac), as shown in the Fig. 2·8.

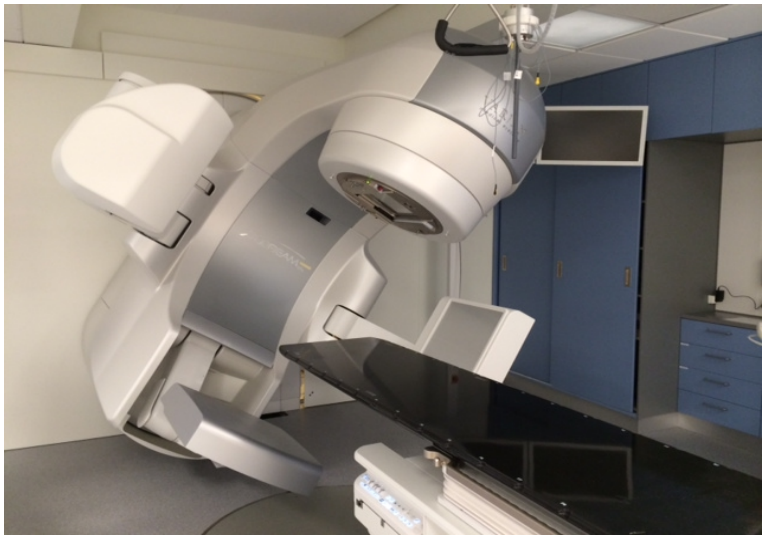

Figure 2·8: The Varian TrueBeam Linear Accelerator system with an additional kilovoltage CBCT for imaging in treatment room, Oslo University Hospital, the Radiumhospital

.

A linac generates high energy X-rays. The Linac fires high energy electrons at a metal target.

When electrons hit the target, high energy photons are produced and are creating a beam. The beam is shaped into a defined beam by collimator. The gantry of linac rotates around the patient couch so that the patient receives radiation from different directions.

2.5.7 Step 7: Plan Adaptation (if necessary)

The aim of ART is modify the original plan so that the dose distribution is adapted to the daily geometry changes as represented by the image acquired for positioning. It demands high speed of the algorithms.

2.6 External Beam Radiotherapy with Linac and Brachytherapy

In cancer treatment, there are two general classes of radiation therapy: external beam radiation therapy and brachytherapy. **External beam radiotherapy (EBRT**) is literally introduced as the most common type of radiation therapy. It refers to the techniques where a machine delivers radiation (in the form of x-rays or accelerated particles) from outside the patient to the tumour. **Brachytherapy** is treatment in which the radioactive source is placed near or in contact with tumour, with using of intracavitary, interstial or intraluminial placement of the treatment source.

In the past 30 years, it has been the modern era of radiation therapy. Many sophisticated treatment modalities have been developed with the aim to improve the therapeutic ratio by reducing doses to adjacent normal tissues. Some of the treatment modalities are described in the following sections.

2.6.1 Intensity Modulated Radiotherapy and Volumetric Modulated Arc Therapy

Three-dimensional conformal radiotherapy (3D-CRT) is termed used for radiotherapy techniques that can shape the dose to match the shape of the target by delivering radiation beam from different direction.

Intensity modulated radiotherapy (IMRT) is a form of 3D CRT during which small fields - beamlets with different intensity are constructed and combined through inverse treatment

planning to create an optimal dose distribution. The intensity or the fluence (i.e., the number of photons per area) is modulated by combining MLC fields dynamically, or statically, or by rotating the gantry.

Volumetric modulated arc therapy (VMAT) is referred as intensity modulated arc therapy. It is an IMRT technique that delivers radiation on a linac using cone beam that continuously rotates around the patient. Each rotation called an arc, and one or more arc might be used. During each rotation, the cone beam is continuously shaped (modulated) by MLCs. In VMAT, dose rate (how much radiation delivered for each second) and gantry speech (how fast beam rotates) are optimized to generate highly conformal dose distribution. Treatment time is shorter in VMAT compared to IMRT technique.

2.6.2 Image Guided Radiotherapy

The most widely concept of image-guided radiotherapy (IGRT) is using three-dimensional imaging in treatment room before, during and/or after the radiotherapy [25]. In the modern radiotherapy, the contribution of IGRT is proven, it has been helping to control the treatment uncertainties in order to reduce the PTV margins and thus certain coverage of target and minimize the dose to normal tissues. It is the key development to enable daily practice the dosimetric benefits of IMRT/VMAT. A large variety of IGRT technology is being used clinically. The most widely used is CT or CBCT. Another potential option for visualizing tumour itself and soft-tissues is MRI/linac integration, coming in the near future.

2.6.3 Brachytherapy

Brachytherapy is a type of internal radiation therapy in which a radioactive material is placed inside the body, close to the tumour in order to kill the cancer cell or shrinks the tumour. Some tumours are treated with brachytherapy alone or in combination with EBRT. For locally advanced cervical cancer treatment, patients receive EBRT and brachytherapy is usually initiated in the later part of treatment (after 4 to 6 weeks of EBRT).

2.7 Image Registrations

The theory below is based on AAPM TG132 [30].

Image registration is the process to define the spatial relationship between two image sets: a reference image set (e.g., the image dataset that another image dataset is being to registered to) and a target image set (e.g., the image dataset that is being transformed or deformed to match the reference image) [30]. In the image registration process, the transformation function is applied to the target image set to align it to the reference image (point to point correspondence). The mapped data from the target dataset can be combined and displayed on or with the reference dataset in a process, called fusion.

Image registration is classified into two categories, rigid image registration and deformable image registration.

2.7.1 Rigid Image Registration

Rigid registration defines the spatial relationship between each volumetric image set by changing translation and rotation in three dimensions (right-left, antorior-poterior, superior-inferior). The transformation function preserves the distance between all points in the image.

It is typically used for image guidance, for example 3D fusion of kv-CBCT to planning CT provides translation shifts on linear accelerator table. It is also common used for planning image sets.

2.7.2 Deformable Image Registration

Deformable image registration (DIR) determines the geometric transformation between two images to map them onto a common coordinate system. The spatial relationship can be "deformed" to match all areas of the volumetric images. It is a non-linear process that includes not only rigid transformation (i.e., translation/or rotation) but also deformations (e.g., stretching and shrinking). It is used when a rigid registration cannot accurately match all areas of the image.

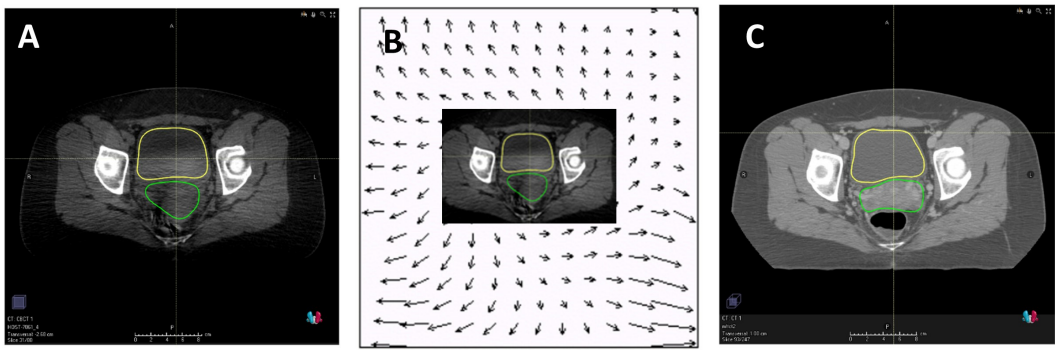

Figure 2·9: DIR theory. A: Target image: is image that will be deformed to match the reference image , B: Registered image, C: Reference image.

The Fig. 2·9 shows deformable image registration process warps the target image via deformable vector field (DVFs) to align the target image to the reference image. DVF defines the motion of each image voxel from the target image to the reference image. The size and direction of the arrows represent the magnitude and direction of DVF. This produces a registered image.

In the field of radiation therapy, DIR can be used in mapping structures from one image set to another image set for faster contouring. In dose accumulation process, the DVFs from DIR is applied to map a fraction dose distribution from the target image set to a reference image set (e.g., from the daily CBCT to the planning CT). The deformed fraction doses propagated in this way can be summed up. The delivered accumulated dose can be used to report the delivered dose or to compare with the planning/prescription dose (dose tracking/monitoring) in order to trigger, for example adaptive re-plan [59].

DIR algorithm

The DIR algorithm in RayStation TPS is Hybrid DIR (ANACONDA = ANAtomically CONstrained Deformable Algorithm [92]). This algorithm is the best suited for adaptive radiation therapy. The objective function is a linear combination of four linear terms. 1. image similarity term; 2. grid regularization term, which aims at keeping the deformed image grid smooth and invertible; 3. a shaped base regularization term which works to keep the deformable anatomically reasonable when regions of interest are present in the reference image; 4. a penalty term which is added to the optimization problem when controlling structures are used, aiming at deforming the selected structure in the reference image to the corresponding structure in the target image.

Deformable Image Registration and Dose Accumulation

The theory below is based on Chapter 5 in ART book [89].

The deformable organ registration (DOR) needs to be performed for accurately evaluating the cumulative dose distributions delivered to the CTV. In the DOR, an organ is divided into many sub-volumes, and the relative position of each sub-volume varies from fraction to fraction. Assume v is the sub-volume of an organ, V, that is, $v \in V$, it has a coordinate of $\vec{x}(v) \in R^3$. The displacement of the sub-volumes of the organ is subjected to the constraints of the tissue elastic properties. Let $\vec{x}_{ref}(v)$ be the position of v in reference CT, then its position at fraction i becomes:

$$\vec{x_i}(v) = \vec{x}_{ref}(v) + \vec{\delta_i}(v) + TM_i(V) \tag{2.13}$$

where $\vec{\delta_i}(v)$ is the displacement of the sub-volume v, $TM_i(V)$ is the rigid transformation matrix used in online image guidance and it affects the whole image set. If online image guidance is not performed, then $TM_i(V) = 0$. Assume that we have a series of moving image (M), each corresponding to a treatment fraction. Every image i has a dose matrix $D_i(x)$ assigned to it. The dose matrix can originate from an EBRT dose planning and is a description of the distribution of radiation dose given in the fraction corresponding to image i. Then, the accumulated dose distribution after k fractions is:

$$CD_k(v) = \sum_{i=1}^{k} D_i(\vec{x}(v)) \tag{2.14}$$

2.8 Dose Tracking

Dose tracking process is a process in which the accumulated delivered dose to patients is tracked and compared to accumulated planned dose. It can be evaluated quantitatively based on computing fraction dose on daily imaging (for example CBCT). The process of dose tracking is described in detail in **Section 3.6**. Then, by evaluating accumulated dose, to assess treatment plan success.

Chapter 3

Materials and Methods

3.1 Patients and Radiation Treatment Planning in the EMBRACE II Study

The clinical data of 8 patients treated for locally-advanced cervical cancer (FIGO stages Ib or higher) were retrospectively investigated in this project work. The patients underwent treatments in Oslo University Hospital-Radiumhospital (Oslo, Norway), and were included in the EMBRACE II study (Image guided intensity modulated External beam Radiochemotherapy and MRI based adaptive BRAcytherapy in locally advanced CErvical Cancer) [35].

3.1.1 Image Acquisitions During the Course of Treatment

Computed tomography (CT) images (planCT), MR-images and cone beam computed tomography (25 daily CBCTs) were acquired for every patient.

Procedure for MR: patients were asked not to eat 4 hours prior to the image acquisition. Then, at the MR update they were asked to actively empty the rectum with clyster. The patients were also asked to empty their bladder.

Procedure for CT and prior to each fraction: patients followed the drinking protocol (empty bladder, drink 300 ml water, 30 min prior to CT and treatment). No instruction regarding the rectum.

Thus, the bladder would be rather empty on MR and comfortably full on plan CT and CBCT. The rectum would be more or less empty on MR but can vary a bit on CT and CBCT.

The planCT images were acquired with patients in the head first supine position. The CT scan is a GE Discovery MI and is part of a PET/CT procedure with diagnostic quality. It gives 2-mm slice thickness and 512 × 512 pixels. Then, MR-images were aquired with a Siemens Skyra 3T. Patients underwent CBCT scanning prior to every treatment fraction and fused to planCT image (rigid registration) for a correction of the patient's position. Finally, all CBCT images were imported into RayStation (RaySearch, v 9.0, RaySearch Laboratories, Stockholm, Sweden) TPS via the network.

3.1.2 Target and Organ-At-Risks Delineation

Target Delineation

The contours of target volumes and OARs were done on the MRI and CT scans. Then, MRI scans were fused to the planCT images using bone rigid registration. The target volumes and OARs were delineated on the fused images by a radiation oncologist according to the planning procedure for primary irradiation of cervical cancer (Oslo University Hospital)[6] as below:

- GTVp_MR: was defined as a primary tumour which was visible on T2-weighted MR image.
- GTVn# (CT/MR): pathology enlarged lymph nodes which were delineated on CT.
- GTVp_PET: was primary tumour which was defined on FDG PET-CT.
- CTVp_HR (MR): was an extension of GTVp_MR and the rest of cervix which was not infiltrated by tumour on MR.
- CTVp_LR (CT): included original CTVp_HR, GTVp_PET and the rest of cervix on CT. In addition parametria on both sides, whole uterus was included as well as involved vagina with a 20 mm margin. In the level of cervix a 5mm margin from the CTVp_HR in the anterior and posterior direction were applied.
- CTVe (MR/CT): Lymph notes area lymph node regions which includes relevant blood vessels with a minimum of 7mm perivascular tissue.

OARS delineation

Bladder, rectum, sigmoid, bowel, femoralhead_L, femoralhead_R, kidney_L, kidney_R, spinal cord, duodenum, caudal equina, PIBS* (Postterior Inferior Border of Symphysis, point that lies in the vagina at the level of the posterior, lower border of the symphysis), and PIBS-2cm (point that lies in vagina, 2 cm caudal for PIBS) were delineated on the planCT.

3.1.3 Margins to create ITV and PTV

The margins were set-up according to planning procedure for primary irradiation of cervical cancer (Oslo University Hospital)[6] as below: The ITVp_LR margins were added individually from the movement that was seen on CT- and MR-images. It was recommended to start with standard margins and adjust individually for each patient. A ITV_45 for the whole pelvis was created by combining the ITVp_LR and the CTVe. Additional margin of 5 mm was applied to create PTV_45. Fig. 3·1 shows contours of targets and OARs with margins on CT image for one patient.

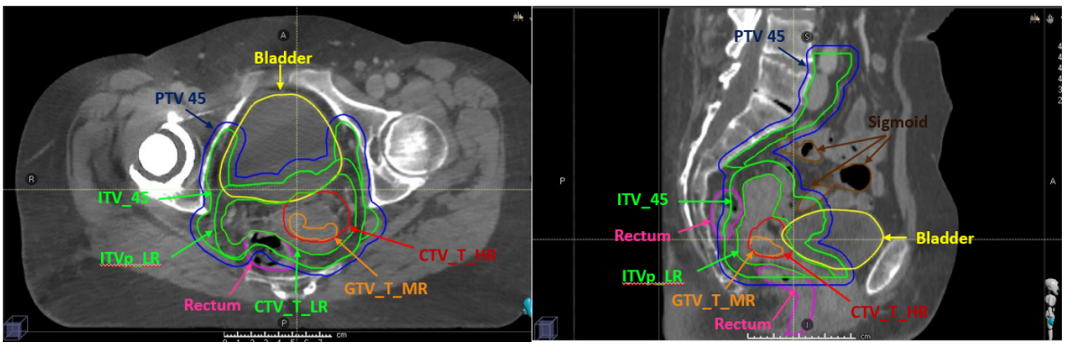

Figure 3·1: Delineations of targets and OARs with margins on CT image for patient 10. On the left: in transversal plane. On the right: in sagittal plane. Figure was taken from RayStation TPS.

3.1.4 Plan Evaluation

The treatment plans were evaluated for target and OARs using DVHs, isodose curves from RayStation TPS and dose statistics based on treatment planning procedure from Oslo University Hospital [6]. The dosimetric parameters were shown in the Table 3.1 and Table 3.2.

Table 3.1: Dose objectives to the target volumes [6].

Volume	Goals	Acceptance
ITV_45	$Dmin > 42.8$ Gy	
PTV_45	V95 % > 42.8 Gy	$V95\% = 42.8$ Gy

Table 3.2: Dose constraints to OARs [6].

Organ	Goals	Acceptance
Bladder	$Dmax < 105\%$ (47.3 Gy)	$V40Gy < 60\%$ $V30Gy < 80\%$
Rectum	$Dmax < 105\%$ (47.3 Gy)	$V40Gy < 75\%$ $V30Gy < 95\%$

3.1.5 Treatment Delivery

A Varian linear accelerator with energy of 6MV X –ray equipped with a kv –CBCT was used. The treatment was delivered by VMAT technique with two or three arcs, following the daily CBCT before every fraction.

The patients received EBRT to the CTVp and CTVe (1. 8 Gy × 25 fractions, to a total dose of 45 Gy) and a possibly simultaneously integrated boost to (2.2 –2.3 Gy × 25 fractions) to a CTVn (positive lymph nodes). The EBRT was given with one fraction everyday and five days per week. The patients received in addition brachytherapy with (7.8 Gy × 4 fractions) and weekly Cisplatin 40 mg/m^2. The maximum total treatment time included EBRT and brachytherapy and chemotherapy is 50 days according to the EMBRACE II protocol.
Fig. 3·2 shows an example of dose distributions on transversal and sagittal planes on planning CT image for one patient.

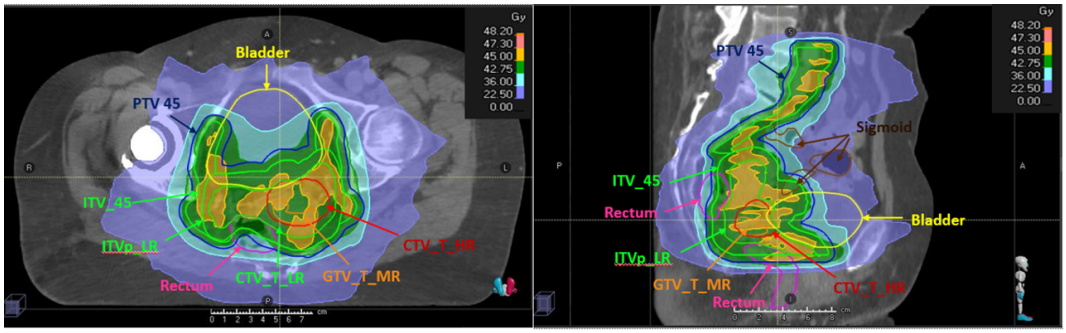

Figure 3·2: An example of treatment dose distribution on plan CT. On the left: In transversal plane; On the right: In sagittal plane. Images taken from RayStation TPS.

3.2 Analysis of Organ-At-Risk Volume variations

In order to enquire whether the bladder volume was stable or changed throughout the course of treatment, the bladder was delineated in all daily CBCTs for all the patients. Then, the bladder volumes were quantified based on bladder segmented ROIs on daily CBCTs, recorded from RayStation TPS. The bladder volume change ($\triangle V$) can be calculated as in the following equation:

$$\triangle V = V_k - V_p \tag{3.1}$$

where V_p is the volume measured on the planCT and V_k is the volume measured on the CBCT scan in fraction k.

3.3 Compute Delivered Fractional Dose Calculation on daily CBCTs

The description of this method was based on guideline for RayStation TPS from RaySearch Laboratories AB's presentation.

In order to perform dose tracking over the fractions during the course of treatment, the daily fraction dose was re-calculated based on daily CBCT image. It was computed using the "Dose Tracking" function in the "Adaptive Radiation" module in the RayStation TPS.

The CBCT values are not in Hounsfield units as CT. Hence, there is no direct mapping over densities. In RayStation TPS, conversion of CBCT values to densities is achieved by automatic

segmentation of the CBCT image into a number of different tissue regions, such as air, lung, adipose tissue, catalyst bone, and other. Then, a technique in RayStation TPS created a density table by mapping mass density values in g/cm^3 to the CBCT gray levels for these tissue regions. Fig. 3·3 (right) shows an example of the tissue based HU-to-density curve and the density table that were generated by the RayStation TPS. A sliding bar in the "image stack gray level histogram", as shown in the Fig. 3·3 (left), was used for manually adjusting the tissue specific thresholds to improve the values applied to create the CBCT density table.

The external ROI was created on each CBCT on limited field-of-view by a function in RayStation TPS. The original treatment plan was transferred to the CBCT images, following rigid image registration Subsection 2.7.1 and re-calculated the dose on each CBCT image set.

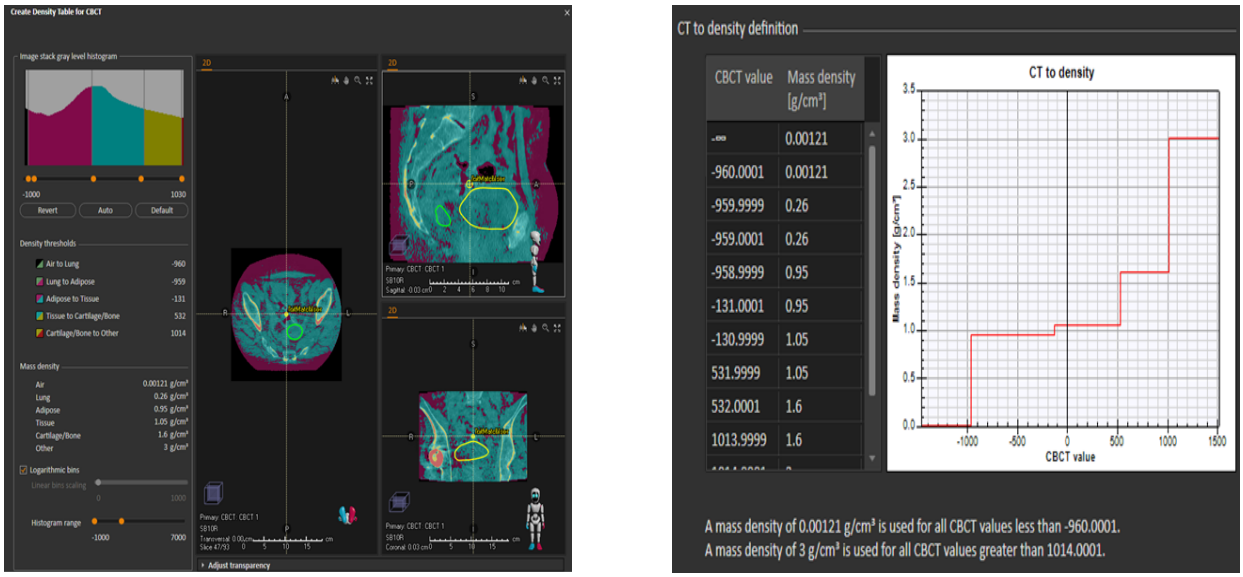

Figure 3·3: Left image: Tissue segmentation following density threshold on a pelvic area of a cervix cancer patient, and Right image: Tissue specific HU-to-density curves for CBCT image generated in RayStation TPS.

3.4 Dose Accumulation By Simple DVH Parameter Addition-based Method

Once the fraction dose was computed based on daily CBCT image, the accumulated delivered dose could be calculated by direct addition of DVH parameters. The clinical dose metrics such as D98 received by CTV_T_LR and Dmean, D2, and D50 received by bladder were accumulated.

Target and organ movement and deformation are crucial issues of determining where the dose is

actually delivered over the course of radiotherapy treatment [27]. Fig. 3·4(a) shows the target and OAR and dose distribution at planning. Fig. 3·4(b) illustrates target and OAR and dose distribution during one of the fractions where target and OAR have been deformed and OAR has moved into the high dose region.

In the current study, to account for target and OAR inter-fractional motion, a DIR algorithm was used for registering the daily CBCT image set to the plan CT image set. Then, DIR was applied for deforming dose and accumulating delivered dose. This method will be described in details in the following sections.

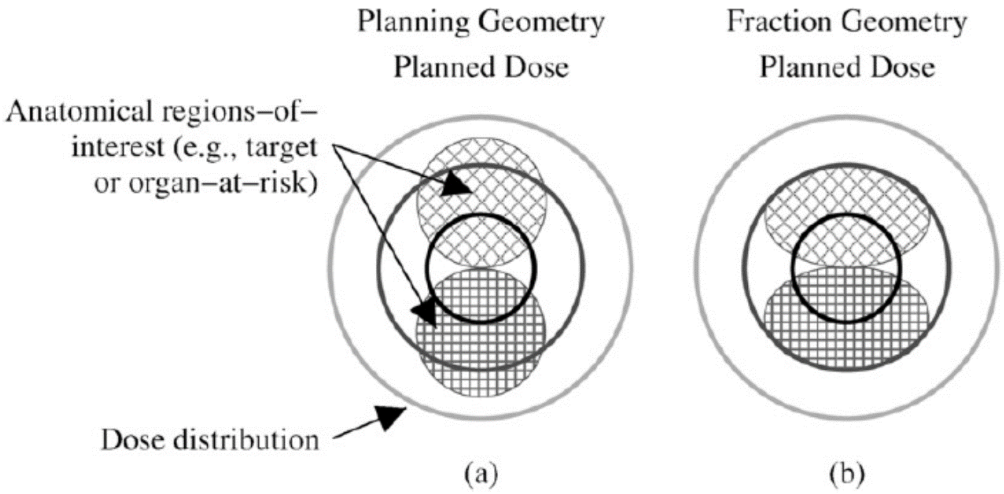

Figure 3·4: Two dimensional illustration of dose distribution, figure taken from Stewart, et.al. [27]. (a) The anatomy and dose distribution at planning. The OAR is located just below the target volume. (b) The anatomy and dose distribution during one of the fractions.

3.5 Deformable Image Registration

3.5.1 DIR Process

The DIR workflow is illustrated in the Fig. 3·5.

The CT image was used as the reference image, and the daily CBCT image was used as the target image. The DIR algorithm maps the ROIs geometry in the target image into the corresponding ROIs geometry in the reference planCT image. It should be noted that before DIR, the rigid registration, served as a starting point, was as good as possible.

The Hybrid DIR (ANACONDA = ANAtomically CONstrained Deformable Algorithm [92]) in RayStation TPS was used. It can be run with image information only, or in combination with anatomical information. The hybrid DIR algorithm in RayStation TPS have been being developed over the time to optimize the algorithm. It was demonstrated that controlling structures ROIs (regions of interest) and \or POI(s) (point of interest) as a guidance for ANACONDA algorithm improve the DIR accuracy. In order to prove this, in the current study, DIRs were performed in three scenarios: **case 1:** with controlling ROIs and POIs (only for patient 13 due to large deformation of CTV_T_LR); **case 2:** with controlling ROIs (for other 6 patients); **case 3:** only use image information (intensity) (for all 7 patients). Then, for individual patient, the accuracy of DIRs in these scenarios were qualitatively and quantitatively assessed and compared to each other. After all, the best case was chosen.

The controlling strutures (ROIs), such as CTV_T_LR and bladder and POIs, such as fundus points were defined on both planCT image and daily CBCT images. It was noted that, for a good DIR, the CTVp_LR on planCT image was modified to CTV_T_LR, in which the parametria on both sides of CTVp_LR was excluded because it was not well visible on CBCT images. The modification of CTVp_LR on planCT image and the segmentations of ROIs (CTV_T_LR and bladder) on daily CBCTs were done by the author of this thesis, with supervision of a doctor.

More details about how to improve DIR accuracy were added in the Appendix Section. A.1.

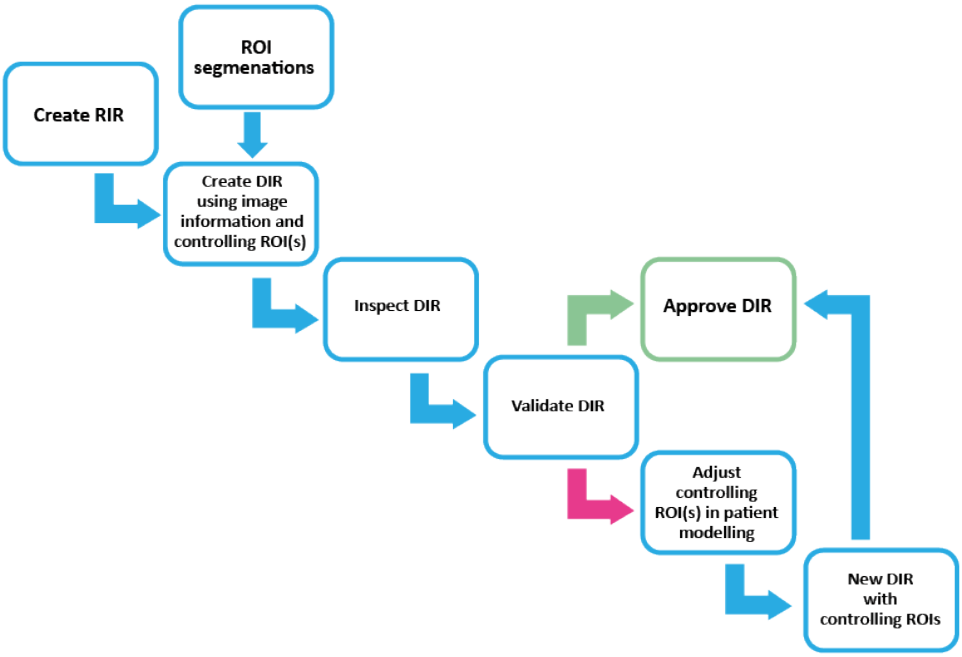

Figure 3·5: Deformable Image Registration workflow, *adopted from a guideline for DIR in RayStation version 9B, RaySearch Laboratories AB, Sweden.* RIR = Rigid Image Registration, DIR = Deformable Image Registration.

3.5.2 Evaluation of DIR Geometric Performance

The accuracy of DIR needs to be validated since the dose accumulation result is highly dependent on it. The validation of DIR was followed the AAPM TG 132 report [30].

Qualitative Evaluation of DIR Performance

In this study, the evaluation of DIR through visual inspection was performed using validation tools in RayStation. ROIs on reference image were shown in solid and ROIs on target image were shown in dashed, as illustrated in the Fig. 3·6. Qualitative validation of DIR performance was based on overlaps between ROIs on reference image and deformed ROIs from target image, i.e., good overlaps between ROIs after DIR showed a good registration. This process was supervised by an experience medical physicist.

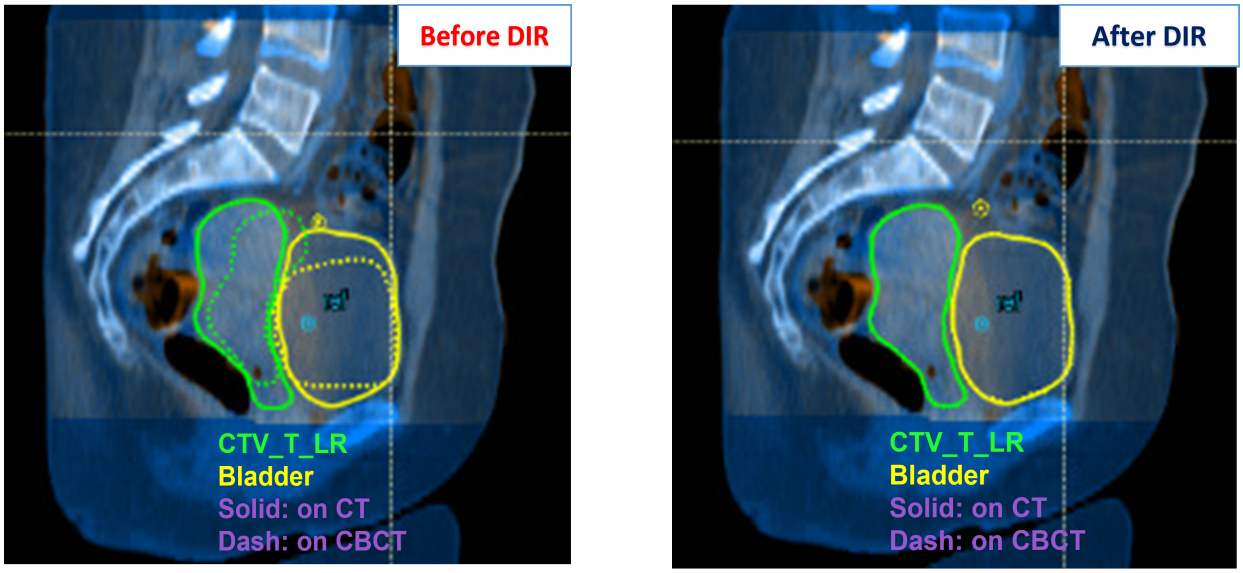

Figure 3·6: Qualitative Evaluation of DIR: An example of DIR from daily CBCT to planCT for patient 18: Before DIR and after DIR images. Images taken from RayStation TPS

Quantitative Evaluation of DIR Performance

The Dice Similarity Coefficient (DSC) metric was used for quantitative evaluation of DIR in this study. DSC is statistics used for comparing the similarity of two samples. DSC quantifies the spatial overlap of the contours on the reference images (planCT) with the contours on the target images (daily CBCT image), i.e., overlaps of contours of CTV_T_LR and bladder.
The DSC between two regions is calculated as in the following formula:

$$DSC = \frac{2 \mid V_r \bigcap V_d \mid}{\mid V_r \mid + \mid V_d \mid} \tag{3.2}$$

In the formula, V_r represents the volume of the contour on PlanCT image of reference and V_d represents the volume of the contours from the target image deformed by DIR. The values of DSC range from 0 to 1, with higher DSC values indicating the better overlap between two volumes.

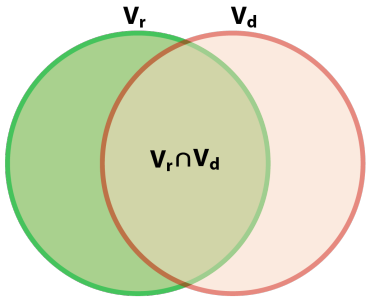

Figure 3·7: Dice Similarity Coefficient (DSC). V_r = Volume of the contour on PlanCT image of reference and V_d = Volume of the contours from the target image deformed by DIR

.

There is no consensus for standard DSC which gives good DIR standard. The DSC calculations are dependent on the volume of the structure, therefore very large or very small structures may have different expected DSC values for contour uncertainty [30].

In the recent study, the reasonable DIRs were approved by a function in RayStation TPS for being used further in dose deform and dose accumulation in the dose tracking process, i.e., the bad DIRs were excluded. The RayStation TPS can estimate dose for the fraction that deform dose was missing. The DVH dose parameters for deformed delivered dose from the fraction which missed dose deform was assumed similar as DVH dose parameters calculated on daily CBCT image.

3.6 Dose Tracking

The dose tracking process relies on five steps [59], as illustrated in Fig. 3·8. Each step is described in details in separate sections.

- **Step 1 (Deformable Image Registration):** All daily CBCT images were registered to CT using DIR. The detailed of DIR process is described in the Section 3.5.
- **Step 2 (Daily fraction Dose Calculation):** The daily fraction dose was computed on CBCT image, using the treatment parameters (the detailed process is described in the Section 3.3).

- **Step 3 (Dose Mapping/Deform dose):** The deformable vector field (DVFs) obtained with CBCT-to-CT in the DIR were used to map all CBCT fraction doses to the CT frame of reference (the detailed process is Section 3.6.1).
- **Step 4 (Dose Accumulation/Dose Summation):** the detailed process is described in the Section 3.6.2.
- **Step 5 (Dose Comparison):** The accumulated delivered dose can be compared to the accumulated planned dose, as in Section 3.8.

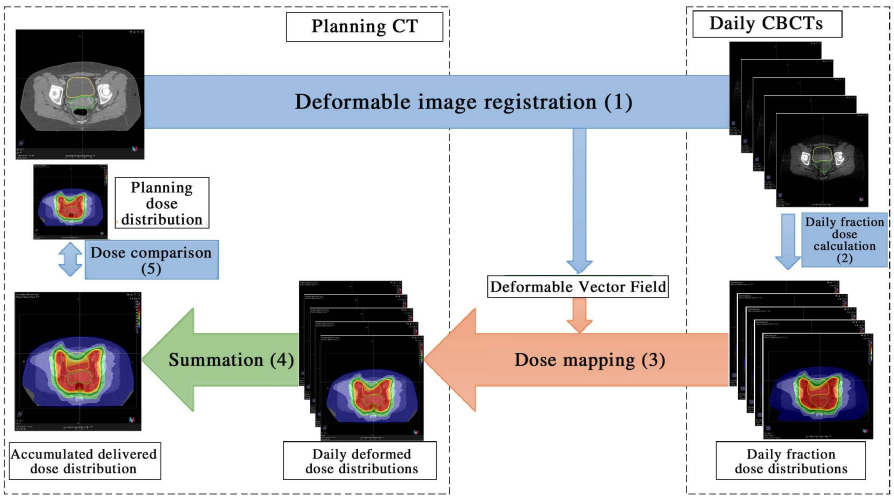

Figure 3·8: Dose tracking workflow includes five steps, adopted from *B. Rigaud et al.* [59]. Step 1: Deformation Image Registration (DIR). Step 2:Daily Fraction Dose Calculation. Step 3: Dose Mapping. Step 4: Accumulation/Summuation. Step 5: Dose Comparison.

A brief guidelines of dose tracking process on RayStation TPS could be found in the Appendix Section. A.1.

3.6.1 Dose mapping/Deform Dose

The monitoring of daily fraction dose on CBCTs provides useful dosimetric information. However, the dose is being compared on two different image sets (on planCT-the reference image set and on CBCT-target image set). In order to compare the delivered dose with the planned dose on the same image set, the distribution dose on the CBCT was deformed to the planCT. The process is illustrated in the Fig. 3·9.

With the approved DIRs and daily fraction doses computed based on CBCTs, doses can be deformed from the daily CBCTs to the planCT with function "Deform Dose" in the "Dose Tracking" module in RayStation TPS.

3.6.2 Dose Accumulation/Dose Summation

The dose accumulation is defined by the addition of the dose distributions at different fractions from daily CBCTs mapped to the planCT, by applying the dose distribution for each fraction. Once daily dose distributions have been deformed back to the planCT, the propagated dose distributions are summed up for computing the accumulated dose on the plan CT. The process is illustrated in the Fig. 3·9.

The algorithms of daily fraction dose calculation, dose deformation, as well as dose accumulation in RayStation TPS, have been discussed in literature [12, 92].

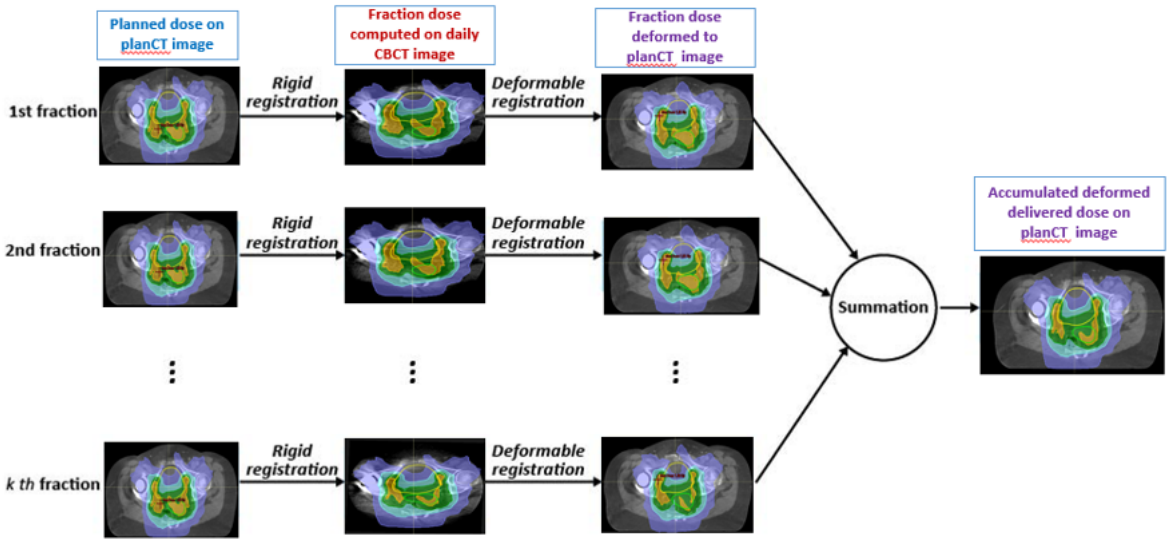

Figure 3·9: Accumulated Delivered Dose by DIR Method, adopted from *Y. Cui et al.* [13].

3.7 Dose Tracking in Two Methods: Dose Accumulation by DIR-based And Dose Accumulation By DVH Parameter Addition-based Methods

3.7.1 Visual Inspection of Dose Distribution and DVHs

The dose distributions from deformable dose accumulation and planned dose accumulation were compared in terms of isodose curves and DVHs.

3.7.2 Dose Tracking Using Dosimetric Metrics: D98, D50, and D2

Cumulatives DVHs parameters of the CTV_T_LR and bladder were calculated based on accumulated dose distributions. The accumulated delivered dose were calculated by two calculation methods, i.e., the dose accumulation by the DIR-based method as in the subsection Subsection 3.6.2 and the dose accumulation by the simple DVH parameter addition-based as in the Section 3.4.

The clinical DVH dose metrics such as D98 received by CTV_T_LR and Dmean, D50, and D2 received by bladder calculated by these two methods were used for the dose tracking, i.e., compared accumulated delivered dose with the accumulated planned dose.

These clinical DVH dose metrics were also used in Wilcoxon signed-rank test for comparing the accumulated delivered dose calculated by the DIR-based method and by the simple DVH parameters addition-based.

3.8 Dose Comparisons

This subsection describes the comparison modes in the step 5 in the dose tracking process. Contents were based on guideline for RayStation version 9B, RaySearch Laboratories AB, Sweden.

The four options for dose comparison in the RayStation TPS include **Fraction, Deformation, Accumulation and Total Dose dose comparison modes:**

- **Fraction comparison:** Compares planned dose vs. delivered dose per fraction (i.e., computed fraction dose).
- **Deformation comparison:** Compares deformed delivered dose vs. delivered dose per fraction.
- **Accumulation comparison:** Compares planned dose vs. deformed delivered dose for the selected fractions.
- **Total dose comparison:** Compares planned dose vs. estimated delivered dose for all fractions.

3.9 Perform Dose Tracking on Reduced Margins

In order to secure high precision of external beam radiotherapy, patient-based margins have been applied to account for target and organ motion or tumour regression [60, 32]. However, large margins may counteract the benefits of IMRT/VMAT that aims to spare normal tissues and conformal dose to target volumes, yet too small margins for patients who have large target and organ motion may lead to under-dosing to target volume and over-dosing to the normal tissues. The individualised ITV margins have been introduced in EMBRACE II [61]. This was denoted as a large margin in the current study, and its contour was created as the description in Subsection 3.1.3.

In this project, a treatment plan with 10 mm ITV (denoted as a small margin) was investigated in the dose tracking process. Further more, it was compared to the large margin plan. It should be noted that only patient 10 was performed with this small margin plan.

Fig. 3·10 shows the contours of target volumes, OARs, and margins on the plan CT for the patient 10 in the small margin plan. The ITV_T_LR_10mm was created by a medical physicist. First, a CTV_T_LR was created without taking into account the MR-information, and then 10 mm margin around this volume was applied. In this way the possible movement of the CTV_T_LR would not be taken into account therefore, the small bump on ITVp_LR (in green color) was removed.

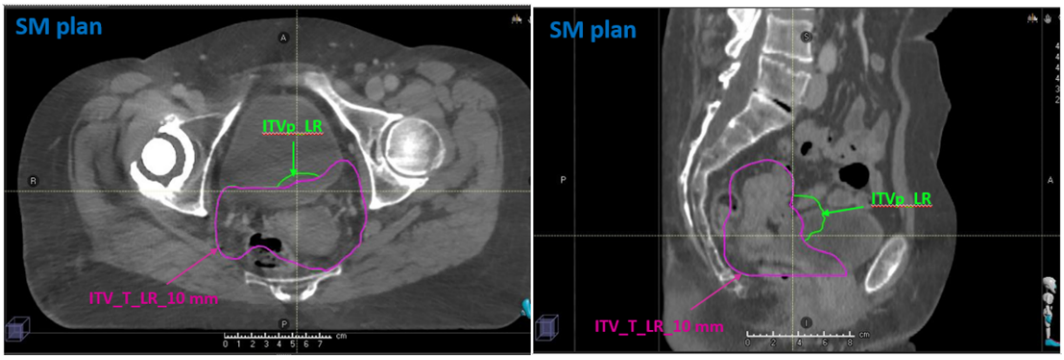

Figure 3·10: Contours on plan CT for SM plan for patient 10. On the left: In transversal plane; On the right: In sagittal plane. SM = Small margin. Images taken from RayStation TPS.

3.10 Statistical Methods

In this study, the following statistical methods have been used for data analysis:

- **Correlation coefficient:** quantifies the relationship between two variables. It is determined by the following formula:

$$r = \frac{\Sigma(x_i - \overline{x})(y_i - \overline{y})}{\sqrt{\Sigma(x_i - \overline{x})^2 \Sigma(y_i - \overline{y})^2}} \tag{3.3}$$

  where r is correlation coefficient; x_i is values of the x-variable in a sample; $\overline{x}$ is mean of the values of x-variable; y_i is values of the y-variable in a sample; $\overline{y}$ is mean of the values of y-variable;

  Correlation coefficient ranges from -1 to $+1$ which indicates the direction and strength of the relationship between two variables.

- **A least-squares linear regression:** is performed to fit linear models.

- **Regression statistics :** is used for exploring the correlations between two or more variables.

- **Box-and-whisker plot:** is used to display the five-number summary (the minimum, first quartile, median, third quartile, and maximum) of a set of data. The box represents the lower and upper quartiles (IQR), the band inside the box is the median value. The whisker represents the largest (lowest) value within 1,5 IQR of the upper (lower) quartile.

Dots above or below the whispers are outliers.

- **Wilcoxon signed-rank test:** is a non-parametric statistical test. It used to investigate if there is a difference between two related datasets.
- **Paired sample t-test:** is a type of t-test which is used to determine if there is a significant difference between two means of two data sets. It is used when the data in dataset has normal distribution and the data points in two data sets are related in paired.

$p < 0.05$ was considered statistically significant. Statistical analysis was carried out using Python statistics programming language and Data Analysis Module in the Excel Microsoft 365.

Chapter 4

Results

4.1 Assessment of Bladder Inter-fractional Volume Variations on Daily CBCTs

4.1.1 Bladder Inter-fractional Volume Variations

In the analysis of inter-fractional bladder volume variations, one of the 8 patients was excluded. This patient had bad quality CBCT images, as such, it was not possible to segment the bladder ROIs on CBCT images for quantifying the bladder volume. The other 7 patients, the bladder volumes were quantified on daily CBCT images for assessment.

The boxplot in the Fig. 4·1 shows the bladder inter-fractional volume variations during 25 fractions for all patients. Also, the bladder volumes on the plan CTs are illustrated in red dots and the mean bladder volumes calculated over fractions on daily CBCTs are showed in blue dots. As can be seen from this figure, patient 17 and 18 show larger bladder volume variations, while patient 11 and patient 13 have smaller bladder volume variations compared to the others. The mean bladder volumes on CBCTs for these patients were 149.04 ml, 167.05 ml, 87.21 ml, and 67.59 ml, respectively, compared with 153.47 ml, 251.4 ml, 79.49 ml, and 87.91 ml, respectively, on planning CT images. Moreover, patient 3, 10, 11, 13, and 17, the mean bladder volumes on CBCTs were closed to the bladder volumes on the plan CTs, while for patient 18 and 19 mean bladder volumes on CBCTs were lower than bladder volumes on the plan CTs.

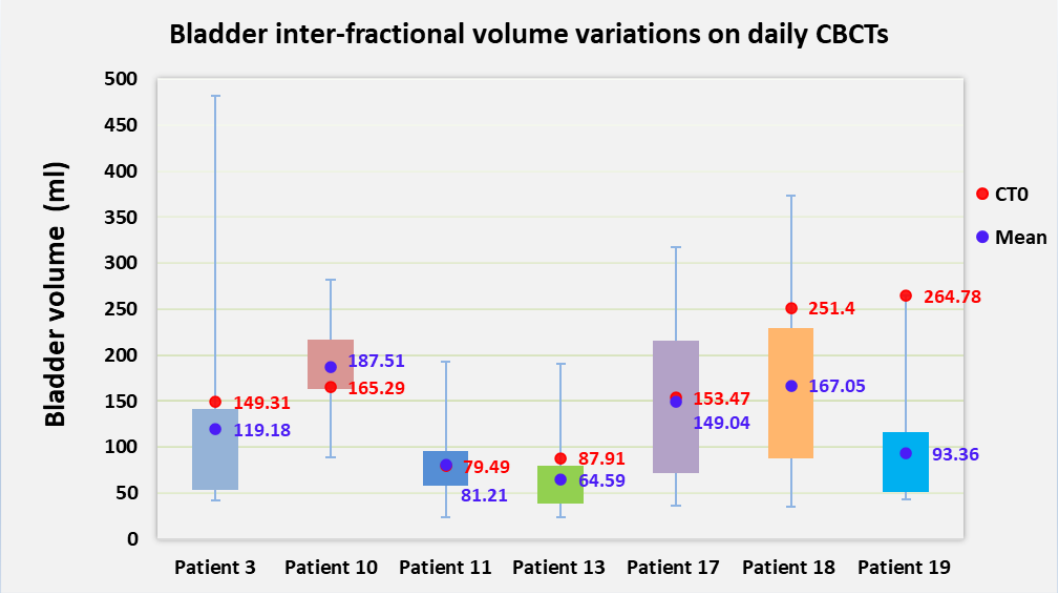

Figure 4·1: Boxplots of bladder inter-fractional volume variations during 25 fractions. Red dots show bladder volumes on planning CT image, and blue dots show average bladder volumes calculated over 25 fractions on CBCT images.

4.1.2 Bladder Volume Variations and Time Trends

Individual Bladder Volume Variations and Time Trends

With regards to individual patient, Fig. 4·2 shows bladder volumes observed on CT and CBCTs during the course of treatment. The regression statistics results (referred to the Appendix Subsection. A.3.3) revealed insignificant correlation between bladder volumes and the time of the treatment.

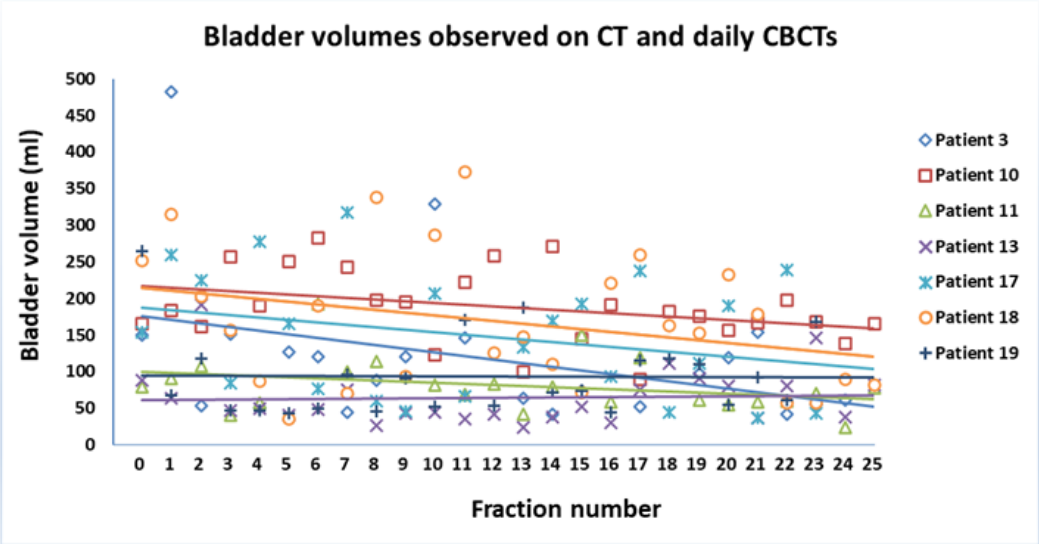

Figure 4·2: Individual patient bladder volume observed on CT and CBCTs. Fraction number 0 = Fraction on CT plan image; Fraction number 1-25 = Fractions on CBCT images.

Population Mean Bladder Volume Variation and Time Trend

Taken patients as a group (population), the Fig. 4·3 shows population mean bladder volumes during 25 fractions of radiotherapy treatment. The population mean bladder volume at planning on CT was 164 ±79 ml (1SD) (range 80 – 265 ml). During the course of treatment (25 fractions), the mean bladder volume was decreased to 108 ±70 (1SD). The regression statistics demonstrated that mean bladder volumes of population significantly declined during the course of treatment ($p = 0.026$, $R = 0.443$).

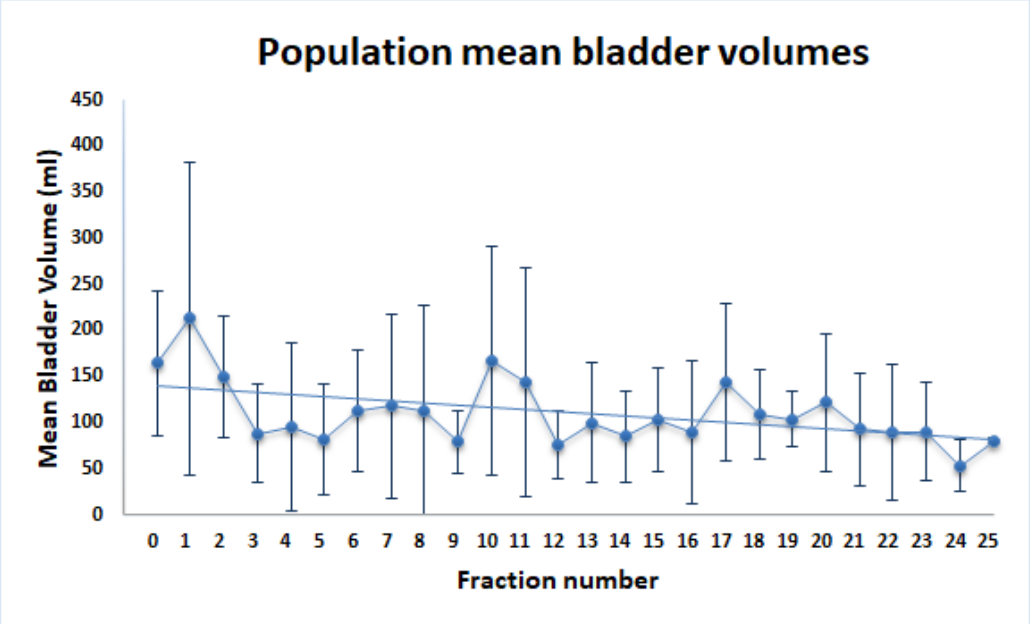

Figure 4·3: Population mean bladder volume during 25 fractions of radiotherapy treatment. Fraction number 0 = Fraction on CT plan image; Fraction number 1-25 = Fractions on CBCT images.

4.2 Evaluations of DIR Accuracy

4.2.1 Comparisons of Dice Similarity Coefficients in Hybrid DIR Algorithms with and without Controlling ROIs and/or POIs

Referred to the method in the Subsection 3.5.1.

The hybrid DIR algorithm in corporation with controlling ROIs (CTV_T_LR and bladder structures delineated on CT and CBCT images) and in some case additional controlling point-of-interest POIs (fundus points were chosen) enable to increase the DSCs.

The investigation was performed in patient 13 who had large structures deformation. The Fig. 4·4 and the Fig. 4·5 showed comparisons of the DSCs over all fractions for CTV_T_LR and bladder in hybrid DIR algorithm for three cases, i.e., case 1: with controlling ROIs and POI(s), case 2: with controlling ROIs, and case 3: without controlling ROIs and/or POIs (only used image information). In the t-test of the DSCs, the statistical difference between the DIRs, i.e., difference between DSC datasets in case 1 and case 2, and case 2 and case 3 ($p < 0.05$). As

can be seen from these two figures, for both CTV_T_LR and bladder, the hybrid DIR algorithm in case 1 gave the highest DSCs for all fractions. In contrast, the hybrid DIR algorithm in case 3 gave the lowest DSCs for all fractions. It was noted that, for other patients, visual inspections and quantitative evaluations of DIR (DSCs) demonstrated that the hybrid DIR algorithm in case 2 gave the reasonable DSCs (results not shown).

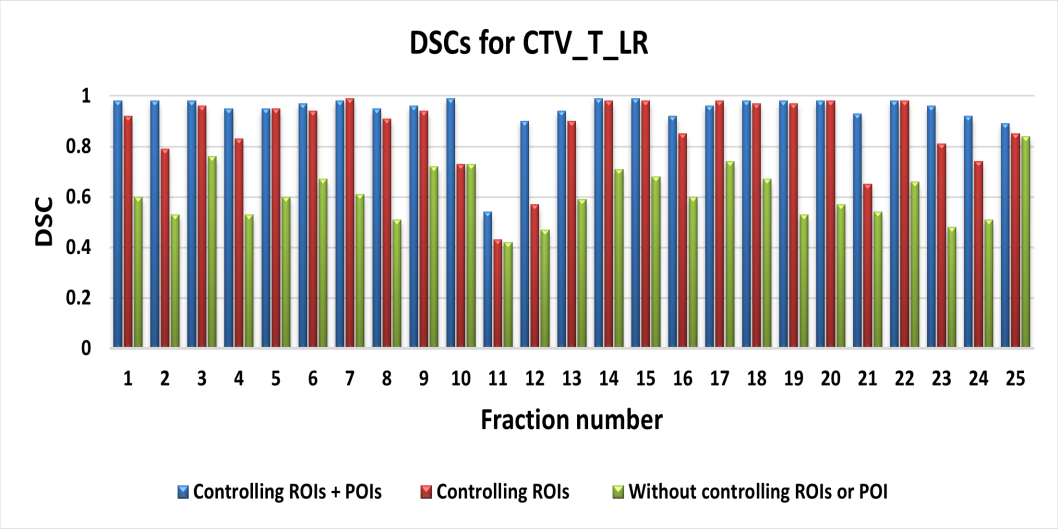

Figure 4·4: Comparison of DSCs for CTV_T_LR in hybrid DIR algorithms with and without using controlling ROIs and POIs. Results from patient 13.

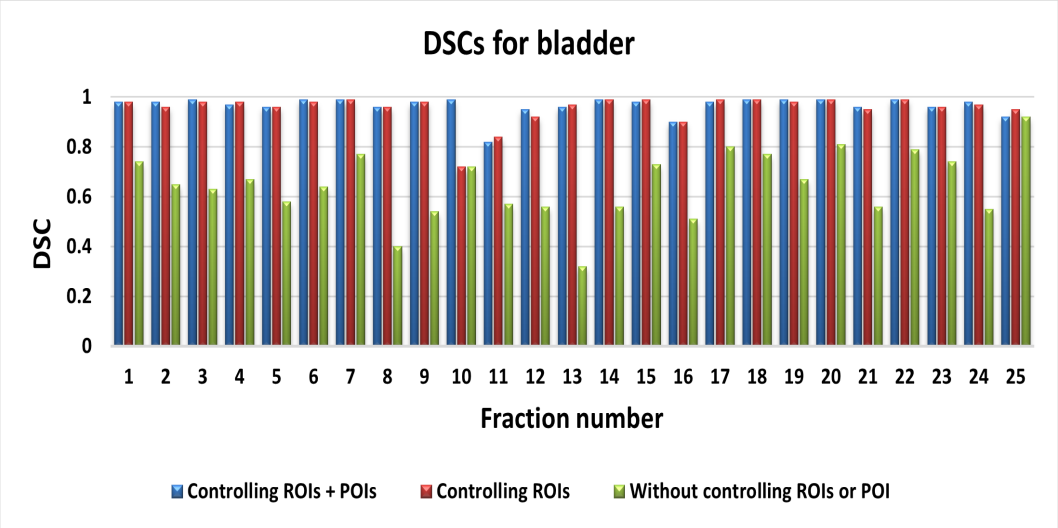

Figure 4·5: Comparison of DSCs for bladder in hybrid DIR algorithms with and without using controlling ROIs and POIs. Results from patient 13.

4.2.2 Qualitative Evaluation of DIR

Referred to the method in the Subsection 3.5.2.

The Fig. 4·6 (left) shows examples of the controlling ROIs (CTV_T_LR and bladder) and POI (fundus point) on plan CT and CBCT images before DIR in the sagittal plane. The algorithms in the RayStation TPS mapped the ROI geometry in the reference image (plan CT) and the corresponding ROI geometry in the target image (daily CBCT). The qualitative validation for DIR accuracy was done through visual inspection in the RayStation TPS. For all deformable fusion views, the ROIs in the reference image were shown in solid, the ROIs in the target image were shown in dash. The Fig. 4·6 (right) shows that the ROIs defined in both image sets, solid and dashed structures and fundus points were overlapped, i.e., it is a good DIR.

Among 8 patients studied, one patient was excluded from DIR due to bad quality of daily CBCT images. Among 175 DIRs for 7 patients, there were 10 bad DIRs accuracy. These daily fractions were excluded from deform dose and dose accumulation.

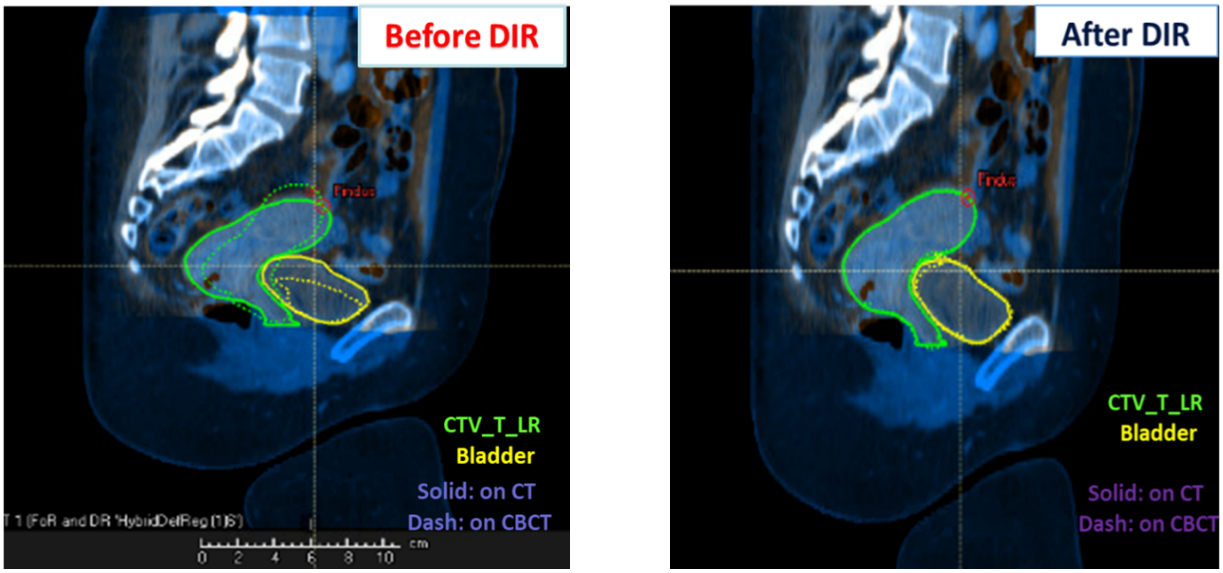

Figure 4·6: Qualitative Evaluation of DIR: Before DIR and after DIR images. Results for patient 13, taken from RayStation TPS.

4.2.3 Quantitative Evaluation of DIR

Referred to the method in the Subsection 3.5.2.

The boxplots in the Fig. 4·7 and the Fig. 4·8 showed the DSCs results over all fractions for CTV_T_LR and bladder, respectively, for individual patient.

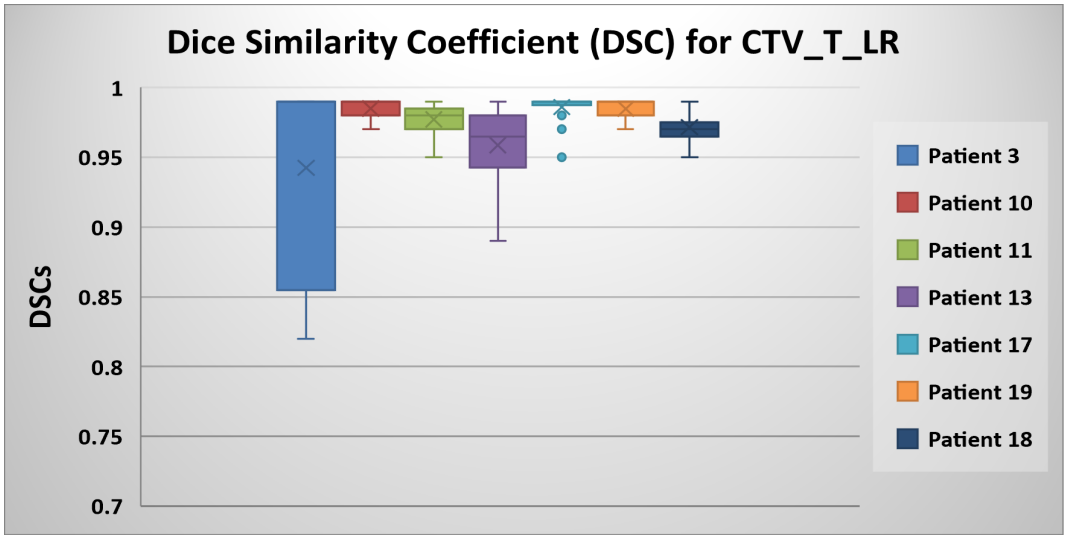

Figure 4·7: Boxplots of Dice Similarity Coefficient (DSC) over all fractions for CTV_T_LR. The bottom edge, the central mark, and the top edge of the box indicate the 25th, the 50th, and the 75th percentiles, respectively. The whiskers extend to the most extreme data points not considered outliers [$< Q3 + 1.5 * (Q3 - Q1)$ or $> Q1 - 1.5 * (Q3 - Q1)$], and the outliers are plotted individually using the dots symbol.

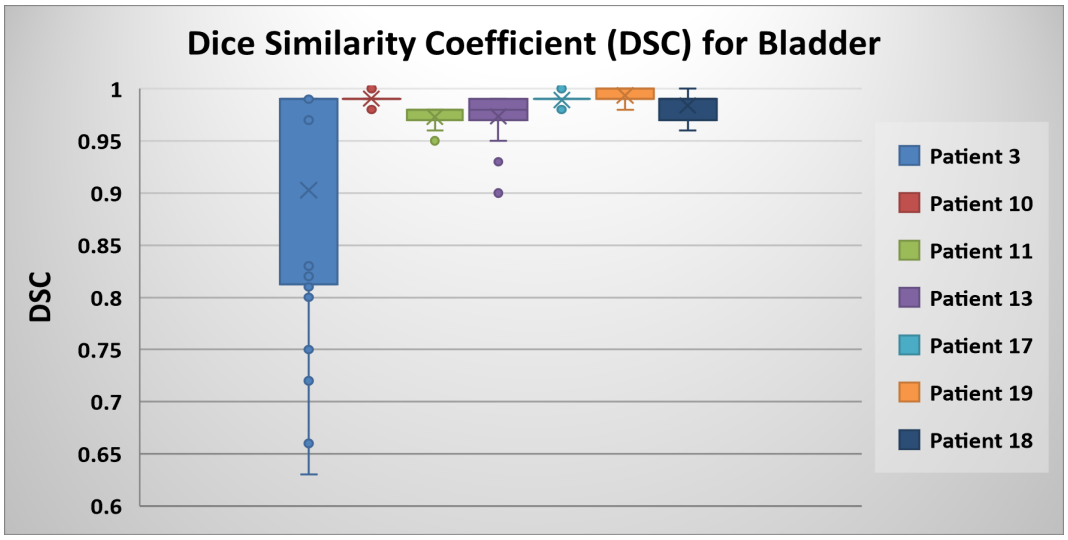

Figure 4·8: Boxplots of Dice Similarity Coefficient (DSC) over all fractions for bladder. The bottom edge, the central mark, and the top edge of the box indicate the 25th, the 50th, and the 75th percentiles, respectively. The whiskers extend to the most extreme data points not considered outliers [$< Q3 + 1.5 * (Q3 - Q1)$ or $> Q1 - 1.5 * (Q3 - Q1)$], and the outliers are plotted individually using the dots symbol.

For every patient, the mean DSC calculated over all fractions for CTV_T_LR and bladder were reported in the Table. 4.1. For the CTV_T_LR, the mean DSC calculated over 7 patients was 0.96 (ranging from 0.94 to 0.98 with SD of about 0.02). For the bladder, the mean DSC

calculated over 7 patients was 0.97 (ranging from 0.9 to 0.99 with SD of about 0.02).

Table 4.1: Table of the mean dice similarity coefficient (DSCs) over all fraction for CTV_T_LR and bladder.

Patient number	3	10	11	13	17	18	19
Mean DSC for CTV_T_LR	0.94	0.98	0.97	0.95	0.98	0.97	0.98
Mean DSC for bladder	0.9	0.99	0.97	0.97	0.98	0.98	0.99

4.3 Accumulated delivered dose

Referred to the methods in Subsections: 3.4, 3.6.2, 3.7, and 3.8.

It should be noted that only good DIRs performance after qualitative and quantitative validations were approved (done by a function in RayStation TPS) for being used further in dose deform and delivered dose accumulation as it was explained in method Subsections 3.5.2. The dose tracking was performed for 7 studied patients (who have good DIRs). It was assessed individually.

4.3.1 Visual Inspection of Dose Distribution

The fractional delivered dose computed on daily CBCT was deformed to the plan CT by the DIR method. Fig. 4·9 shows the dose distributions for CTV_T_LR (green line contour) and bladder (yellow line contour) for the planned accumulated dose on the plan CT (left) and deformed delivered accumulated dose (right). The dose distributions of these two accumulated doses were qualitatively inspected and visually compared slide by slide. As can be seen in this figure, 45 Gy isodose distributions were slightly different between the delivered accumulated dose and the planned accumulated dose at the end of treatment, while the other isodoses distributions were quite similar.

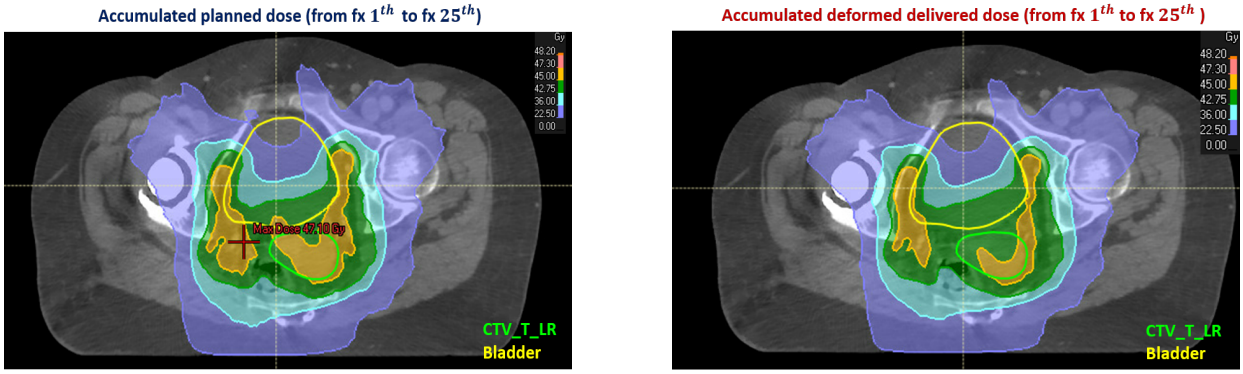

Figure 4·9: The accumulated dose distribution for CTV_T_LR (green line contour) and bladder (yellow line contour) for the planned accumulated dose (left) and deformed delivered accumulated dose (accumulated delivered dose by DIR-based process)(right) on plan CT (from fx 1 to fx 25). Images for patient 10 from RayStation TPS.

4.3.2 Visual Inspection using DVHs

Figure Fig. 4·10 shows the DVHs for the CTV_T_LR and the bladder of patient 10. The DVHs for planned accumulated dose (dotted lines) and for delivered accumulated dose (solid lines) were compared. It can be seen there was very little difference in DVH curves for both CTV_T_LR and bladder, i.e., accumulated planned dose was very similar with delivered accumulated dose.

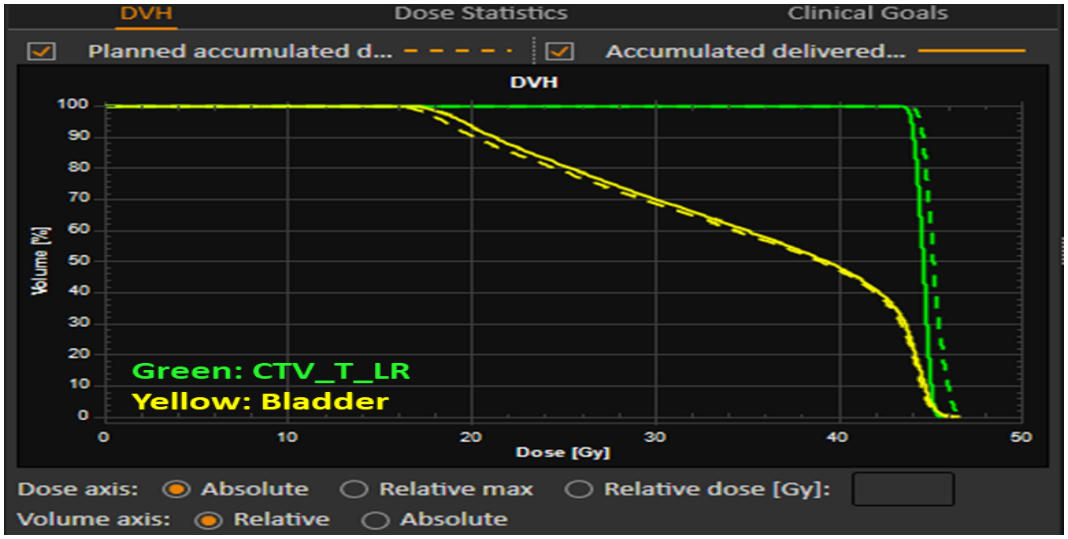

Figure 4·10: Dose-volume histogram (DVH) shows the comparison between accumulated planned dose and accumulated delivered dose by DIR-based method. The DVH was generated in RayStation TPS.

4.3.3 Dose Tracking Using Dosimetric Metrics: D98, D50, Dmean, and D2

The dose metrics: Near minimum dose (D98) received by CTV_T_LR, Dmedian (D50), and near maximum dose (D2) received by bladder were computed and presented in dose tracking results. The figures were shown in this part as the results for all studied patients in the same graphs. The results for each patient and Dmean to bladder were referred to the Appendix Section. A.2.

The accumulated delivered dose variation from the initial plan was tracked. It was noted that the accumulated delivered doses were calculated by two methods. The dose tracking results in two methods were compared.

Fig. 4·11 illustrates dose tracking results for the near minimum dose (D98) received by CTV_T_LR from both methods. For all patients, the accumulated delivered doses were slightly changed from the initial plan during the course of treatment. Table 4.2 shows the accumulated delivered doses for all the patients and the results indicated a lightly decreased compared to the initial plan at the end of treatment, except for patient 17, the results showed slightly increased. The dose differences ranged from 0.29 Gy to 2.05 Gy lower (in the DIR-based method) and from 0.35 Gy to 1.37 Gy lower than initial plan (in the simple DVH parameter addition-based method). Except for patient 17, the dose tracking results in both methods showed accumulated delivered dose increased from initial plan, with 0.87 Gy higher at the end of treatment for DIR-method. In the simple DVH parameter addition-based method, the accumulated dose values showed: from fx 1 to fx 10 increased linearly from 0.02 Gy to 0.27 Gy; from fx 11 to 15 decreased linearly from 0.08 Gy; from fx 16 to 25 increased linearly from 0.02 Gy to 0.37 Gy.

For all patients, as observed in Fig. 4·11A and Fig. 4·11B, the results of the dose tracking in these two methods were similar during the course of treatment. As reported in Table 4.2, at the end of treatment, the accumulated delivered doses calculated by the DIR-based method were closed to the accumulated delivered doses calculated by the simple DVH parameter addition-based method.

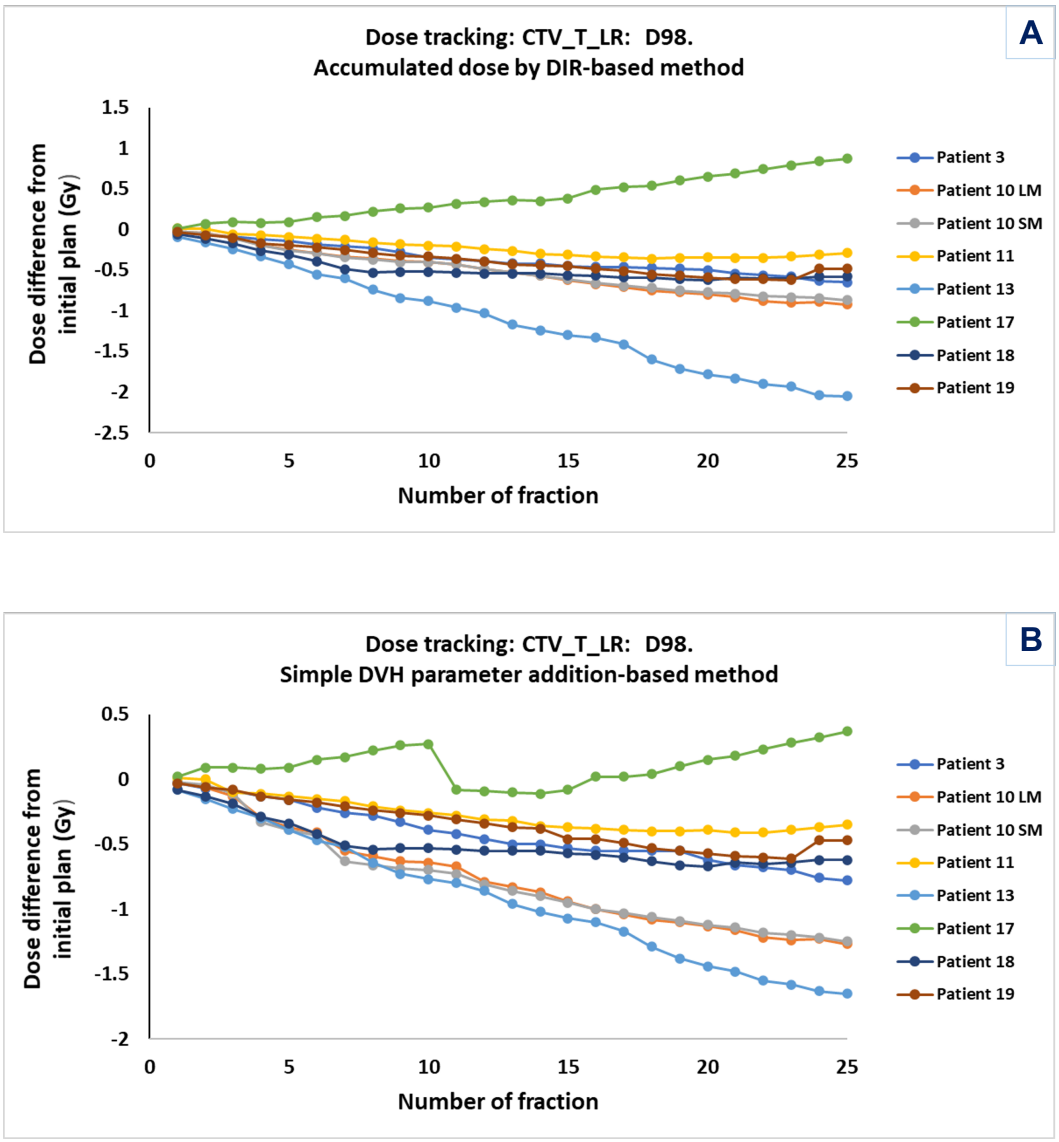

Figure 4·11: Dose tracking: D98 received by CTV_T_LR: comparison between accumulated planned dose and accumulated delivered dose during treatment in two methods: **A.** Accumulated delivered dose by DIR-based method and **B.** Accumulated delivered dose by simple DVH addition-based method. *Dose difference from initial plan = accumulated delivered dose – accumulated planned dose.* The minus sign indicates the accumulated delivered dose is lower than the initial plan.

Table 4.2: Dose volume histogram (DVH) parameters for CTV_T_LR: D98. *Dose difference between two method = dose difference by simple DVH parameter based method - by DIR based method.*

CTV_T_LR D98	**Patient**	**Accumulated planned dose (Gy)**	**Accumulated delivered dose by DIR (Gy)**	**Accumulated delivered dose by simple DVH parameter addition (Gy)**
	3	44.5	43.85	43.72
	10	44.5	43.58	43.23
	11	44.5	44.21	44.15
	13	44.5	42.45	42.85
	17	44.5	45.37	44.87
	18	44.5	43.92	43.88
	19	44.5	44.02	44.03
Dose differences (Gy)	**Patient**	**By DIR from initial plan**	**By simple DVH parameter addition from initial plan**	**Between two methods**
	3	-0.65	-0.78	-0.13
	10	-0.92	-1.27	-0.35
	11	-0.29	-0.35	-0.06
	13	-2.05	-1.65	0.4
	17	0.87	0.37	-0.5
	18	-0.58	-0.62	-0.04
	19	-0.48	-0.47	0.01
p-values (Wilcoxon signed-rank test)		**p = 0.0099**	**p = 0.0099**	**p = 0.7984**

Concerning the accumulated delivered dose to the OAR, the figure Fig. 4·12 illustrates the dose tracking for near-maximum (D2) received by bladder. For all patients, the accumulated delivered doses were lightly altered from the initial plan during the course of treatment. D2 values can be observed in Table 4.3. For some patients, the accumulated delivered dose were lower than the initial plans (ranged from no change to about 1 Gy) in both methods. While in the others, the accumulated delivered dose showed increasing compared to the initial plan (ranged from 0.1 Gy to 1.23 Gy) at the end of treatment.

For all patients, as observed in Fig. 4·12A and Fig. 4·12B, the the dose tracking results in two methods were similar during the course of treatment. As reported in Table 4.3, at the end of treatment, the accumulated delivered dose calculated by the DIR-based method was insignificantly different from the accumulated delivered dose calculated by the simple DVH parameter addition-based method.

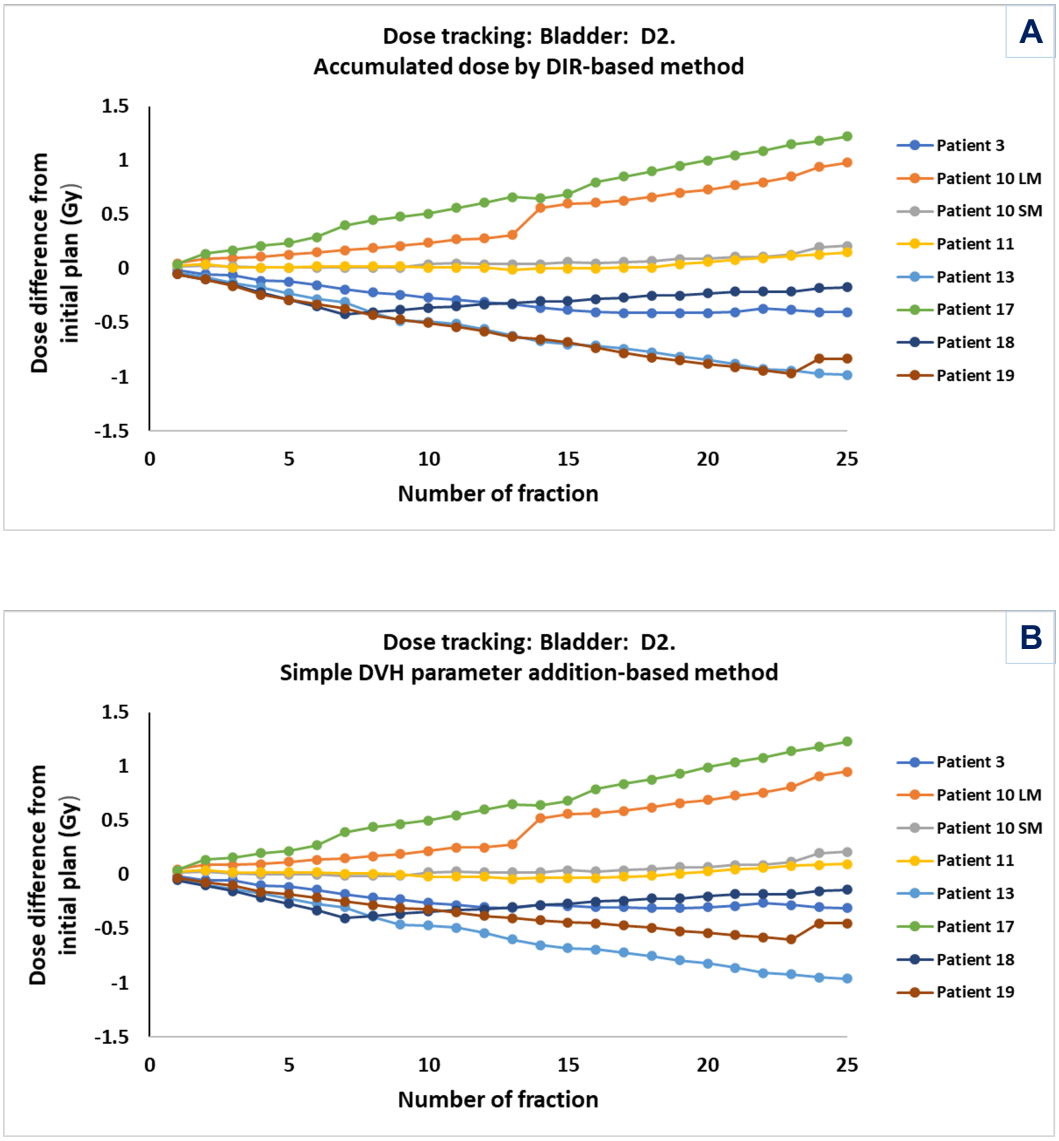

Figure 4·12: Dose tracking: D2 received by bladder: comparison between accumulated planned dose and accumulated delivered dose during treatment in two methods: **A.** Accumulated delivered dose by DIR-based method and **B.** Accumulated delivered dose by simple DVH addition-based method. *Dose difference from initial plan = accumulated delivered dose – accumulated planned dose.* The minus sign indicates the accumulated delivered dose is lower than the initial plan.

Table 4.3: Dose volume histogram (DVH) parameters for Bladder: D2. *Dose difference between two method = dose difference by simple DVH parameter based method - by DIR based method.*

Bladder: D2	**Patient**	**Accumulated planned dose (Gy)**	**Accumulated delivered dose by DIR (Gy)**	**Accumulated delivered dose by simple DVH parameter addition (Gy)**
	3	45.25	44.85	44.94
	10	45.75	46.73	46.7
	11	45.75	45.9	45.85
	13	45.75	44.77	44.79
	17	46	47.22	47.23
	18	45.75	45.58	45.61
	19	45.75	44.92	45.3
Dose differences (Gy)	**Patient**	**By DIR from initial plan**	**By simple DVH parameter addition from initial plan**	**Between two methods**
	3	-0.4	-0.31	0.09
	10	0.98	0.95	-0.03
	11	0.15	0.1	-0.05
	13	-0.98	-0.96	0.02
	17	1.22	1.23	0.01
	18	-0.17	-0.14	0.03
	19	-0.83	-0.45	0.38
p-values (Wilcoxon signed-rank test		**p = 0.6312**	**p = 0.7897**	**p = 0.8335**

With regard to D50 received by bladder, Fig. 4·13 shows the dose tracking for median dose (D50) received by bladder. The accumulated delivered doses were slightly varied from the initial plan during the course of treatment. As demonstrated in Table 4.4, the accumulated delivered dose results showed no change for some patients, whereas some others showed decreased ranged from (0.88 Gy to 3 Gy), and others showed increased (ranged from 0.24 to 0.85 Gy) compared to initial plan at the end of treatment.

For all patients, as observed in Fig. 4·13A and Fig. 4·13B, the the dose tracking results in these two methods were similar during the course of treatment. As reported in Table 4.4, at

the end of treatment, compared to the initial doses, for some patients, the dose differences by the simple DVH parameter addition-based method were lower than by the DIR-based method (ranged from 0.45 to 0.95 Gy lower), while for other patients, they were higher (ranged from 0.12 to 1.25 Gy higher). No difference between two methods was showed for patient 3.

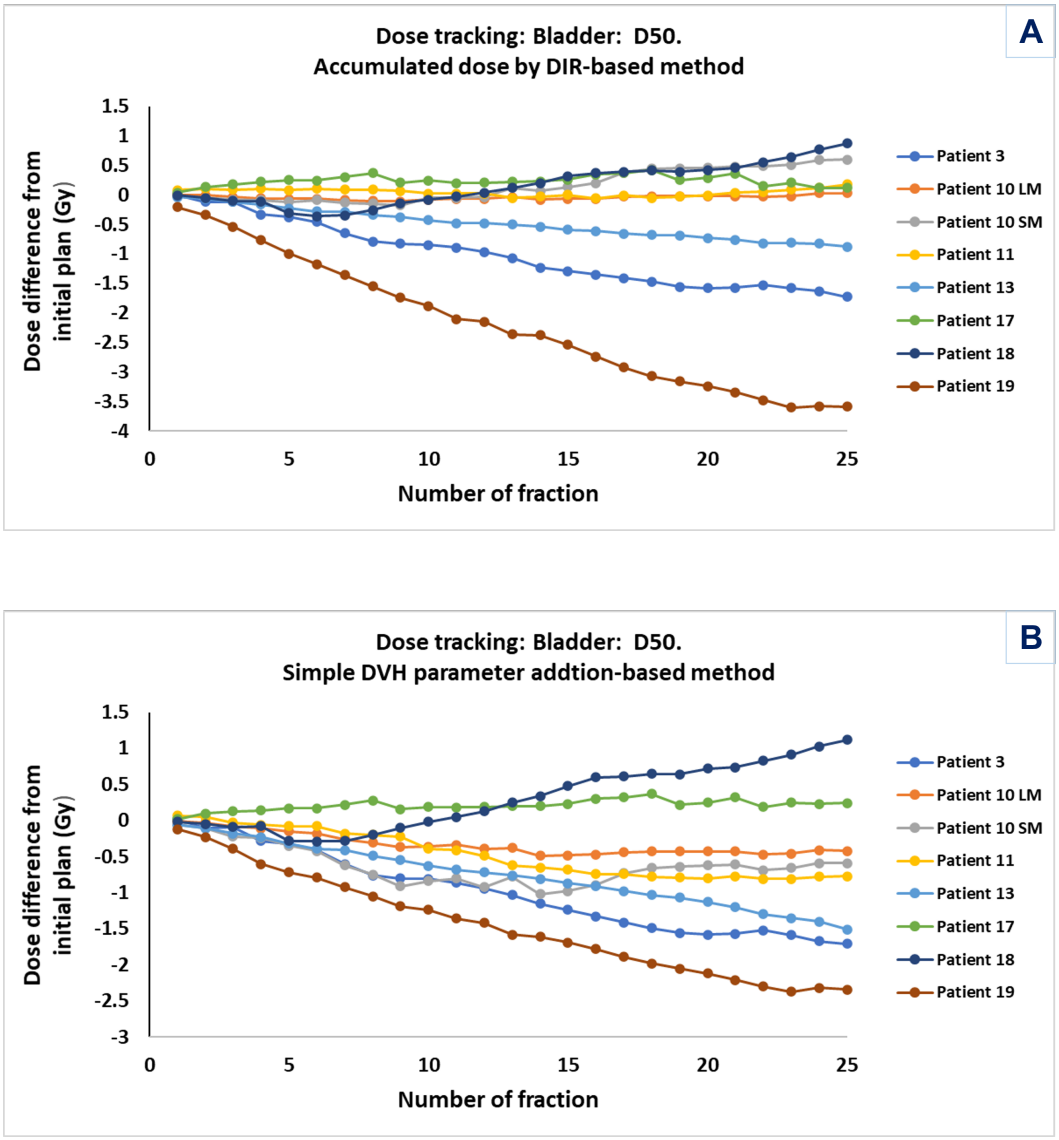

Figure 4·13: Dose tracking: D50 received by bladder: comparison between accumulated planned dose and accumulated delivered dose during treatment in two methods: **A.** Accumulated delivered dose by DIR-based method and **B.** Accumulated delivered dose by simple DVH addition-based method. *Dose difference from initial plan = accumulated delivered dose – accumulated planned dose.* The minus sign indicates the accumulated delivered dose is lower than the initial plan.

Table 4.4: Dose volume histogram (DVH) parameters for Bladder: D50. *Dose difference between two method = dose difference by simple DVH parameter based method - by DIR based method.*

Bladder: D50	**Patient**	**Accumulated planned dose (Gy)**	**Accumulated delivered dose by DIR (Gy)**	**Accumulated delivered dose by simple DVH parameter addition (Gy)**
	3	43.25	41.52	41.54
	10	42.5	42.53	42.08
	11	43.5	43.68	42.73
	13	43.75	42.87	42.24
	17	44.5	44.62	44.74
	18	41	41.87	42.12
	19	44.5	40.91	42.16
Dose differences (Gy)	**Patient**	**By DIR from initial plan**	**By simple DVH parameter addition from initial plan**	**Between two methods**
	3	-1.73	-1.71	0.02
	10	0.03	-0.42	-0.45
	11	0.18	-0.77	-0.95
	13	-0.88	-1.51	-0.63
	17	0.12	0.24	0.12
	18	0.87	1.12	0.25
	19	-3.59	-2.34	1.25
p-values (Wilcoxon signed-rank test)		**p = 0.4945**	**p = 0.2698**	**p = 0.9999**

As regards to dosimetric metrics D98 received by CTV_T_LR, Dmean, D50, and D2 received by bladder, the results of the Wilcoxon signed-rank tests for studied patients were showed in Table 4.2, Table 4.3, and Table 4.4. As can be observed, the p-values indicated no significant difference between accumulated delivered dose and planned dose. In addition, there was no significant difference between accumulated delivered dose calculated by DIR-method and accumulated delivered dose calculated by the simple DVH parameter addition-based method.

4.4 Comparison of Dose Tracking for Large Margin and Small Margin Plans

4.4.1 Comparison of Dose Distributions in Planning CTs for Large Margin and Small Margin Plans

Fig. 4·14 and Fig. 4·15 illustrate dose distributions displayed on a transversal slice and a sagittal slice in the large margin and small plans on the planning CTs. The dose distributions were illustrated very similar in both plans.

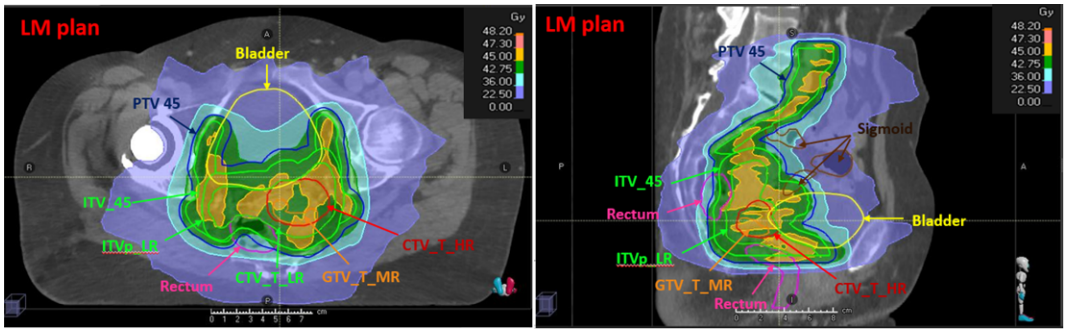

Figure 4·14: Dose distribution in large margin plan on the planning CT image for patient 10. LM = Large Margin. On the left: In transversal plane; On the right: In sagittal plane. Images taken from RayStation TPS.

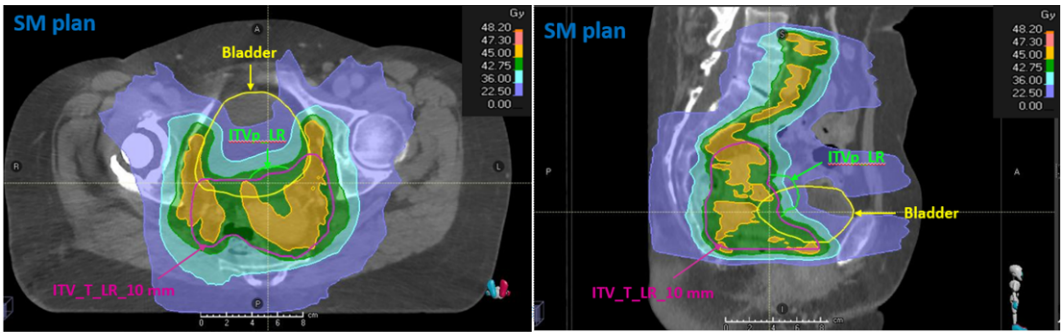

Figure 4·15: Dose distribution in small margin plan on the planning CT for patient 10. SM = Small Margin. On the left: In transversal plane; On the right: In sagittal plane. Images taken from RayStation TPS.

4.4.2 Comparison of Dose Tracking Using Dosimetric Metrics: D98, D50, and D2 in Large Margin and Small Margin Plans

Fig. 4·16 illustrates the dose tracking results regarding near minimum dose (D98) received by CTV_T_LR during the course of treatment for both LM and SM plans.

Fig. 4·16.A reveals the accumulated delivered doses over the fractions that were calculated by DIR-based method. LM and SM plans revealed very similar results. The accumulated delivered doses were slightly decreased during the course of treatment. At the end of treatment, it was reported 0.92 Gy lower (in LM plan) and 0.87 Gy lower (in SM plan) than the initial planned doses, as shown in Table 4.5.

Fig. 4·16.B shows the accumulated delivered doses over the fractions that were calculated by simple DVH addition-based method. The dose tracking results in LM and SM plans also illustrated very similar results during the course of treatment. At the end of treatment, it was revealed 1.27 Gy lower (in LM plan) and 1.25 Gy lower (in SM plan), compared to the the initial plan dose, as reported in Table 4.5.

In both plans, the accumulated delivered dose differences from initial plan calculated by DIR-based method was very similar to by simple DVH parameters addition-based method, by 0.35 and 0.38 Gy, respectively, as reported in Table 4.5.

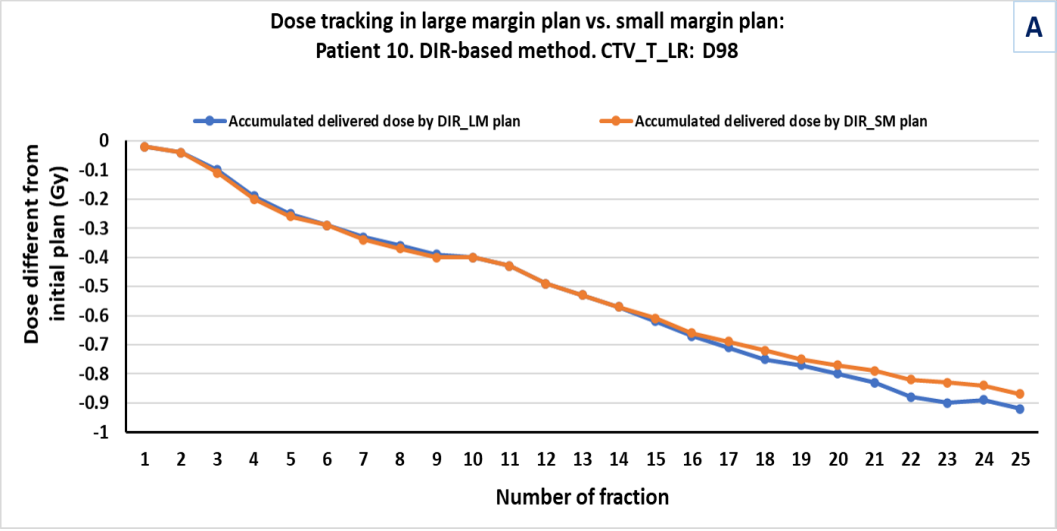

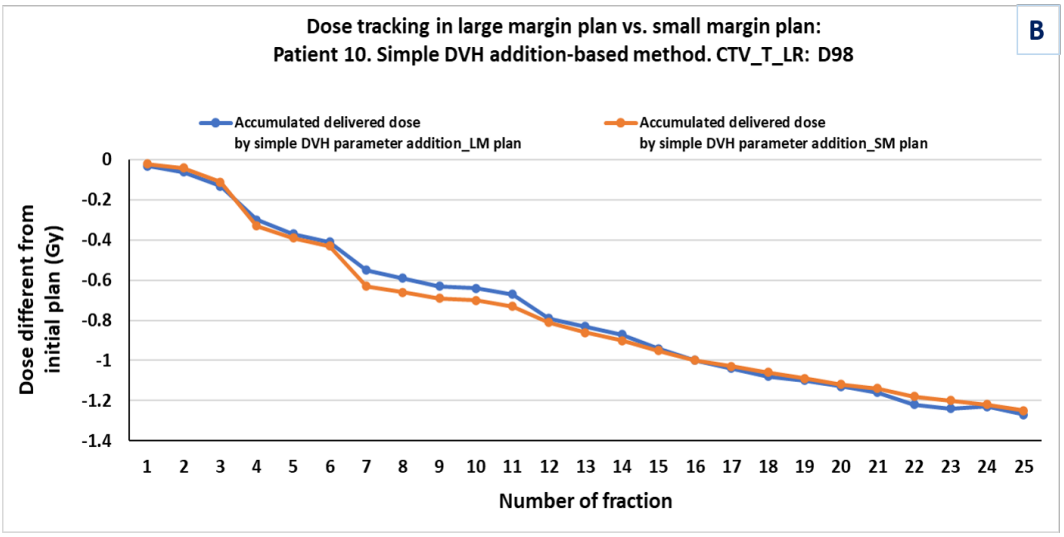

Figure 4·16: Dose tracking patient 10: CTV_T_LR:D98: comparison between large margin and small margin plans. A. Accumulated delivered dose calculated in DIR-based method, and B. Accumulated delivered dose calculated in simple DVH parameter addition-based method. LM = Large Margin. SM = Small Margin

Table 4.5: Dose volume histogram (DVH) parameters for CTV_T_LR: D98. LM = Large margin plan; SM = Small margin plan. *Dose difference between two method = dose difference by simple DVH parameter based method - by DIR based method.*

CTV_T_LR D98	**Patient**	**Accumulated planned dose (Gy)**	**Accumulated delivered dose by DIR (Gy)**	**Accumulated delivered dose by simple DVH parameter addition (Gy)**
	10 (LM)	44.5	43.58	43.23
	10 (SM)	44.25	43.38	43
Dose differences (Gy)	**Patient**	**By DIR from initial plan**	**By simple DVH parameter addition from initial plan**	**Between two methods**
	10 (LM)	-0.92	-1.27	-0.35
	10 (SM)	-0.87	-1.25	-0.38

Fig. 4·17 shows the dose tracking results as for near maximum dose (D2) received by bladder during the course of treatment for both LM and SM plans.

Fig. 4·17.A shows the accumulated delivered doses over the fractions that were calculated by DIR-based method. For both plans, the accumulated delivered doses were lightly increased during the course of treatment. At the end of treatment, it was reported 0.98 Gy higher (in LM plan) and 0.21 Gy (in SM plan) than the initial planned doses, as outlined in Table 4.6.

Fig. 4·17.B illustrates the accumulated delivered doses over the fractions that were calculated by simple DVH addition-based method. The dose tracking results showed very similar results as in DIR-based method, as shown in Table 4.6.

The accumulated delivered dose differences from initial plan calculated by DIR-based method was the same as by simple DVH parameters addition-based method, as reported in Table 4.6.

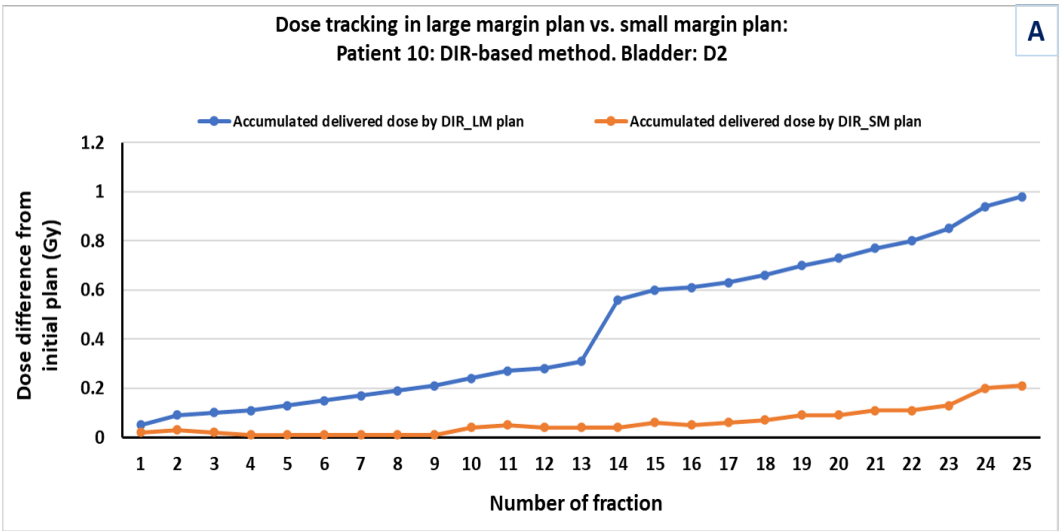

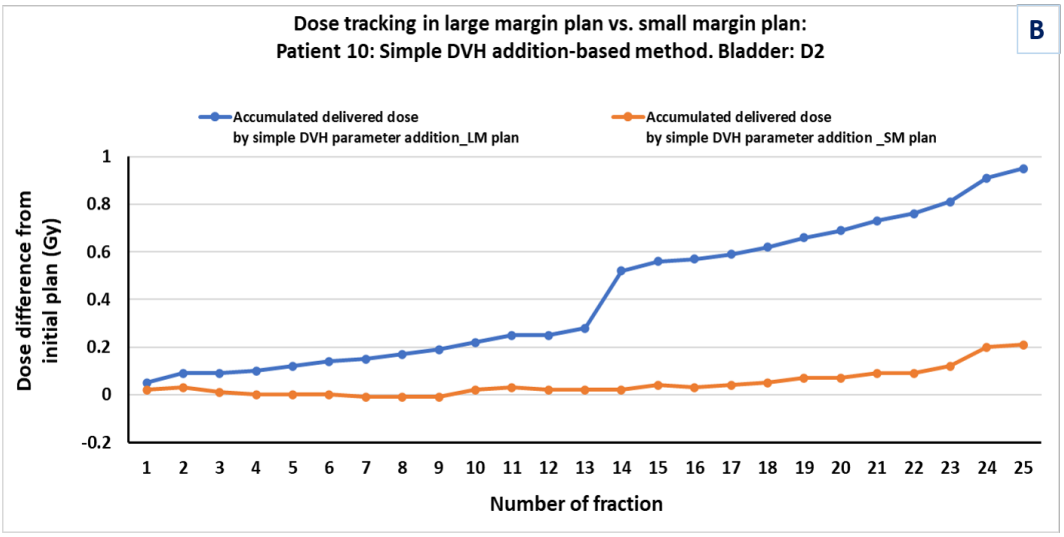

Figure 4·17: Dose tracking patient 10: Bladder: D2: comparison between large margin and small margin plans. A. Accumulated delivered dose calculated in DIR-based method, and B. Accumulated delivered dose calculated in simple DVH parameter addition-based method. LM = Large Margin. SM = Small Margin

Table 4.6: Dose volume histogram (DVH) parameters for Bladder: D2. LM = Large margin plan; SM = Small margin plan. *Dose difference between two method = dose difference by simple DVH parameter based method - by DIR based method.*

Bladder: D2	**Patient**	**Accumulated planned dose (Gy)**	**Accumulated delivered dose by DIR (Gy)**	**Accumulated delivered dose by simple DVH parameter addition (Gy)**
	10 (LM)	45.75	46.73	46.7
	10 (SM)	45.25	45.46	45.46
Dose differences (Gy)	**Patient**	**By DIR from initial plan**	**By simple DVH parameter addition from initial plan**	**Between two methods**
	10 (LM)	0.98	0.95	-0.03
	10 (SM)	0.21	0.21	0

Fig. 4·18 shows the dose tracking results as regards the D50 received by bladder during the course of treatment for both LM and SM plans.

Fig. 4·18.A illustrates the accumulated delivered doses over the fractions that were calculated by DIR-based method. In the LM plan, the accumulated delivered doses were not differentiated from the initial plan over fractions during the course of treatment. In the SM plan, the accumulated delivered doses revealed slightly decreased from fraction 1 to fraction 9, then increased from fraction 10 to fraction 25. At the end of treatment, it was 0.6 Gy higher, as reported in Table 4.7.

Fig. 4·18.B shows the accumulated delivered doses over the fractions that were calculated by simple DVH parameter addition-based method. For LM plan, the accumulated delivered doses were slightly decreased over the fractions during the course of treatment. While for SM plan, the accumulated delivered doses were lightly deceased from fraction 1 to fraction 14, about 1 Gy lower (after 14 fractions compared to the initial plan), then, increased very little from fraction 14 to fraction 25. At the end of treatment, it was reported 0.42 Gy lower (in LM plan) and 0.59 Gy lower (in SM plan) than the initial plan, as shown in Table 4.7.

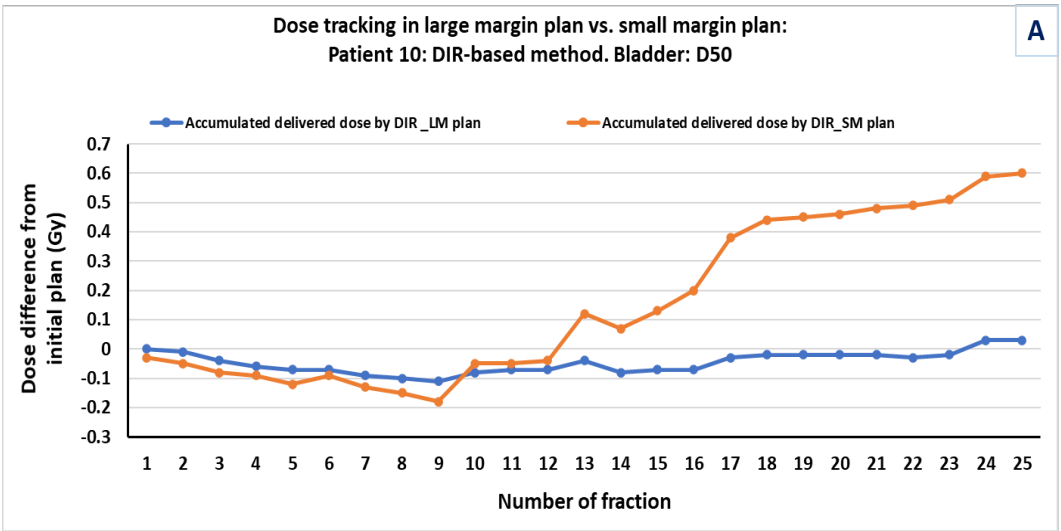

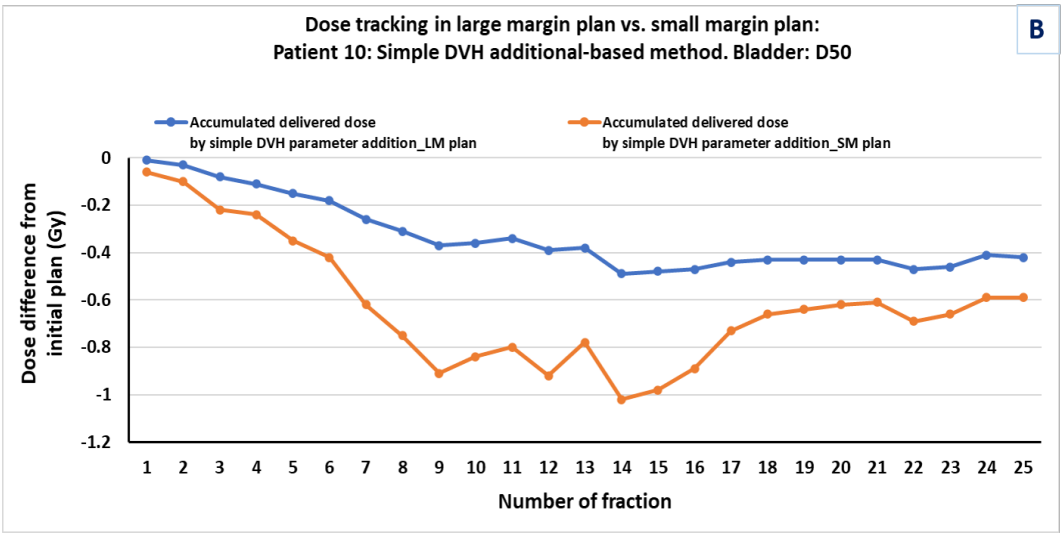

Figure 4·18: Dose tracking patient 10: Badder: D50: comparison between large margin and small margin plans. A. Accumulated delivered dose calculated in DIR-based method, and B. Accumulated delivered dose calculated in simple DVH parameter addition-based method. LM = Large Margin. SM = Small Margin

Table 4.7: Dose volume histogram (DVH) parameters for Bladder: D50. LM = Large margin plan; SM = Small margin plan. *Dose difference between two method = dose difference by simple DVH parameter based method - by DIR based method.*

Bladder: D50	**Patient**	**Accumulated planned dose (Gy)**	**Accumulated delivered dose by DIR (Gy)**	**Accumulated delivered dose by simple DVH parameter addition (Gy)**
	10 (LM)	42.5	42.53	42.08
	10 (SM)	39	39.6	38.41
Dose differences (Gy)	**Patient**	**By DIR from initial plan**	**By simple DVH parameter addition from initial plan**	**Between two methods**
	10 (LM)	0.03	-0.42	-0.45
	10 (SM)	0.6	-0.59	-1.19

Chapter 5

Discussions

Among 8 studied patients, one patient was excluded due to many bad quality of daily CBCT images, i.e., too much image scattering, it was impossible to delineations of either CTV_T_LR or bladder.

5.1 Bladder Inter-fractional Volume Variations on Daily CBCTs

In cervical cancer radiation therapy, precisely accounting for daily uncertainties in the target position is an important goal. The sources of uncertainties may arise from set-up variations, inter- and intra-fractional motion, with inter-fractional motion usually being the largest contribution [56]. The volume variations in adjacent anatomical structures of the cervix such as bladder may lead the movement of the target volume and/or normal organ within the pelvis. Consequently, it impacts on the accuracy of the irradiation plan [51].

For cervical cancer radiotherapy, patients are commonly treated with comfortably full bladder with a rationale for better OARs sparing. This is usually achieved by asking the patient to follow a specific procedure prior to CT simulation and each fraction, a so called drinking protocol. However, bladder volume variation is unpredictable. This may be due to the patient's poor compliance, naturally anatomical alterations during radiotherapy or toxicity [81]. Therefore, it has become customary to measure the patient's bladder volume using volumetric imaging modality (such as CBCT imaging) prior to daily radiation therapy for cervical cancer treatment. In this study, despite the patients followed the drinking protocol regrading the significance and method of pretreatment fluid intake, the bladder volume quantified by CBCT images during the 25 fractions of treatment varied from 53 to 213 ml. Some patients showed larger variations

than the others. It was found that population mean bladder volume at planning of 164 ± 79 ml (1SD) reduced to 108 ± 70 ml (1SD) in 5 weeks. Regarding to the individual patient, there was insignificant correlation between bladder volumes and the time of treatment, as referred to regression statistics result in the Appendix Subsection. A.3.3. However, the population mean bladder volumes showed slight, but significant declining trend during treatment (25 fraction, $p < 0,05$). This result is in line with the previous studies. Ahmad et al. [57] showed that the population mean bladder volume at planning CT of 378 ± 209 ml (1SD) reduced to 109 ± 88 ml (1SD) in 6 weeks, while Luo et al. [20] reported that bladder volume at the end of treatment were reduced by 63.5%. Huang et al. [71] noted a 44% variation in bladder volume during the course of fractionated pelvic radiotherapy, and noted high doses being delivered than initially planning doses. Xin Wang et al. [78] found that the mean volume of bladder was 156 with large range $(1.7 - 626.5)$ ml. In those studies, the studied patients were also followed the drinking protocols.

Although this study did not investigate correlations between bladder volume inter-fractional changes and the target and organ movements, the inter-fractional changes in bladder volume during the course of treatment has been found in agreement with other studies (as been discussed above). Previous studies have demonstrated the variable bladder filling effects on the target and organ shapes and motions [14, 56, 60, 64]. Huh et al. [64] compared the magnetic resonance images taken before and during pelvic radiotherapy and noted a significant change in the uterine movement and position due to variable bladder filling. Chan et al. [56] reported that for every 10-ml decline in the bladder volume, the uterine canal moved 8 mm inferiorly, the uterine fundus 18 mm inferiorly, and the cervical 3 mm anteriorly. Jadon et al. [60] reviewed the literature regarding variable organ motions and concluded that a compromise on uterine coverage was noted with variable bladder volumes. Soumya et al. [14] claimed that variable bladder filling led to a considerable displacement of utero-cervical central of mass in the anterior-posterior (z-axis) and superior-inferior (y-axis) without compromising the target volume coverage. Published literature shows the dosimetric impacts of bladder inter-fractional volume changes have been investigated [14, 32, 38]. Lim et al. [32] explored the impact of internal anatomic changes on the dose delivered to the tumour and OARs and concluded that planned dose was not the same as simulated delivered dose, but when taken as a group, this was not statistically significant. Ye et al. [38] reported that the full bladder filling could protect bowel in cervical cancer treatment with IMRT plans. Soumya et al. [14] concluded that bladder

filling variations have an impact on cervico-uterine motion/shape, thereby impacting the dose to the target and OARs. It was recommended to have threshold bladder volume of at least $70 - 75\%$ of optimally filled bladder during daily treatment.

5.2 Evaluation of DIR Accuracy

Recently, DIR has been investigated for quantification of target and OARs motion, dose accumulation in deforming geometry, and multi-modality image fusion during the course of radiation therapy [18, 28, 43].

In this study, DIR was integrated in the dose accumulation process for deforming dose. The plan CT and daily CBCTs were referred to two image sets to be performed deformable image registration (DIR). Daily CBCT was the moving/target dataset (e.g., the dataset that was being transformed and deformed to match the plan CT), while plan CT was the stationary/reference dataset (e.g., the dataset that daily CBCT image was being registered to) [30]. The hybrid DIR algorithm (ANACONDA) was used in RayStation TPS has been reported by Weistrand and Svensson [92] and the quality of the DIR results were evaluated according to the recommendations in the report from American Association of Physicists in Medicine (AAPM) task group TG132 [30]. The algorithms in the RayStation TPS mapped the ROI geometry in the reference image (plan CT) and the corresponding deformed ROI geometry in the target image by the function overlap. The Dice Similarity Coefficient (DSC) method was used for quantitative evaluation of DIR. According to the recommendation of AAPM TG132 [30], the DSC tolerance should be from 0.8 to 0.9 in order to be qualified for deforming dose in the dose accumulation process. As can be seen in the results Table. 4.1, the mean DSCs value for both CTV_T_LR and bladder for all 7 patients were higher than 0.9. Therefore they were considered to be good enough for deforming dose. Nevertheless, in the Fig. 4·7 and the Fig. 4·8 show some DSCs outliers values. It might due to bad quality of CBCT images, resulting in inaccurate delineations of controlling ROIs, and therefore bad DIRs. These fractions were excluded from dose accumulation. It has been also claimed that, DSC calculations are dependent on the volume of the structure, and therefore very large or very small structures may have different expected DSC values[30]. In this study, even thought the bladder volumes changed during the course of treatment (as discussed in the previous section), the DSCs for bladder showed

reasonable results (mean DSCs > 0.9). It should be noted that the CTV_T_LR volumes during the treatment were not quantified in this project.

The hybrid DIR algorithm in corporation with controlling ROIs (CTV_T_LR and bladder delineated on plan CT and daily CBCTs in this study) and in some case additional controlling POIs (fundus points were choosen) showed the ability to increase the DSCs, as shown in the Fig. 4·4 and the Fig. 4·5. The contours of the CTV_T_LR and bladder were used as region-of-interest (ROIs) to guide image deformation in the hybrid DIR and to evaluate DIR. They aimed at deforming the selected structure in the target image to the corresponding structures in the reference image [52]. Thus, users should delineate the ROIs carefully because they were used as controlling ROIs applied to DIR algorithm. The DIR accuracy was affected directly by the accuracy of the contouring. The inter-inspector in this study is an experient medical physicist who gave good supervision on the qualitative validation of DIR. In a previous study, Motegi et al. [33] evaluated hybrid DIR algorithm in RayStation and MIM Maestro, demonstrated the use of ROIs to guide image deformation had possibility to reduce unrealistic image deformation. The mean DSC at the centroid of the ROIs were 0.9. In another study, Kim et al. [24] investigated a hybrid DIR algorithm based on the intensity-based DIR algorithm combined with the feature-based technique and reported that high DSCs for bladder (0.9).

DIR method is crucial in the dose accumulation process. The dosimetric impact of using DIR methods on dose accumulation will be discussed later in the dose tracking section, section 5.3. Noisy CT images, poor quality of CBCT images, as well as bad soft-tissue contrasts on CBCT images are obstacle to DIR algorithms. Errors and uncertainties in DIR process translate to the mapped/deform and accumulated dose distributions. For the clinical use, for example integration of DIR in the dose accumulation process, the limitation of the hybrid DIR should be taken into account. Zhong et al. [21] reported that DIR using the CBCT for the prostate region has poor accuracy because of unfavourable conditions such as noise, poor low-contrast resolution, and abdominal motion artifacts. RayStation implemented shape-based grid regularization in the optimization problem for the anatomically reasonable deformation [92]. Therefore, the hybrid DIR algorithm in RayStation could be robust for image pairs with poor quality caused by noise and artifacts [92].

In cervical cancer radiotherapy, target and organ motion and deformation in pelvis are unpre-

dictable. To evaluate the irradiated dose for target and OARs accurately, dose accumulation between different treatment fraction is required. Application of DIR in dose deform and dose accumulation is essential. However, the limitation of validation methods for DIR is remaining challenge for transferring of DIR into clinical routines. Future work for an accurate and efficient patient-specific validation should be defined, and appropriate metrics should be carried out for both geometric and dosimetric DIR accuracy, as discussed by C. Paganelli et al. [90]. The AAPM TG132 [30] recommended three methods to assess the registration results: physical phantom system end-to-end tests, digital phantom tests, and clinical data tests. A comprehensive commissioning process should include all three components.

5.3 Dose Tracking

5.3.1 Impact of Computed Fraction Dose Based on Daily CBCT on Dose Accumulation

The daily fraction dose was computed based on daily CBCT image, then this was deformed to the planning CT for dose accumulation by the used of the deformable vector field found during the DIR process. Therefore, the uncertainties in calculation of daily dose would impact on the results of the delivered dose accumulation. In this study, tissue specific HU-to-density curves generation technique was used in the RayStation TPS to calibrate the CBCT's HU table. This approach might provide accurate dose calculation based on CBCT image as demonstrations in the previous studies [9, 22]. However, the manual procedure for creating density table offered by the RayStation TPS can be subjective and user dependent for the choice of each tissue grey level ranges for different tissues. In addition, the manual contouring of CTV_T_LR and bladder structures on daily CBCT images might affect on the accuracy of the dose calculation.

The field-of-view (FOV) for CBCT was inevitably smaller than that of plan CT. The RayStation TPS provide a function for creating external ROI on the limited FOV. It should be noted that validation of the accuracy of the CBCT-based dose calculation was out of the scope of this project. Nevertheless, it has been investigated in various studies and less than 3% difference was found when comparing the CBCT-based with the CT-based dose calculation [73, 82].

5.3.2 Impact of DIR Accuracy on Deformable Dose Accumulation

DIR is essential for the recently development in radiation therapy. In this study, DIR was integrated in the dose accumulation process as can be seen in the work-flow in the Subsection 3.6.2. This method gives possibility of quantifying the actual distribution of radiation dose absorbed from each fraction (on daily CBCT image) and mapping the dose back to a common reference image (planning CT image). Then, the deformed dose from each fraction is accumulated for evaluating the total dose distribution. This method facilitates the dose tracking process, i.e., comparing the actually accumulated delivered dose to the accumulated planned dose. The dose accumulation by DIR-based technique has been investigated in many scientific researches [18, 31, 54, 76, 77, 70, 84]. The deformation vector fields (DVFs) exported in DIR between planning CT (pCT) and daily CBCT represent the shift value and direction for a particular voxel to match a corresponding voxel. Therefore, the accumulated delivered dose by DIR-based method is influences by the accuracy of DIR. The effect of DVF uncertainties on dose mapping is complex and depends on several factors, such as the spatial locations of both DVF errors and the dose gradient, deformable algorithm, the image content, the presence of homogeneous regions, and tissue changes [90, 92].

The assessment of the DIR accuracy was discussed in details in the Section 5.2. There has been no definite consensus about the clinically meaningful DSC value. Although the DIR-based dose accumulation is sensitive to DIR, a DSC of ~ 0.8 is acceptable for integrating in dose accumulation, according to AAPM TG132 [30]. In this study, the mean DSCs for CTV and bladder for all patients were greater than 0.9. Total of 10 DIRs were excluded from dose accumulation due to bad DIR quality. It was highlighted in other studies that the regions of poor image contrast were more prone to larger variability in mapped dose [75, 92]. As discussed by Schultheiss and Tome et al. [72], the factors such as image distortion, noise and artifacts, large target and organ motion effects the accuracy of deformable dose accumulation. The influence of the accuracy of DIR methods on the estimation of dose accumulation on both target and the organ dose was demonstrated by Nopnop et al. [76]. A method of sampling image registration errors and their impact on the mapped dose was developed by Morphy et al.[40]. Still, the opinion of deforming dose by DIR-based method and the different methods for validation of DIR accuracy lead to ongoing researches [90].

5.3.3 Dose Tracking: Accumulated Delivered Dose calculated by Two Methods: by DIR-based and by Simple DVH Parameter Addition-based method

Dose tracking was performed for monitoring the actual accumulated dose during the treatment and the accumulated delivered dose was compared to accumulated planned dose. Significantly differences might indicate that either the patient was not properly positioned before treatment or that the anatomy has changed during the treatment. Chritensen et al. [19] published one of the first researches of dose accumulation using DIR. It was reported that the deformation modelling of the accumulated dose distribution to the organs was achievable. Traditionally, according to GEC ESTRO recommendation, accumulated delivered dose is calculated by simple DVH parameter addition-based method [61]. It was underlying assumption that the ROI is identical and high-dose region located in the same part of the organ in each fraction. However, organ motion, the changes in target volumes and changes in shape and volume for OARs are challenges for this accumulated dose method. The simple summation of dose in the direct DVH parameter addition will overestimate the dose if the high-dose region moves to a new location [3]. To approach this problem, local anatomical variations between fractions must be accounted for by mapping the fraction doses to a common coordinate system before accumulation. It is thought that DIR could be used to perform this task. However, the dose tracking results showed no statistical difference compared to the simple DVH parameter addition-based method. The accumulated delivered CTV_T_LR D98 were lower than the accumulated planned dose, for six out of seven studied patients at the end of the treatment for both methods. Among those, patient 13 showed the highest dose deviation with around 2 Gy lower dose compared to the planned dose for both methods. In contrast, patient 17 was shown higher accumulated delivered dose, compared to the initial plan (as seen in the Table 4.2). Bladder 50 and D2 showed small variations among the patients, some patients received higher, others received lower accumulated delivered dose at the end of treatment (as shown in the Table 4.3, and Table 4.4). However, the dose variations for both CTV_T_LR and bladder from initial plan were clinical acceptance. The non- clinically significant differences observed may be explained by the use of a full bladder protocol and a generous margin plan which means that movement of the target and OAR is already taken into account. Still, some small dose differences could be derived from uncertainties in the fraction dose computed on CBCTs (as considered in the Subsection 5.3.1) and dose deformation (as discussed in the Subsection 5.3.2). For cervical cancer treatment, some other previous researches claimed the use of DIR to accumulate the EBRT doses did not

show large differences to the initial plan dose for the target, but some differences were observed for OARs [27, 65, 32].

Some previous studies have also considered these two dose accumulation methods. Abe et al. [70] assessed cumulative dose distributions in combined radiotherapy for cervical cancer using DIR and concluded that no significant differences in accumulated dose D90 received by HR-CTV and D2cc for rectum and bladder. Similar results were demonstrated by Zeng et al. [28]. Zakariaee et al. [63] claimed that the simple DVH parameters addition-based method over-estimated the bladder dose as compared to DIR-based method, specially when adjacent high dose volumes were considered. In another study, Jamema et al. [67] reported that D2cc region of bladder and rectum was quite stable in terms of spatial location for direct dose accumulation, whereas hot-spots in the sigmoid and bowel had large spatial variation between brachytherapy fractions. It was indicated that, the simple DVH parameters addition-based method might be a good approximate dose accumulation in bladder and rectum, whereas significant uncertainties might arise for sigmoid and bowel. Rubeaux et al. [42] explored accumulated dose by two methods using a numerical phantom. It was illustrated the significant results between two methods and claimed the need for DIR-based method to accumulate dose.

Even though the results in this study, as well as in other studies showed no significant difference in DVH parameters between the DIR-based and the simple DVH parameter addition-based methods for dose accumulation, DIR-based dose accumulation was proven significant useful to visualize the cumulative delivered dose of the target and OARs and to compare to cumulative planned dose in the same plan CT image for cervical cancer in routine clinics. In treatment plan strategies for proton therapy produce more conformal dose distribution [8], DIR-based method may be requisite for accumulating delivered dose. Still, many important and practical concerns need to be tackled for a successful dose tracking procedure, for example intra-fraction motion, the organ segmentations, CBCT image quality, and the accuracy of DIR algorithms. A significant progress has been improved in DIR algorithms in RayStation TPS, a comprehensive dosimetric evaluation method should be undertaken for assessment of deformable dose. It is beyond the scope of this project.

5.3.4 Dose Tracking results for Large Margin And Small Margin Plans

A safety margin to ensure high precision of clinical radiotherapy has been researched by Marcel van Herk [45]. Tumour and organ movement, deformation, and volume change were recognized to occur during pelvic radiotherapy for cervical cancer treatment (as discussed earlier, in the Section 5.1), thereby challenge the accuracy of the EBRT. To secure the target and avoid excessive normal tissue irradiation, margins have been applied [32, 49, 60]. Larger patient-based margins may counteract the benefits of IMRT/VMAT that aims a highly conformal dose and sparing normal tissues, yet too small margins can lead to under-dosing in patients with large target movement. The individualised ITV margins for patients have been introduced in EMBRACE II study [62]. This means that all of the patients in the present study have an ITV where the movement of the uterus between large (on plan CT image) and small (on plan MR image) bladder filling were taken into account. As described above, this could explain the result of the small difference between planned and delivered dose.

It was therefore of relevance to investigate whether a smaller standardized margin based upon the information on the plan CT only will change this results. Thus, the dose tracking was performed for one (patient 10) for evaluation of delivered dose to CTV_T_LR and bladder during the treatment with a small margin (SM) plan. The results showed small differences between delivered accumulated doses to CTV_T_LR and bladder and planned accumulated dose for both plans (as can be seen in Table 4.5, Table 4.6, and Table 4.7). As can be seen, in SM plan, the D98 received by CTV_T_LR was similar in both plans, while D2 dose to bladder was reduced about 0.75 Gy in SM plan compared to LM plan in both accumulated dose calculation methods. Regarding D50 received by bladder, it showed 0,17 Gy lower in SM plan compared to LM in the simple DVH parameter addition-based method, while it was 0,6 Gy higher in DIR-based method. The differences in results between those two methods might be due to uncertainties in DIR, resulting the uncertainties in deformable dose. In both plans, the non-clinically significant differences between actual dose from initial dose and good CTV_T_LR coverage observed might be explained by the use of a bladder filling protocol and both generous margins for this patient. The results revealed that smaller PTV margin of 10 mm is sufficient for this patient. Similarly, Lim et al. [32] demonstrated that with large margin whole pelvis IMRT (20 mm PTV, 10 mm inferior), the planned dose was different from delivered dose, however, taken as a group (20 studied patients), this was not statistically significant. For smaller margin (5 mm PTV),

adequate target coverage was yielded in most patients, except for one patient who exhibited immoderate and unpredictable internal target movement. As regards to OARs, actual delivered doses were significant reduced in 5 mm margin plan. Therefore, it was demonstrated that 5 mm margins could be sufficient of primary tumour coverage in IGRT-IMRT. It was noted in Lim's study that DIR-based method was also used for calculating dose accumulation. Ahmad et al. [58] evaluated dosimetric in an online margin-of-the-day treatment strategy that based on a single planning CT scan and a pre-treatment generated IMRT plan with incremental CTV-PTV margins with steps of 5 mm and compared with population-based margin (15 mm). It was reported that among 14 studied patients (total dose 46 Gy, 23 fractions), 15 mm recommended margin resulted in cervix-uterus under-dose in 6 patients, 25% of the fractions could be treated with a margin of 5 mm, 58 % of fractions with a margin up to 15 mm, and 81% with a margin up to 25 mm. In another investigation, Nina et al. [49] investigated organ motion based on CBCT and generated individualized ITVs (for 23 patients) from pre-treatment MRI and CT scans with full and empty bladders. It was outlined the median of ITV margins related to uterus and cervix was 12 mm. In both Ahmad [58] and Nina [49] researches, accumulated doses were calculated by the simple DVH parameter addition-based method.

As discussed, the target motion is affected by various factors, e.g. bladder, rectal, and bowel fillings, which is patient specific and unpredicted during the course of cervical cancer treatment. Consequently, it impacts on actual dose delivered to target and OARs. CBCT-based monitoring or another IGRT methods is practical for assessment of target and organ motions. In the recent study, only one patient was performed with reducing margin plan. The patient cohort should be larger so as to achieve better exploration. The patients with less motion during treatment could be benefit from a plan with smaller margins. Actual dose monitoring of target dose coverage and actual dose delivered to OARs in case of further reduced margin, down to 5 mm of target coverage may be worthwhile. Integration of DIR in the dose tracking process is useful for facilitating the adaptive planning in practical clinics. It should be taken into consideration as a novel approach for reducing toxicity in cervical cancer patients treated with VMAT or more advanced technique such as proton therapy.

5.4 Some Limitations

This study has some limitations. Firstly, this was retrospective study on 8 patients with locally advanced cancers. The patient cohort should be larger so as to achieve better exploration, especially regarding to the small margin analysis, in which only one patient was investigated. Secondly, in this study only CTV_T_LR and bladder were considered. Assessment of inter-fraction movement, change in shape and volume of rectum would be interesting. However, the delineation of rectum on daily CBCT was challenging. Also, manual delineations of CTV_T_LR and bladder on daily CBCT (done by the author of this project) may contain uncertainties. Thirdly, poor quality of CBCT images impact on the manual delineations of target and OAR, DIRs, computation of daily fraction dose, deform dose, and accumulated dose. They were discussed in details in the previous sections. Fourthly, even though a significant progress has been improved in DIR algorithms in RayStation TPS, lack of comprehensive dosimetric evaluation method was limited for assessment of deform dose. Fifthly, concerning about workload involving contouring, dose accumulation, and replanning on the daily volume imaging (CBCT or MRI imaging datasets) are not currently a viable in the clinics.

Chapter 6

Conclusions

6.1 OARs volumes inter-fractional variation

Despite that all of the studied patients followed the drinking protocol, the bladder volumes changes varied among the patients.

It is necessary to assess the bladder inter-fractional volumes change as it affects on target and organ motion, thereby impacting the dose to the target and OARs.

6.2 Deformable Image Registration

It was proved that the ANACONDA DIR algorithm in combination with controlling ROIs showed better DIR accuracy than only relied on image information. Also in some case with large structure deformation, controlling POIs in addition to controlling ROIs showed the improvement of DIR accuracy.

This DIR process plays an important role in dose deform and dose accumulation. Therefore, it should be evaluated carefully.

6.3 Dose tracking

6.3.1 Accumulated Delivered Dose

According to clinical objectives for CTV_T_LR and constraints dose for bladder, there were no clinically significant differences between accumulated delivered dose and accumulated plan dose for all 7 studied patients. The non-clinically significant differences observed may be explained by the use of a full bladder protocol and a generous individual ITV margin for individual patient that account for the movement in both plan CT image and plan MR image.

6.3.2 Comparison of DIR-based Method and Simple DVH addition- based method

The dose tracking results showed no statistical differences between these two cumulative dose calculation methods, namely the DIR-based and simple DVH parameter addition-based methods. Still, DIR-based dose accumulation was proven significant useful to visualize the cumulative delivered dose of the target and OARs and to compare to cumulative planned dose in the same plan CT image for cervical cancer radiotherapy in routine clinics.

6.3.3 Comparison of Dose Tracking for Large and Small Margin Plans

The results showed slight differences between delivered accumulated doses to CTV_T_LR and bladder and planned accumulated dose for large margin and small margin plans (patient 10). However, the deviations were clinical acceptances. Moreover, the results revealed that smaller PTV margin of 10 mm was sufficient for this patient in covering the CTV_T_LR and no overdose to bladder.

Chapter 7

Significance And Future Work

This study employed DIR in the dose tracking process for deforming and accumulating dose. It is meaningful for facilitating the adaptive planning in practical clinics for radiation therapy. It should be taken into consideration as a novel approach for reducing toxicity in cervical cancer patients treated with VMAT or more advanced technique such as proton therapy. It was claimed that the volume of the structure affects on DSC calculation [30]. Therefore, correlation between the volumes of target and OARs and DIR accuracy would be interesting, i.e, investigate if the very small or very big volumes of the structures would impact on the DIR accuracy. The clinical data could be worthwhile to the development of DIR algorithm in RayStation TPS.

A comprehensive process for validating both geometric and dosimetric DIR accuracy should be accomplished. The AAPM TG132 [30] has recommended a comprehensive process that includes three methods, such as physical phantom, digital phantom and clinical data tests. Moreover, quantification about the influence of DIR uncertainties on dose accumulation in the dose tracking process is important.

Reduced margin plans analysis with, for example 10 mm and 5 mm ITV margins, should be carried out for more number of patients and perhaps for proton treatment plan. Then, dose tracking needs to be performed aiming to monitoring dosimetric individually and assisting decision on re-planning.

Researchers worldwide have concerned about automatic contouring, automatic planning and automatic dose tracking in treatment planning system with the help of machine learning in order to minimize time in treatment planning process. In addition, the potential MRI-Linac in the treatment room for volumetric imaging in real-time during radiotherapy has been explored for optimal imaging which can capture the most significant organ motion in real-time. It would

hopefully provide more realistic in order to facilitate for novel approach to adaptive replanning in clinics.

Appendix A

Appendix

A.1 RayStation Guidelines from ROIs Segmentations to Dose Tracking

Step 1: Segmentation ROIs (CTV_T_LR and bladder) manually on CBCTs:, using module: **Patient Modelling**.

- Use: **Structure Definition**

Step 2: Create CTV_T_LR_TriMesh and bladder_TriMesh
This step makes the TriMesh (smoother ROIs) that will be used for ROIs controlling for DIRs later, using module **: Patient Modeling**.

- Use **Deformable Registration**
- Use **Controlling ROIs**
  - Use *Create New Mesh from reference geometry.* Choose: *CTV_T_LR* and *Bladder.*
    - *Mesh detail: Default*
    - *Smoothing radius: 0,5*

Step 3: Perform DIRs
This step performs DIRs (from CBCTs to CT). Do for all daily CBCTs (for all fractions), using module **: Patient Modelling**.

- Use **Deformable Registration**

- In *New Registration*. Choose *Hybrid Intensity and structure based*.
  - Reference Image: CT
  - Target Image Sets: CBCTs
  - Controlling ROI(s) or/ and POI(s)
    * Choose: *CTV_T_LR_TriMesh*
    * Choose: *Bladder_TriMesh*

Step 4: Validate DIRs

This step validates DIRs qualitatively and quantitatively in order to choose good DIRs for dose accumulation.

1. **Qualitative validation:** Inspection use Fusion image with **overlap** function.
   - Use module **Patient Modelling**
   - Use Deformation Registration
     - Select, for example **CBCT1**
     - Go to **Fusion** view. Fusion type **Overlay**. Showed deformed ROIs/POIs. See *Undeformed* or *Deformed*.
     - Deformed: Good (100 % overlay).
2. **Quantitative validation:** Use Dice Similarity Coefficient (DSCs) statistics.
   - Use module **Patient Modelling**
   - Use Deformation Registration
     - Go to *Deformation*. Select, for example **CBCT1**
     - Go to *Sagital View panel*. Click *ROI Geometry Statistics*.
     - Select target image set: CBCT:CBCT1
     - Record DSCs for interested ROIs.

After **qualitative validation** and **quantitative validation**, good DIRs are approved for **dose accumulation** in **dose tracking** process.

Step 5: Dose accumulation and Dose Tracking

This step will do dose accumulation and dose comparison. The four different dose comparison modes in RayStation that include:

- **Fraction comparison**
- **Deformation comparison**
- **Accumulation comparison**
- **Total dose comparison**

A.2 Dose Tracking Results

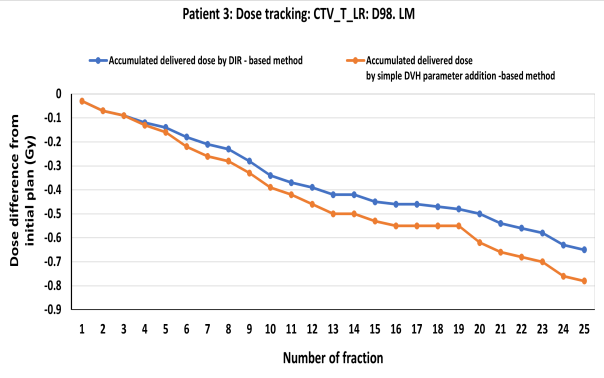

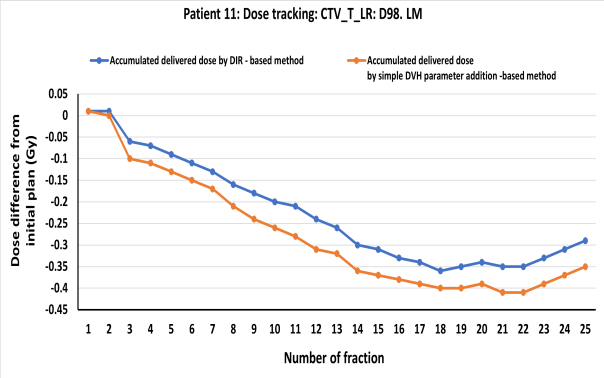

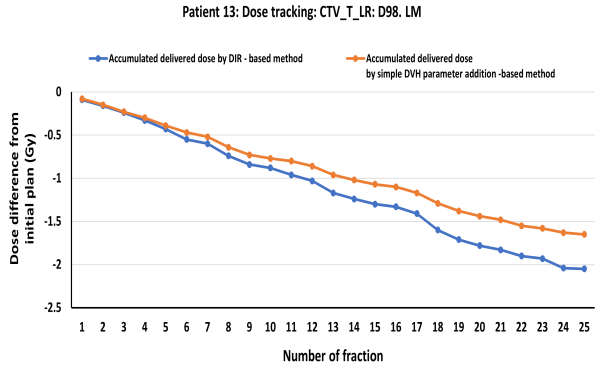

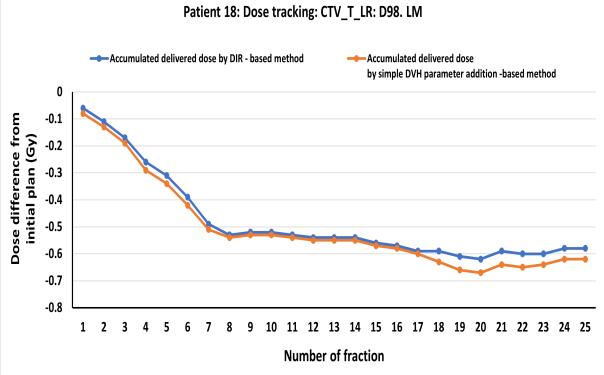

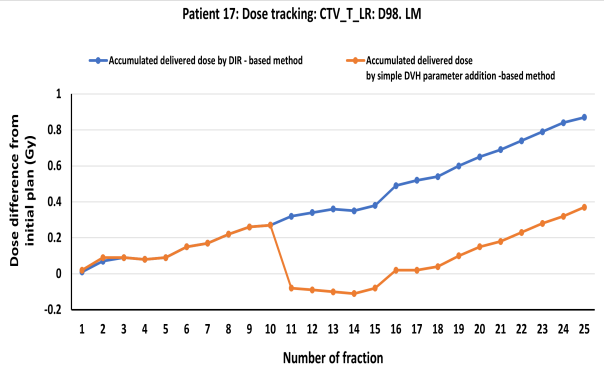

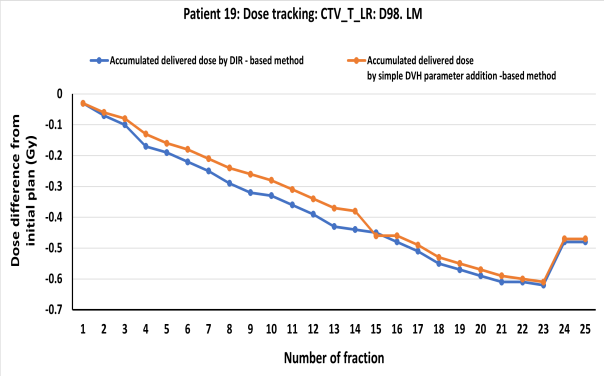

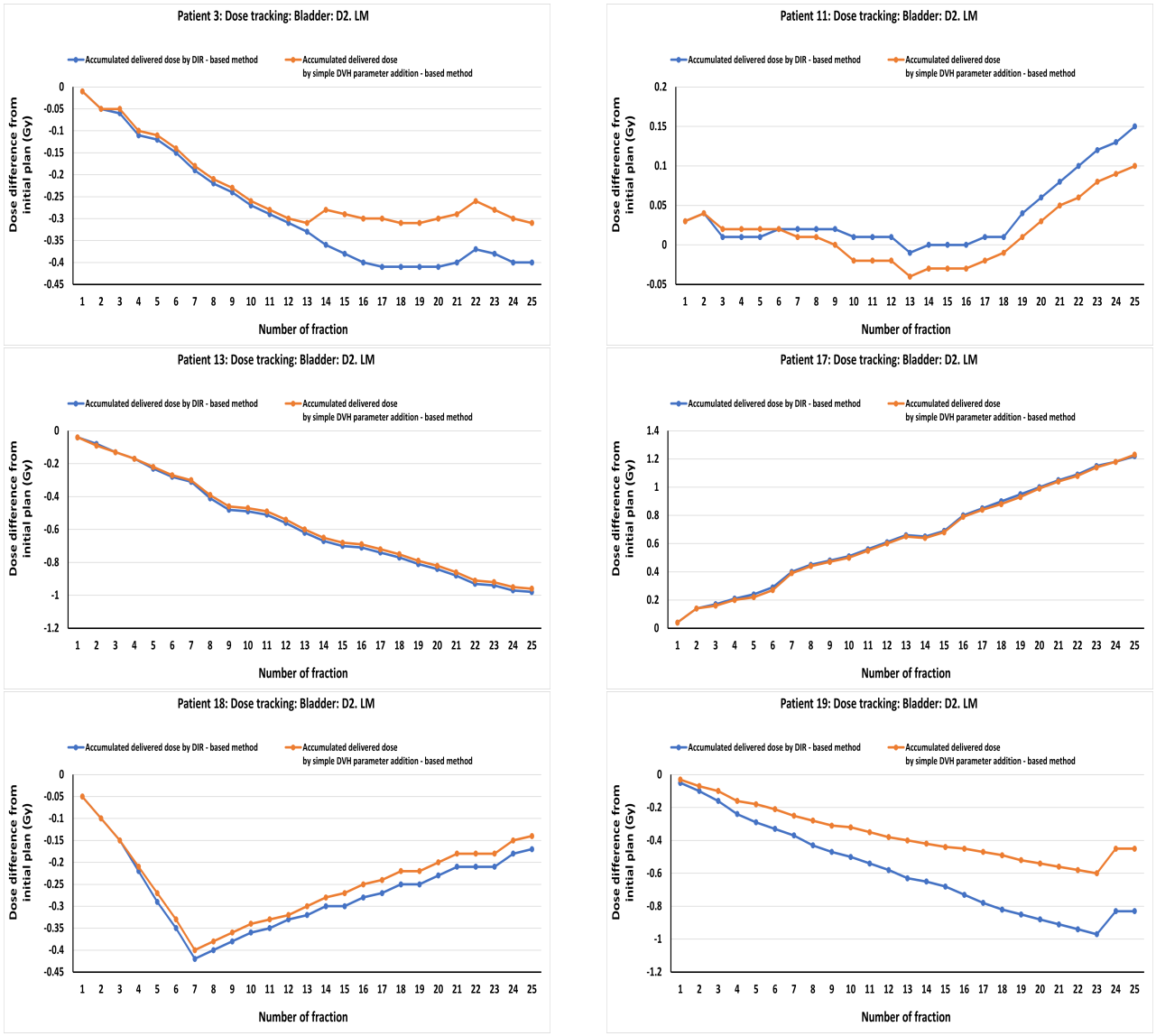

Figure A·1: Dose tracking results for all patient: Bladder: D2. Accumulated delivered doses were calculated by DIR-based method and simple DVH parameter addition-based method.

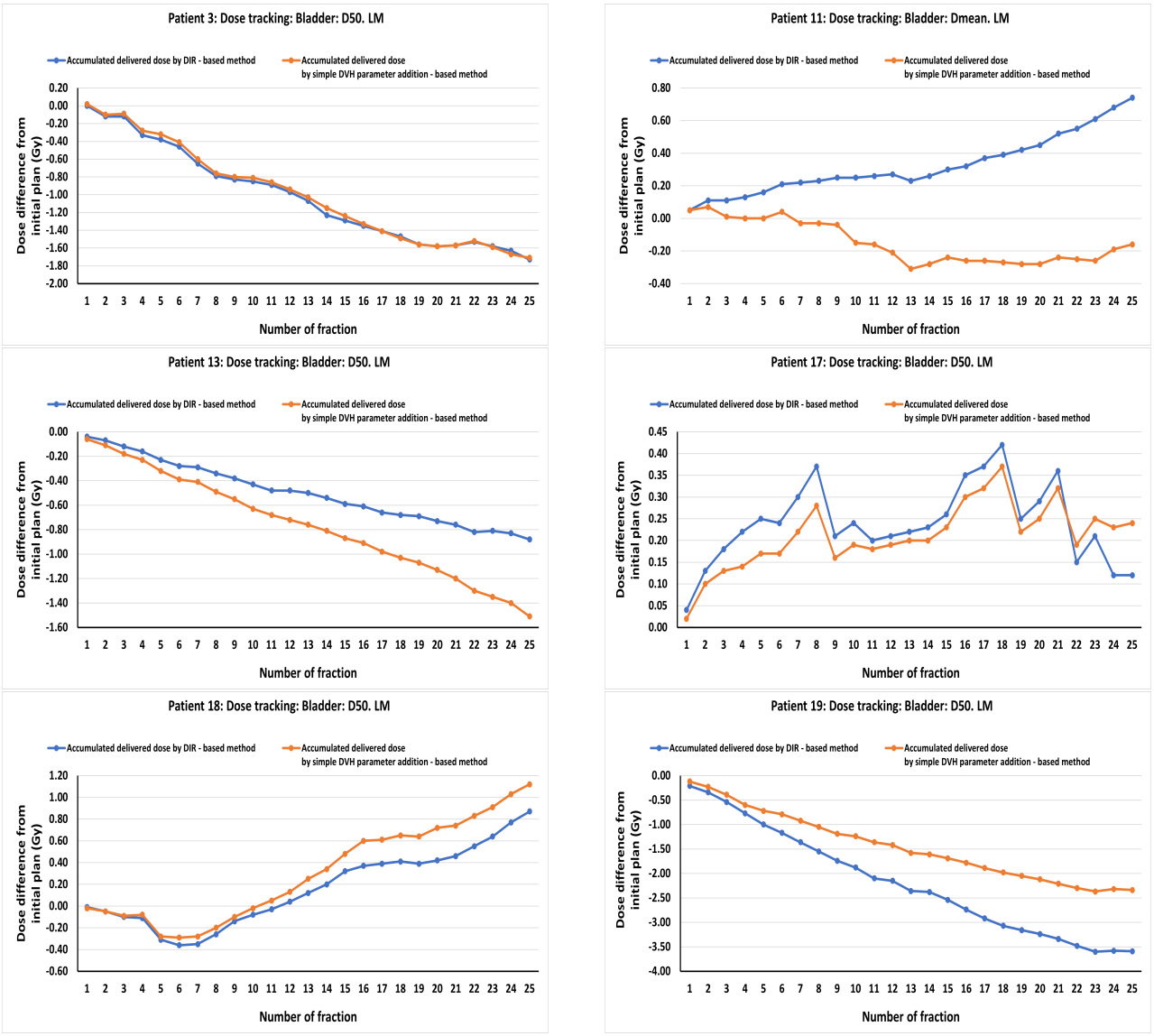

Figure A·2: Dose tracking results for all patient: Bladder: D50 or Dmean. Accumulated delivered doses were calculated by DIR-based method and simple DVH parameter addition-based method.

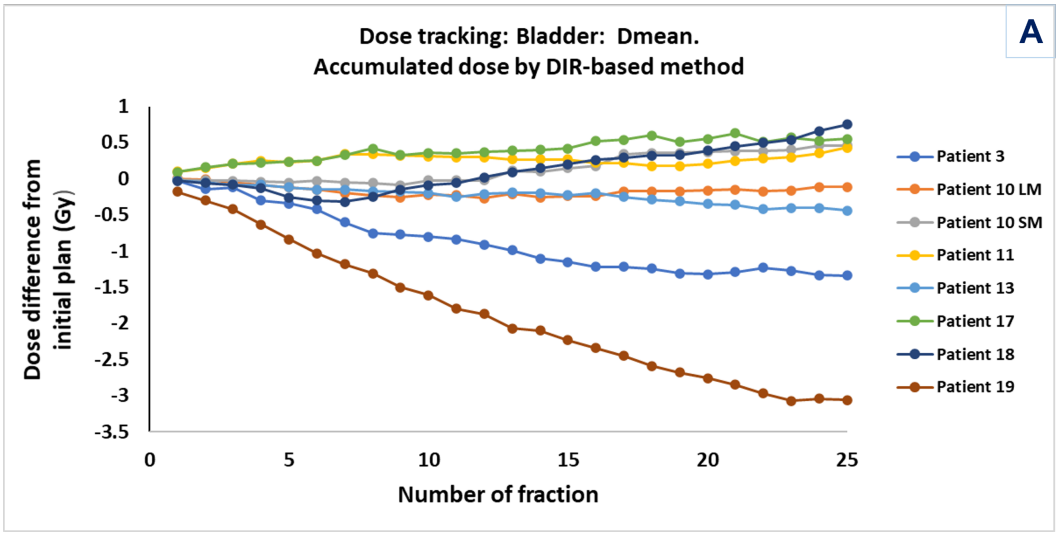

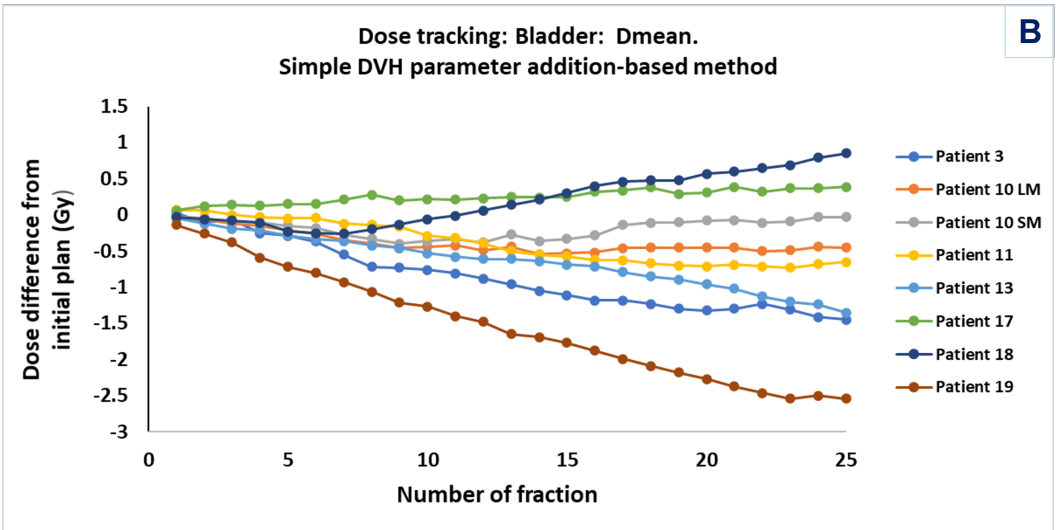

Figure A·3: Dose tracking: Dmean received by bladder: comparison between accumulated planned dose and accumulated delivered dose during treatment in two methods: **A.** Accumulated delivered dose by DIR-based method and **B.** Accumulated delivered dose by simple DVH addition-based method. *Dose difference from initial plan = accumulated delivered dose – accumulated planned dose.* The minus sign indicates the accumulated delivered dose is lower than the initial plan.

Table A.1: Dose volume histogram (DVH) parameters for Bladder: Dmean. LM = Large margin plan. *Dose difference between two method = dose difference by simple DVH parameter based method - by DIR based method.*

Bladder: Dmean	**Patient**	**Accumulated planned dose (Gy)**	**Accumulated delivered dose by DIR (Gy)**	**Accumulated delivered dose by simple DVH parameter addition (Gy)**
	3	41	39.66	39.55
	10 (LM)	40	39.89	39.55
	11	40.5	40.93	39.85
	13	41.75	41.31	40.4
	17	42	42.55	42.39
	18	38.75	39.5	39.6
	19	42.5	39.44	39.96
Dose differences (Gy)	**Patient**	**By DIR from initial plan**	**By simple DVH parameter addition from initial plan**	**Between two methods**
	3	-1.34	-1.45	-0.11
	10 (LM)	-0.11	-0.45	-0.34
	11	0.43	-0.65	-1.08
	13	-0.44	-1.35	-0.91
	17	0.55	0.39	-0.16
	18	0.75	0.85	0.1
	19	-3.06	-2.54	0.52
p-values (Wilcoxon signed-rank test)		**p = 0.5737**	**p = 0.2268**	**p = 0.8747**

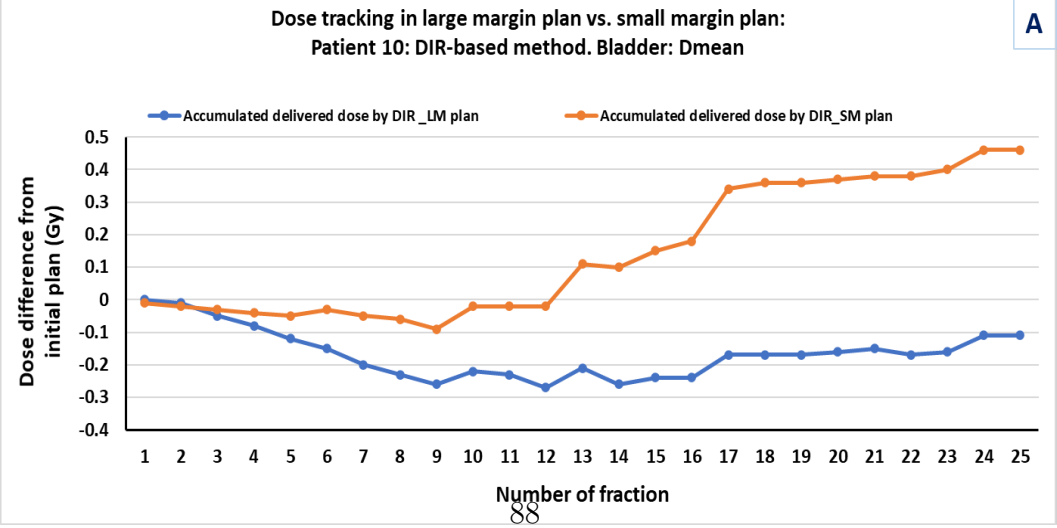

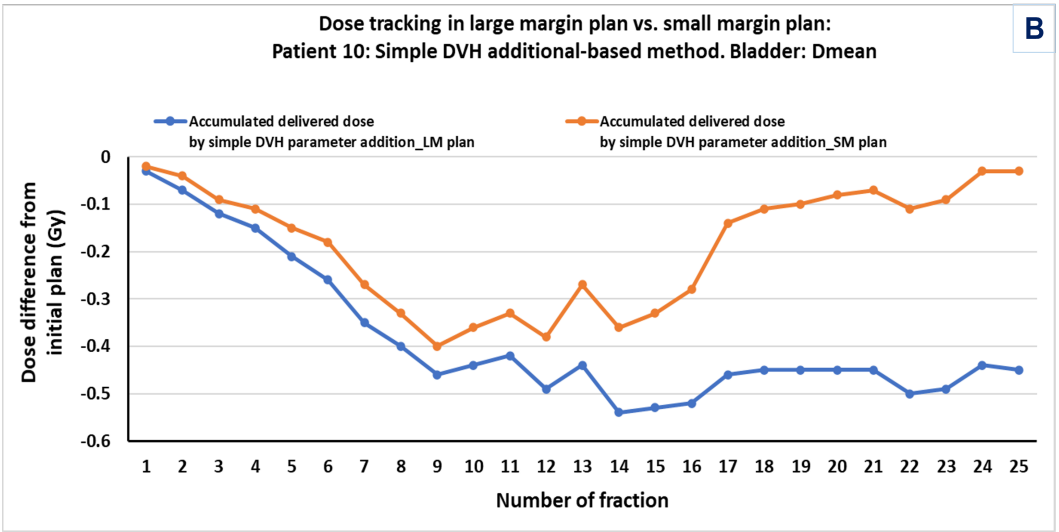

Figure A·4: Dose tracking patient 10: Badder: Dmean: comparison between large margin and small margin plans. A. Accumulated delivered dose calculated in DIR-based method, and B. Accumulated delivered dose calculated in simple DVH parameter addition-based method. LM = Large Margin. SM = Small Margin

Table A.2: Dose volume histogram (DVH) parameters for Bladder: Dmean. LM = Large margin plan; SM = Small margin plan. *Dose difference between two method = dose difference by simple DVH parameter based method - by DIR based method.*

Bladder: Dmean	**Patient**	**Accumulated planned dose (Gy)**	**Accumulated delivered dose by DIR (Gy)**	**Accumulated delivered dose by simple DVH parameter addition (Gy)**
	10 (LM)	40	39.89	39.55
	10 (SM)	35.25	35.71	35.22
Dose differences (Gy)	**Patient**	**By DIR from initial plan**	**By simple DVH parameter addition from initial plan**	**Between two methods**
	10 (LM)	-0.11	-0.45	-0.34
	10 (SM)	0.46	-0.03	-0.49

A.3 Correlation between bladder volume changes and D98 to CTV_T_LR changes

A.3.1 Calculation

The bladder volume changes can be calculated as described in Section 3.2

The D98 to CTV_T_LR changes can be calculated as follows:

$$\triangle D = D_k - D_p \tag{A.1}$$

where D_p is the dose on the planCT and D_k is the delivered dose computed on the CBCT in fraction k or the deformed delivered dose in fraction k.

A.3.2 Results

The correlation coefficients between volume changes and dose changes (D98 to CTV_T_LR) were found in the below table:

	Patient 3	Patient 10 LM	Patient 10 SM	Patient 11	Patient 13	Patient 17	Patient 18	Patient 19
Correlation coeff. Volume changes vs fx D98 to CTV changes (DIR-based method)	-0.33514	-0.40476435	-0.474216835	-0.098281	0.115865	-0.400241	-0.00509	-0.029326
Correlation coeff. Volume changes vs fx D98 to CTV changes (computed on CBCT)	-0.20778	-0.39996441	-0.30960118	-0.054863	0.034271	0.098855	-0.034538	-0.023595

Figure A·5: Correlation coefficients between bladder volume changes and D98 to CTV changes.

A.3.3 Regression statistics results for bladder volumes on CT and daily CBCTs and time trending

	Patient 3	Patient 10	Patient 11	Patient 13	Patient 17	Patient 18	Patient 19
R-value	-0.36	-0.35	-0.31	-0.04	-0.28	-0.13	-0.001
R-square	0.135	0.123	0.098	0.002	0.079	0.009	8.43x10^-5
p-value	0.092402	0.078563	0.144951	0.82576569	0.19222455	0.1320752	0.9660439

Figure A·6: Regression statistics results for bladder volumes on CT and daily CBCTs and time trending.

A.4 Raw Data

Raw data were recorded from RayStation TPS

A.4.1 Bladder Volume on daily CBCTs

CBCT fraction #	Patient 3	Patient 4	Patient 11	Patient 13	Patient 17	Patient 19	Patient 18	Patient 10
CBCT 1	481.94	Bad image quality	90.17	64.04	259.22	67.57	314.53	182.85
CBCT 2	52.86	Bad image quality	108.08	190.72	225.23	117.26	202.26	161.68
CBCT 3	151.4	Bad image quality	40.26	46.7	84.33	47.57	155.84	257.02
CBCT 4	50.92	Bad image quality	56.71	49.56	277.94	46.73	86.56	189.48
CBCT 5	126.8	Bad image quality		40.27	165.7	43.2	35.2	250.76
CBCT 6	120.31	Bad image quality	192.68	48.41	77	49.15	189.96	282.02
CBCT 7	44.69	Bad image quality	100.21	75.74	317.07	96.42	70.61	242.94
CBCT 8	88.34	Bad image quality	113.42	26.23	59.44	45.57	338.18	197.87
CBCT 9	120.4	Bad image quality		42.75	45.93	91.25	93.73	195.32
CBCT 10	328.5	Bad image quality	81.94	44.65	206.54	52.53	286.92	122.52
CBCT 11	146.69	Bad image quality	68.86	35.24	66.32	170.93	372.8	222.57
CBCT 12		Bad image quality	82.42	41.37		53.65	124.97	258.11
CBCT 13	64.02	Bad image quality	41.23	24.3	132.98	186.63	147.15	100.34
CBCT 14	41.63	Bad image quality	79.51	37.39	169.03	71.02	110.53	270.72
CBCT 15	73.53	Bad image quality	150.33	52.01	192.94	73.77	71.53	145.15
CBCT 16		Bad image quality	58.35	30.55	93.55	44.42	220.44	191.7
CBCT 17	51.49	Bad image quality	119.45	75.86	237.74	115.39	259.42	89.36
CBCT 18		Bad image quality		111.87	44.06	117.19	163.1	181.79
CBCT 19	97.58	Bad image quality	60.96	90.38	111.08	109.98	152.02	175.39
CBCT 20	119.59	Bad image quality	54.54	80.03	189.54	54.85	232.54	155.72
CBCT 21	154.23	Bad image quality	58.53	37.22	36.86	91.46	178.32	166.96
CBCT 22	42.18	Bad image quality	59.35	80.02	238.71	60.92	57.37	197.88
CBCT 23	54.59	Bad image quality	69.98	145.85	43.41	168.52	56.75	168.39
CBCT 24	61.05	Bad image quality	23.84	38.44			89.6	138.02
CBCT 25			77.54	81.94			81.78	165.65

Figure A·7: Bladder volume raw data.

A.4.2 DSCs for CTV_T_LR and Bladder

DIR	Patient 3	Patient 10	Patient 11	Patient 13 (controlling ROIs & POIs)	Patient 13 (controlling ROIs, no POIs)	Patient 13 (no controlling ROIs & POIs)	Patient 17	Patient 18	Patient 19
CBCT1 -> CT	0.99	0.99	0.99	0.97	0.92	0.6	0.99	0.99	0.99
CBCT2 -> CT	0.99	0.99	0.98	0.97	0.79	0.53	0.99	0.99	0.99
CBCT3 -> CT	0.99	0.97	0.95	0.98	0.96	0.76	0.99	0.99	0.98
CBCT4 -> CT	0.99	0.96	0.99	0.92	0.83	0.53	0.99	0.96	0.98
CBCT5 -> CT	0.99	0.98		0.94	0.95	0.6	0.99	0.95	0.99
CBCT6 -> CT	0.99	0.99	0.96	0.95	0.94	0.67	0.99	0.99	0.98
CBCT7 -> CT	0.99	0.89	0.99	0.98	0.99	0.61	0.99	0.99	0.98
CBCT8 -> CT	0.98	0.99	0.99	0.92	0.91	0.51	0.97	0.97	0.98
CBCT9 -> CT	0.99	0.99		0.95	0.94	0.72	0.99	0.96	0.99
CBCT10 -> CT	0.84	0.99	0.99	0.98	0.73	0.73	0.99	0.97	0.99
CBCT11 -> CT	0.82	0.98	0.99	0.47	0.43	0.42	0.97	0.97	0.99
CBCT12 -> CT		0.99	0.99	0.87	0.57	0.47		0.97	0.97
CBCT13 -> CT	0.83	0.97	0.99	0.9	0.9	0.59	0.98	0.98	0.99
CBCT14 -> CT		0.99	0.96	0.99	0.98	0.71	0.99	0.97	0.99
CBCT15 -> CT	0.83	0.98	0.99	0.99	0.98	0.68	0.99	0.97	0.98
CBCT16 -> CT		0.98		0.85	0.85	0.6	0.99	0.97	0.98
CBCT17 -> CT	0.82	0.98	0.96	0.96	0.98	0.74	0.99	0.97	0.99
CBCT18 -> CT	0.75	0.98		0.97	0.97	0.67	0.99	0.97	0.99
CBCT19 -> CT	0.86	0.98	0.99	0.98	0.97	0.53	0.99	0.97	0.98
CBCT20 -> CT	0.99	0.99	0.99	0.98	0.98	0.57	0.99	0.97	0.98
CBCT21 -> CT	0.99	0.99	0.97	0.88	0.65	0.54	0.98	0.97	0.99
CBCT22 -> CT	0.99	0.99	0.99	0.98	0.98	0.66	0.98	0.96	0.98
CBCT23 -> CT	0.99	0.98	0.94	0.92	0.81	0.48	0.99	0.96	0.99
CBCT24 -> CT	0.99	0.98	0.99	0.89	0.74	0.51		0.96	
CBCT25 ->CT		0.99	0.99	0.84		0.84		0.97	

Figure A·8: DSCs for CTV.

DIR	Patient 3	Patient 10	Patient 11	Patient 13 (controlling ROIs & POIs)	Patient 13 (controlling ROIs, no POIs)	Patient 13 (no controlling ROIs & POIs)	Patient 17	Patient 18	Patient 19
CBCT1 -> CT	0.72	0.99	0.98	0.98	0.98	0.74	0.99	1	1
CBCT2 -> CT	0.99	1	0.97	0.98	0.96	0.65	0.99	1	1
CBCT3 -> CT	0.99	0.98	0.95	0.99	0.98	0.63	0.99	1	0.99
CBCT4 -> CT	0.99	0.99	0.98	0.97	0.98	0.67	0.99	0.98	0.99
CBCT5 -> CT	0.99	0.99		0.96	0.96	0.58	0.99	0.97	0.99
CBCT6 -> CT	0.99	0.99	0.98	0.99	0.98	0.64	0.99	1	0.98
CBCT7 -> CT	0.99	0.99	0.98	0.99	0.99	0.77	0.99	0.99	0.99
CBCT8 -> CT	0.99	0.99	0.98	0.96	0.96	0.4	0.99	0.99	0.99
CBCT9 -> CT	0.99	0.99		0.98	0.98	0.54	0.99	0.97	1
CBCT10 -> CT	0.8	0.99	0.98	0.99	0.72	0.72	0.99	0.99	0.99
CBCT11 -> CT	0.66	0.99	0.98	0.82	0.84	0.57	0.99	0.99	1
CBCT12 -> CT		0.99	0.98	0.95	0.92	0.56		0.99	0.99
CBCT13 -> CT	0.75	0.99	0.98	0.96	0.97	0.32	0.99	0.99	1
CBCT14 -> CT	0.63	0.99	0.97	0.99	0.99	0.56	0.99	0.98	1
CBCT15 -> CT	0.82	0.99	0.98	0.98	0.99	0.73	0.99	0.99	0.99
CBCT16 -> CT		0.98		0.9	0.9	0.51	0.99	0.99	0.99
CBCT17 -> CT	0.81	0.99	0.97	0.98	0.99	0.8	0.99	0.99	1
CBCT18 -> CT	0.83	0.99		0.99	0.99	0.77	0.99	0.99	1
CBCT19 -> CT	0.97	0.99	0.98	0.99	0.98	0.67	0.99	0.98	0.99
CBCT20 -> CT	0.99	0.99	0.98	0.99	0.99	0.81	0.99	0.99	0.99
CBCT21 -> CT	0.99	1	0.95	0.96	0.95	0.56	0.99	0.98	0.99
CBCT22 -> CT	0.99	0.99	0.97	0.99	0.99	0.79	0.99	0.98	0.99
CBCT23 -> CT	0.99	0.99	0.96	0.96	0.96	0.74	0.99	0.97	1
CBCT24 -> CT	0.99		0.96	0.98	0.97	0.55		0.97	
CBCT25 ->CT		1	0.97	0.92		0.92		0.98	

Figure A·9: DSCs for Bladder.

A.4.3 Dose statistics

Dose statistics for CTV

D98 to CTV	Planned fx dose	Delivered fx dose	Deformed delivered fx dose
Fraction 1	1.78	1.75	1.75
Fraction 2	1.78	1.74	1.74
Fraction 3	1.78	1.76	1.76
Fraction 4	1.78	1.74	1.75
Fraction 5	1.78	1.75	1.76
Fraction 6	1.78	1.72	1.74
Fraction 7	1.78	1.74	1.75
Fraction 8	1.78	1.76	1.76
Fraction 9	1.78	1.73	1.73
Fraction 10	1.78	1.72	1.72
Fraction 11	1.78	1.75	1.75
Fraction 12	1.78		
Fraction 13	1.78	1.74	1.75
Fraction 14	1.78	1.78	1.78
Fraction 15	1.78	1.75	1.75
Fraction 16	1.78		
Fraction 17	1.78	1.78	
Fraction 18	1.78	1.78	1.77
Fraction 19	1.78	1.78	
Fraction 20	1.78	1.71	1.76
Fraction 21	1.78	1.74	1.74
Fraction 22	1.78	1.76	1.76
Fraction 23	1.78	1.76	1.76
Fraction 24	1.78	1.72	1.73
Fraction 25	1.78	1.76	1.76

Figure A·10: Patient 3: D98 received by CTV.

D98	Planned fx dose	Delivered fx dose	Deformed delivered fx dose
Fraction 1	1.78	1.74	1.76
Fraction 2	1.78	1.75	1.76
Fraction 3	1.78	1.7	1.72
Fraction 4	1.78	1.61	1.69
Fraction 5	1.78	1.71	1.72
Fraction 6	1.78	1.74	1.74
Fraction 7	1.78	1.64	1.74
Fraction 8	1.78	1.74	1.75
Fraction 9	1.78	1.74	1.75
Fraction 10	1.78	1.77	1.77
Fraction 11	1.78	1.75	1.75
Fraction 12	1.78	1.69	1.72
Fraction 13	1.78	1.74	1.74
Fraction 14	1.78	1.74	1.74
Fraction 15	1.78	1.71	1.73
Fraction 16	1.78	1.71	1.73
Fraction 17	1.78	1.74	1.74
Fraction 18	1.78	1.74	1.74
Fraction 19	1.78	1.76	1.76
Fraction 20	1.78	1.75	1.75
Fraction 21	1.78	1.75	1.75
Fraction 22	1.78	1.72	1.73
Fraction 23	1.78	1.76	1.76
Fraction 24	1.78	1.79	1.79
Fraction 25	1.78	1.74	1.75

Figure A·11: Patient 10: D98 received by CTV. LM plan.

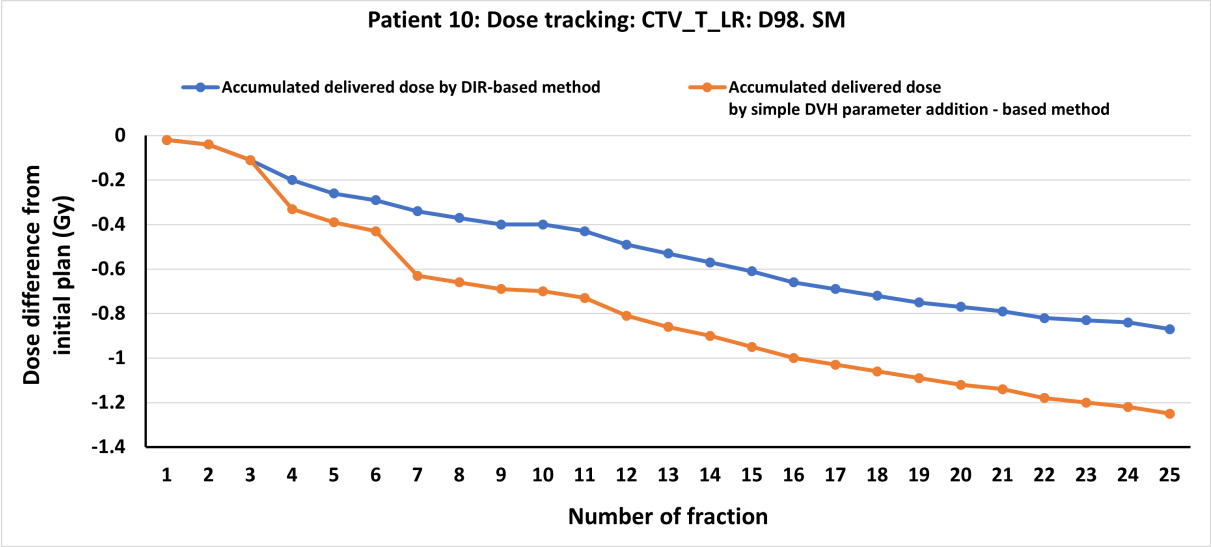

Figure A·12: Patient 10: D98 received by CTV. SM plan.

D98	Planned fx dose	Delivered fx dose	Deformed delivered fx dose
Fraction 1	1.78	1.79	1.79
Fraction 2	1.78	1.77	1.78
Fraction 3	1.78	1.68	1.71
Fraction 4	1.78	1.77	1.77
Fraction 5	1.78		
Fraction 6	1.78	1.76	1.76
Fraction 7	1.78	1.76	1.76
Fraction 8	1.78	1.74	1.75
Fraction 9	1.78		
Fraction 10	1.78	1.76	1.76
Fraction 11	1.78	1.76	1.77
Fraction 12	1.78	1.75	1.75
Fraction 13	1.78	1.77	1.76
Fraction 14	1.78	1.74	1.74
Fraction 15	1.78	1.77	1.77
Fraction 16	1.78		
Fraction 17	1.78	1.77	1.77
Fraction 18	1.78		
Fraction 19	1.78	1.78	1.79
Fraction 20	1.78	1.79	1.79
Fraction 21	1.78	1.76	1.77
Fraction 22	1.78	1.78	1.78
Fraction 23	1.78	1.8	1.8
Fraction 24	1.78	1.8	1.8
Fraction 25	1.78	1.8	1.8

Figure A·13: Patient 11: D98 received by CTV.

D98	Planned fx dose	Delivered fx dose	Deformed delivered fx dose
Fraction 1	1.77	1.7	1.69
Fraction 2	1.77	1.71	1.71
Fraction 3	1.77	1.7	1.7
Fraction 4	1.77	1.71	1.69
Fraction 5	1.77	1.69	1.68
Fraction 6	1.77	1.7	1.66
Fraction 7	1.77	1.73	1.73
Fraction 8	1.77	1.66	1.64
Fraction 9	1.77	1.69	1.68
Fraction 10	1.77	1.74	1.74
Fraction 11	1.77	1.75	
Fraction 12	1.77	1.72	1.71
Fraction 13	1.77	1.68	1.64
Fraction 14	1.77	1.72	1.71
Fraction 15	1.77	1.73	1.72
Fraction 16	1.77	1.75	1.75
Fraction 17	1.77	1.71	1.7
Fraction 18	1.77	1.66	1.59
Fraction 19	1.77	1.69	1.67
Fraction 20	1.77	1.72	1.71
Fraction 21	1.77	1.74	1.73
Fraction 22	1.77	1.71	1.71
Fraction 23	1.77	1.75	1.75
Fraction 24	1.77	1.73	1.67
Fraction 25	1.77	1.76	1.77

Figure A·14: Patient 13: D98 received by CTV.

D98	Planned fx dose	Delivered fx dose	Deformed delivered fx dose
Fraction 1	1.78	1.8	1.79
Fraction 2	1.78	1.85	1.84
Fraction 3	1.78	1.78	1.8
Fraction 4	1.78	1.77	1.77
Fraction 5	1.78	1.79	1.79
Fraction 6	1.78	1.84	1.84
Fraction 7	1.78	1.8	1.8
Fraction 8	1.78	1.83	1.83
Fraction 9	1.78	1.82	1.82
Fraction 10	1.78	1.79	1.79
Fraction 11	1.78	1.43	1.83
Fraction 12	1.78		
Fraction 13	1.78		
Fraction 14	1.78	1.77	1.77
Fraction 15	1.78	1.81	1.81
Fraction 16	1.78	1.88	1.89
Fraction 17	1.78		
Fraction 18	1.78	1.8	1.8
Fraction 19	1.78	1.84	1.84
Fraction 20	1.78	1.83	1.83
Fraction 21	1.78	1.81	1.82
Fraction 22	1.78	1.83	1.83
Fraction 23	1.78	1.83	1.83
Fraction 24	1.78	1.82	1.83
Fraction 25	1.78	1.83	

Figure A·15: Patient 17: D98 received by CTV.

D98	Planned fx dose	Delivered fx dose	Deformed delivered fx dose
Fraction 1	1.78	1.7	1.72
Fraction 2	1.78	1.73	1.73
Fraction 3	1.78	1.72	1.72
Fraction 4	1.78	1.68	1.69
Fraction 5	1.78	1.73	1.73
Fraction 6	1.78	1.7	1.7
Fraction 7	1.78	1.69	1.68
Fraction 8	1.78	1.75	1.74
Fraction 9	1.78	1.79	1.79
Fraction 10	1.78	1.78	1.78
Fraction 11	1.78	1.77	1.77
Fraction 12	1.78	1.77	1.77
Fraction 13	1.78	1.78	1.78
Fraction 14	1.78	1.78	1.78
Fraction 15	1.78	1.76	1.76
Fraction 16	1.78	1.77	1.77
Fraction 17	1.78	1.76	1.76
Fraction 18	1.78	1.75	1.78
Fraction 19	1.78	1.75	1.76
Fraction 20	1.78	1.77	1.77
Fraction 21	1.78	1.81	1.81
Fraction 22	1.78	1.77	1.77
Fraction 23	1.78	1.79	1.78
Fraction 24	1.78	1.8	1.8
Fraction 25	1.78	1.78	1.78

Figure A·16: Patient 18: D98 received by CTV.

D98	Planned fx dose	Delivered fx dose	Deformed delivered fx dose
Fraction 1	1.78	1.75	1.75
Fraction 2	1.78	1.75	1.74
Fraction 3	1.78	1.76	1.75
Fraction 4	1.78	1.73	1.71
Fraction 5	1.78	1.75	1.76
Fraction 6	1.78	1.76	1.75
Fraction 7	1.78	1.75	1.75
Fraction 8	1.78		
Fraction 9	1.78	1.76	1.75
Fraction 10	1.78	1.76	1.77
Fraction 11	1.78	1.75	1.75
Fraction 12	1.78	1.75	1.75
Fraction 13	1.78	1.75	1.74
Fraction 14	1.78	1.77	1.77
Fraction 15	1.78	1.7	1.77
Fraction 16	1.78	1.78	
Fraction 17	1.78		
Fraction 18	1.78	1.74	1.74
Fraction 19	1.78	1.76	1.76
Fraction 20	1.78	1.76	1.76
Fraction 21	1.78	1.76	1.76
Fraction 22	1.78	1.77	1.78
Fraction 23	1.78	1.77	1.77
Fraction 24	1.78	1.92	1.92
Fraction 25	1.78	1.78	1.78

Figure A·17: Patient 19: D98 received by CTV.

Dose statistics for bladder

D_average	Planned fx dose	Delivered fx dose	Deformed delivered fx dose	D50	Planned fx dose	Delivered fx dose	Deformed delivered fx dose	D2	Planned fx dose	Delivered fx dose	Deformed delivered fx dose
Fraction 1	1.64	1.67	1.62		1.73	1.75	1.73		1.81	1.8	1.8
Fraction 2	1.64	1.51	1.52		1.73	1.61	1.61		1.81	1.77	1.77
Fraction 3	1.64	1.67	1.66		1.73	1.74	1.73		1.81	1.81	1.8
Fraction 4	1.64	1.46	1.46		1.73	1.54	1.52		1.81	1.76	1.76
Fraction 5	1.64	1.6	1.6		1.73	1.69	1.68		1.81	1.8	1.8
Fraction 6	1.64	1.56	1.56		1.73	1.64	1.65		1.81	1.78	1.78
Fraction 7	1.64	1.46	1.46		1.73	1.54	1.54		1.81	1.77	1.77
Fraction 8	1.64	1.47	1.49		1.73	1.57	1.59		1.81	1.78	1.78
Fraction 9	1.64	1.63	1.62		1.73	1.69	1.69		1.81	1.79	1.79
Fraction 10	1.64	1.61	1.61		1.73	1.72	1.71		1.81	1.78	1.78
Fraction 11	1.64	1.59	1.6		1.73	1.68	1.69		1.81	1.79	1.79
Fraction 12	1.64				1.73				1.81		
Fraction 13	1.64	1.56	1.56		1.73	1.64	1.63		1.81	1.8	1.79
Fraction 14	1.64	1.55	1.53		1.73	1.61	1.57		1.83	1.84	1.78
Fraction 15	1.64	1.58	1.59		1.73		1.67		1.81	1.8	1.79
Fraction 16	1.64				1.73				1.81		
Fraction 17	1.64	1.64			1.73				1.81	1.81	
Fraction 18	1.64	1.59	1.62		1.73	1.65	1.67		1.81	1.8	1.81
Fraction 19	1.64				1.73				1.81	1.81	
Fraction 20	1.64	1.62	1.63		1.73	1.71	1.71		1.81	1.82	1.81
Fraction 21	1.64	1.66	1.67		1.73	1.74	1.74		1.81	1.82	1.82
Fraction 22	1.64	1.71	1.7		1.73	1.78	1.77		1.81	1.84	1.84
Fraction 23	1.64	1.56	1.6		1.73	1.66	1.68		1.81	1.79	1.8
Fraction 24	1.64	1.54	1.58		1.73	1.65	1.68		1.81	1.79	1.79
Fraction 25	1.64	1.6	1.63		1.73	1.69			1.81	1.8	1.81

Figure A·18: Patient 3: Dmean, D50, and D2 received by Bladder.

D_average	Planned fx dose	Delivered fx dose	Deformed delivered fx dose	D50	Planned fx dose	Delivered fx dose	Deformed delivered fx dose	D2	Planned fx dose	Delivered fx dose	Deformed delivered fx dose
Fraction 1	1.6	1.57	1.6		1.7	1.67	1.7		1.83	1.88	1.88
Fraction 2	1.6	1.56	1.59		1.7	1.66	1.69		1.83	1.84	1.87
Fraction 3	1.6	1.55	1.56		1.7	1.63	1.67		1.83	1.83	1.84
Fraction 4	1.6	1.57	1.57		1.7	1.67	1.68		1.83	1.84	1.84
Fraction 5	1.6	1.54	1.56		1.7	1.66	1.69		1.83	1.85	1.85
Fraction 6	1.6	1.55	1.57		1.7	1.67	1.7		1.83	1.85	1.85
Fraction 7	1.6	1.51	1.55		1.7	1.62	1.68		1.83	1.84	1.85
Fraction 8	1.6	1.55	1.57		1.7	1.65	1.69		1.83	1.85	1.85
Fraction 9	1.6	1.54	1.57		1.7	1.64	1.69		1.83	1.85	1.85
Fraction 10	1.6	1.62	1.64		1.7	1.71	1.73		1.83	1.86	1.86
Fraction 11	1.6	1.62	1.59		1.7	1.72	1.71		1.83	1.86	1.86
Fraction 12	1.6	1.53	1.56		1.7	1.65	1.7		1.83	1.83	1.84
Fraction 13	1.6	1.65	1.66		1.7	1.71	1.73		1.83	1.86	1.86
Fraction 14	1.6	1.5	1.55		1.7	1.61	1.66		1.83	1.84	2.08
Fraction 15	1.6	1.61	1.62		1.7	1.71	1.71		1.83	1.87	1.87
Fraction 16	1.6	1.61	1.6		1.7	1.71	1.7		1.83	1.84	1.84
Fraction 17	1.6	1.66	1.67		1.7	1.73	1.74		1.83	1.85	1.85
Fraction 18	1.6	1.61	1.6		1.7	1.71	1.71		1.83	1.86	1.86
Fraction 19	1.6	1.6	1.6		1.7	1.7	1.7		1.83	1.87	1.87
Fraction 20	1.6	1.6	1.61		1.7	1.7	1.7		1.83	1.86	1.86
Fraction 21	1.6	1.6	1.61		1.7	1.7	1.7		1.83	1.87	1.87
Fraction 22	1.6	1.55	1.58		1.7	1.66	1.69		1.83	1.86	1.86
Fraction 23	1.6	1.61	1.61		1.7	1.71	1.71		1.83	1.88	1.88
Fraction 24	1.6	1.65	1.65		1.7	1.75	1.75		1.83	1.93	1.92
Fraction 25	1.6	1.59	1.6		1.7	1.69	1.7		1.83	1.87	1.87

Figure A·19: Patient 10: Dmean, D50, and D2 received by Bladder. LM plan.

D_average	Planned fx dose	Delivered fx dose	Deformed delivered fx dose	D50	Planned fx dose	Delivered fx dose	Deformed delivered fx dose	D2	Planned fx dose	Delivered fx dose	Deformed delivered fx dose
Fraction 1	1.41	1.39	1.4		1.56	1.5	1.53		1.81	1.83	1.83
Fraction 2	1.41	1.39	1.4		1.56	1.52	1.54		1.81	1.82	1.82
Fraction 3	1.41	1.36	1.4		1.56	1.44	1.53		1.81	1.79	1.8
Fraction 4	1.41	1.39	1.4		1.56	1.54	1.55		1.81	1.8	1.8
Fraction 5	1.41	1.37	1.4		1.56	1.45	1.53		1.81	1.81	1.81
Fraction 6	1.41	1.38	1.43		1.56	1.49	1.59		1.81	1.81	1.81
Fraction 7	1.41	1.32	1.39		1.56	1.36	1.52		1.81	1.8	1.81
Fraction 8	1.41	1.35	1.4		1.56	1.43	1.54		1.81	1.81	1.81
Fraction 9	1.41	1.34	1.38		1.56	1.4	1.53		1.81	1.81	1.81
Fraction 10	1.41	1.45	1.48		1.56	1.63	1.69		1.81	1.84	1.84
Fraction 11	1.41	1.44	1.41		1.56	1.6	1.56		1.81	1.82	1.82
Fraction 12	1.41	1.36	1.41		1.56	1.44	1.57		1.81	1.8	1.8
Fraction 13	1.41	1.52	1.54		1.56	1.7	1.72		1.81	1.81	1.81
Fraction 14	1.41	1.32	1.4		1.56	1.32	1.51		1.81	1.81	1.81
Fraction 15	1.41	1.44	1.46		1.56	1.6	1.62		1.81	1.83	1.83
Fraction 16	1.41	1.46	1.44		1.56	1.65	1.63		1.81	1.8	1.8
Fraction 17	1.41	1.55	1.57		1.56	1.72	1.74		1.81	1.82	1.82
Fraction 18	1.41	1.44	1.43		1.56	1.63	1.62		1.81	1.82	1.82
Fraction 19	1.41	1.42	1.41		1.56	1.58	1.57		1.81	1.83	1.83
Fraction 20	1.41	1.43	1.42		1.56	1.58	1.57		1.81	1.81	1.81
Fraction 21	1.41	1.42	1.42		1.56	1.57	1.58		1.81	1.83	1.83
Fraction 22	1.41	1.37	1.41		1.56	1.48	1.57		1.81	1.81	1.81
Fraction 23	1.41	1.43	1.43		1.56	1.59	1.58		1.81	1.84	1.83
Fraction 24	1.41	1.47	1.47		1.56	1.63	1.64		1.81	1.89	1.88
Fraction 25	1.41	1.41	1.41		1.56	1.56	1.57		1.81	1.82	1.82

Figure A·20: Patient 10: Dmean, D50, and D2 received by Bladder. SM plan.

D_average	Planned fx dose	Delivered fx dose	Deformed delivered fx dose	D50	Planned fx dose	Deformed deliver	Delivered fx dose computed on CBCT	D2	Planned fx dose	Delivered fx dose	Deformed delivered fx dose
Fraction 1	1.62	1.67	1.67		1.74	1.82	1.81		1.83	1.86	1.86
Fraction 2	1.62	1.64	1.68		1.74	1.76	1.72		1.83	1.84	1.84
Fraction 3	1.62	1.56	1.62		1.74	1.73	1.66		1.83	1.81	1.8
Fraction 4	1.62	1.61	1.64		1.74	1.75	1.71		1.83	1.83	1.83
Fraction 5	1.62				1.74	1.72	1.72		1.83		
Fraction 6	1.62	1.66	1.67		1.74	1.76	1.74		1.83	1.83	1.84
Fraction 7	1.62	1.55	1.63		1.74	1.73	1.64		1.83	1.82	1.83
Fraction 8	1.62	1.62	1.63		1.74	1.74	1.72		1.83	1.83	1.83
Fraction 9	1.62				1.74	1.72	1.72		1.83		
Fraction 10	1.62	1.51	1.62		1.74	1.69	1.57		1.83	1.81	1.82
Fraction 11	1.62	1.61	1.63		1.74	1.74	1.72		1.83	1.83	1.83
Fraction 12	1.62	1.57	1.63		1.74	1.74	1.66		1.83	1.83	1.83
Fraction 13	1.62	1.52	1.58		1.74	1.67	1.61		1.83	1.81	1.81
Fraction 14	1.62	1.65	1.65		1.74	1.76	1.71		1.83	1.84	1.84
Fraction 15	1.62	1.66	1.66		1.74	1.77	1.71		1.83	1.83	1.83
Fraction 16	1.62				1.74	1.68	1.68		1.83		
Fraction 17	1.62	1.62	1.67		1.74	1.79	1.74		1.83	1.84	1.84
Fraction 18	1.62				1.74	1.7	1.7		1.83		
Fraction 19	1.62	1.61	1.65		1.74	1.76	1.73		1.83	1.85	1.86
Fraction 20	1.62	1.62	1.65		1.74	1.76	1.73		1.83	1.85	1.85
Fraction 21	1.62	1.66	1.69		1.74	1.79	1.77		1.83	1.85	1.85
Fraction 22	1.62	1.61	1.65		1.74	1.75	1.7		1.83	1.84	1.85
Fraction 23	1.62	1.61	1.68		1.74	1.78	1.74		1.83	1.85	1.85
Fraction 24	1.62	1.69	1.69		1.74	1.77	1.77		1.83	1.84	1.84
Fraction 25	1.62	1.65	1.68		1.74	1.8	1.75		1.83	1.84	1.85

Figure A·21: Patient 11: Dmean, D50, and D2 received by Bladder.

D_average	Planned fx dose	Delivered fx dose	Deformed delivered fx dose	D50	Planned fx dose	Delivered fx dose	Deformed delivered fx dose	D2	Planned fx dose	Delivered fx dose	Deformed delivered fx dose
Fraction 1	1.67	1.62	1.65		1.75	1.69	1.71		1.83	1.79	1.79
Fraction 2	1.67	1.6	1.64		1.75	1.7	1.72		1.83	1.78	1.79
Fraction 3	1.67	1.6	1.64		1.75	1.68	1.7		1.83	1.79	1.78
Fraction 4	1.67	1.65	1.67		1.75	1.7	1.71		1.83	1.79	1.79
Fraction 5	1.67	1.6	1.63		1.75	1.66	1.68		1.83	1.78	1.77
Fraction 6	1.67	1.61	1.64		1.75	1.68	1.7		1.83	1.78	1.78
Fraction 7	1.67	1.65	1.67		1.75	1.73	1.74		1.83	1.8	1.8
Fraction 8	1.67	1.61	1.65		1.75	1.67	1.7		1.83	1.74	1.73
Fraction 9	1.67	1.63	1.66		1.75	1.69	1.71		1.83	1.76	1.76
Fraction 10	1.67	1.6	1.65		1.75	1.67	1.7		1.83	1.82	1.82
Fraction 11	1.67	1.63			1.75	1.7			1.83	1.81	
Fraction 12	1.67	1.64	1.71		1.75	1.71	1.75		1.83	1.78	1.78
Fraction 13	1.67	1.67	1.69		1.75	1.71	1.73		1.83	1.77	1.77
Fraction 14	1.67	1.64	1.66		1.75	1.7	1.71		1.83	1.78	1.78
Fraction 15	1.67	1.62	1.64		1.75	1.69	1.7		1.83	1.8	1.8
Fraction 16	1.67	1.65	1.7		1.75	1.71	1.73		1.83	1.82	1.82
Fraction 17	1.67	1.59	1.62		1.75	1.68	1.7		1.83	1.8	1.8
Fraction 18	1.67	1.61	1.63		1.75	1.7	1.73		1.83	1.8	1.8
Fraction 19	1.67	1.63	1.65		1.75	1.71	1.74		1.83	1.79	1.79
Fraction 20	1.67	1.6	1.63		1.75	1.69	1.71		1.83	1.8	1.8
Fraction 21	1.67	1.61	1.66		1.75	1.68	1.72		1.83	1.79	1.79
Fraction 22	1.67	1.56	1.61		1.75	1.65	1.69		1.83	1.78	1.78
Fraction 23	1.67	1.6	1.69		1.75	1.7	1.76		1.83	1.82	1.82
Fraction 24	1.67	1.63	1.67		1.75	1.7	1.73		1.83	1.8	1.8
Fraction 25	1.67	1.56	1.63		1.75	1.64	1.7		1.83	1.82	1.82

Figure A·22: Patient 13: Dmean, D50, and D2 received by Bladder.

D_average	Planned fx dose	Delivered fx dose	Deformed delivered fx dose	D50	Planned fx dose	Delivered fx dose	Deformed delivered fx dose	D2	Planned fx dose	Delivered fx dose	Deformed delivered fx dose
Fraction 1	1.68	1.68	1.77		1.78	1.8	1.82		1.84	1.88	1.88
Fraction 2	1.68	1.74	1.75		1.78	1.86	1.87		1.84	1.94	1.94
Fraction 3	1.68	1.69	1.73		1.78	1.81	1.83		1.84	1.86	1.87
Fraction 4	1.68	1.67	1.69		1.78	1.79	1.82		1.84	1.88	1.88
Fraction 5	1.68	1.7	1.7		1.78	1.81	1.81		1.84	1.86	1.87
Fraction 6	1.68	1.68	1.69		1.78	1.78	1.77		1.84	1.89	1.89
Fraction 7	1.68	1.74	1.76		1.78	1.83	1.84		1.84	1.96	1.96
Fraction 8	1.68	1.75	1.77		1.78	1.84	1.85		1.84	1.89	1.89
Fraction 9	1.68	1.6	1.59		1.78	1.66	1.62		1.84	1.87	1.87
Fraction 10	1.68	1.7	1.71		1.78	1.81	1.81		1.84	1.87	1.87
Fraction 11	1.68	1.67	1.67		1.78	1.77	1.74		1.84	1.89	1.89
Fraction 12	1.68								1.84		
Fraction 13	1.68								1.84		
Fraction 14	1.68	1.67	1.69		1.78	1.78	1.79		1.84	1.83	1.83
Fraction 15	1.68	1.69	1.7		1.78	1.81	1.81		1.84	1.88	1.88
Fraction 16	1.68	1.75	1.78		1.78	1.85	1.87		1.84	1.95	1.95
Fraction 17	1.68								1.84		
Fraction 18	1.68	1.72	1.74		1.78	1.83	1.83		1.84	1.88	1.88
Fraction 19	1.68	1.59	1.59		1.78	1.63	1.61		1.84	1.89	1.89
Fraction 20	1.68	1.7	1.72		1.78	1.81	1.82		1.84	1.9	1.9
Fraction 21	1.68	1.76	1.76		1.78	1.85	1.85		1.84	1.89	1.89
Fraction 22	1.68	1.61	1.56		1.78	1.65	1.57		1.84	1.88	1.88
Fraction 23	1.68	1.73	1.74		1.78	1.84	1.84		1.84	1.9	1.9
Fraction 24	1.68	1.68	1.64		1.78	1.76	1.69		1.84	1.88	1.88
Fraction 25	1.68								1.84		

Figure A·23: Patient 17: Dmean, D50, and D2 received by Bladder.

D_average	Planned fx dose	Delivered fx dose	Deformed delivered dose	D50	Planned fx dose	Delivered fx dose	Deformed delivered dose	D2	Planned fx dose	Delivered fx dose	Deformed delivered dose
Fraction 1	1.55	1.52	1.52		1.64	1.62	1.63		1.82	1.78	1.78
Fraction 2	1.55	1.52	1.52		1.64	1.61	1.6		1.82	1.78	1.78
Fraction 3	1.55	1.53	1.53		1.64	1.6	1.59		1.82	1.78	1.78
Fraction 4	1.55	1.52	1.5		1.64	1.65	1.63		1.82	1.77	1.76
Fraction 5	1.55	1.43	1.42		1.64	1.44	1.44		1.82	1.77	1.76
Fraction 6	1.55	1.53	1.51		1.64	1.63	1.59		1.82	1.77	1.77
Fraction 7	1.55	1.54	1.53		1.64	1.65	1.65		1.82	1.76	1.76
Fraction 8	1.55	1.61	1.62		1.64	1.72	1.73		1.82	1.85	1.85
Fraction 9	1.55	1.62	1.65		1.64	1.74	1.76		1.82	1.85	1.85
Fraction 10	1.55	1.62	1.61		1.64	1.72	1.7		1.82	1.85	1.85
Fraction 11	1.55	1.6	1.58		1.64	1.71	1.69		1.82	1.84	1.84
Fraction 12	1.55	1.62	1.63		1.64	1.72	1.71		1.82	1.84	1.85
Fraction 13	1.55	1.63	1.62		1.64	1.76	1.72		1.82	1.85	1.84
Fraction 14	1.55	1.62	1.61		1.64	1.73	1.72		1.82	1.85	1.85
Fraction 15	1.55	1.64	1.6		1.64	1.78	1.76		1.82	1.84	1.83
Fraction 16	1.55	1.65	1.61		1.64	1.76	1.69		1.82	1.85	1.85
Fraction 17	1.55	1.61	1.58		1.64				1.82	1.84	1.84
Fraction 18	1.55	1.57	1.58		1.64				1.82	1.85	1.85
Fraction 19	1.55	1.55	1.56		1.64	1.63	1.62		1.82	1.83	1.83
Fraction 20	1.55	1.64	1.61		1.64	1.72	1.67		1.82	1.85	1.85
Fraction 21	1.55	1.58	1.61		1.64	1.66	1.68		1.82	1.85	1.85
Fraction 22	1.55	1.6	1.6		1.64	1.73	1.73		1.82	1.83	1.83
Fraction 23	1.55	1.59	1.59		1.64	1.72	1.73		1.82	1.83	1.83
Fraction 24	1.55	1.65	1.67		1.64	1.76	1.77		1.82	1.86	1.86
Fraction 25	1.55	1.61	1.64		1.64	1.73	1.74		1.82	1.84	1.84

Figure A·24: Patient 18: Dmean, D50, and D2 received by Bladder.

D_average	Planned fx dose	Delivered fx dose	Deformed delivered fx dose	D50	Planned fx dose	Delivered fx dose	Deformed delivered fx dose	D2	Planned fx dose	Delivered fx dose	Deformed delivered fx dose
Fraction 1	1.7	1.58	1.52		1.78	1.66	1.57		1.83	1.8	1.78
Fraction 2	1.7	1.58	1.58		1.78	1.67	1.65		1.83	1.79	1.78
Fraction 3	1.7	1.55	1.58		1.78	1.62	1.58		1.83	1.8	1.77
Fraction 4	1.7	1.51	1.49		1.78	1.57	1.55		1.83	1.77	1.75
Fraction 5	1.7	1.57	1.49		1.78	1.66	1.55		1.83	1.81	1.78
Fraction 6	1.7	1.62	1.51		1.78	1.71	1.61		1.83	1.8	1.79
Fraction 7	1.7	1.57	1.55						1.83	1.79	1.79
Fraction 8	1.7								1.83		
Fraction 9	1.7	1.55	1.51		1.78	1.64	1.59		1.83	1.8	1.79
Fraction 10	1.7	1.64	1.59		1.78	1.73	1.64		1.83	1.82	1.8
Fraction 11	1.7	1.57	1.51		1.78	1.66	1.56		1.83	1.8	1.79
Fraction 12	1.7	1.62	1.63		1.78	1.72	1.73		1.83	1.8	1.79
Fraction 13	1.7	1.53	1.5		1.78	1.62	1.57		1.83	1.81	1.78
Fraction 14	1.7	1.66	1.67		1.78	1.75	1.76		1.83	1.81	1.81
Fraction 15	1.7	1.62	1.57		1.78	1.7	1.62		1.83	1.81	1.8
Fraction 16	1.7	1.61			1.78	1.69	1.58		1.83	1.82	
Fraction 17	1.7								1.83		
Fraction 18	1.7	1.6	1.56		1.78	1.69	1.63		1.83	1.81	1.79
Fraction 19	1.7	1.61	1.61		1.78	1.71	1.69		1.83	1.8	1.8
Fraction 20	1.7	1.61	1.62		1.78	1.71	1.7		1.83	1.81	1.8
Fraction 21	1.7	1.6	1.61		1.78	1.69	1.68		1.83	1.81	1.8
Fraction 22	1.7	1.61	1.58		1.78	1.69	1.64		1.83	1.81	1.8
Fraction 23	1.7	1.62	1.6		1.78	1.71	1.66		1.83	1.81	1.8
Fraction 24	1.7	1.76	1.73		1.78	1.83	1.8		1.83	1.98	1.97
Fraction 25	1.7	1.66	1.68		1.78	1.76	1.77		1.83	1.83	1.83

Figure A·25: Patient 19: Dmean, D50, and D2 received by Bladder.

References

[1] https://www.anatomynote.com/human-anatomy/pelvis-anatomy/symphysis-pubis-and-urinary-bl

[2] *Cervical cancer*. https://www.who.int/health-topics/cervical-cancer#tab=tab_1.

[3] Prescribing, recording, and reporting brachytherapy for cancer of the cervix. *Oxford university press*, (13(1-2)), 2013.

[4] RaySearch Laboratories AB. Deformable image registration. Version 2017, 2017.

[5] L.A. Dawson and D.A. Jaffray. Advances in image - guided radiation therapy. *J. Clin. Oncol.*, (25: 938-946), 2007.

[6] L. H. Djupvik. Doseplanlegging av livmorhalskreft. Dokument ID 39408, 2019.

[7] A. Buchali et al. Impact of the filling status of bladder and rectum on their integral dose distribution and the movement of the uterus in the treatment planning of gynaecological cancer. *Radiother. Oncol.*, 52, 1999.

[8] A. J. Van de Schoot et al. Dosimetric advantages of proton therapy compared with photon therapy using adaptive strategy in cervical cancer. *Acta Oncol (Madr)*, 55, 2016.

[9] A. Richter et al. Investigation of the usability of cone-beam ct data sets for dose calculation. *Radiat Oncol.*, 3, 2008.

[10] A. Taylor et al. An assessment of interfractional uterine and cervical motion: Implications for radiotherapy target volume definition in gynaecoligical cancer. *Radiother Oncol*, 88, 2008.

[11] A.B. Wolbarst et al. Medical imaging: Essentials for physicians. *Wiley online Library*, 2013.

[12] B. Mzenda et al. Modeling anddosimetric performance evaluation of the raystation treatment planning system. *Appl Clin Med Phys*, 15(5), 2014.

[13] C. Yunfeng et al. Deformable dose accumualtion with image guided radiotherapy for final dose evaluation in pelvis cases. *Nucl Med Radiat Ther*, e001, 2011.

[14] D. Soumya et al. Dosimetric impact of variable bladder filling on imrt planning for locally advanced carcinoma cervix. *Journal of the Egyptian National Cancer Institute.*, 32, 2020.

[15] D. Thongphiew et al. Comparison of online igrt technique for prostate imrt treatment: Adaptive vs repositioning correction. *Med. Phys.*, 36, 2009.

[16] D.W. Townsend et al. Pet/ct scanners: a hardware approach to image fusion. *Semin Nucl Med.*, 33(3), 2003.

[17] E. M. Kerhof et al. Intrafraction motion in patients with cervical cancer: The benefit of soft tissue regression using mri. *Radiother Oncol*, 93, 2009.

[18] E. V. H. Laura et al. Role of deformable image registration for delivered dose accumulation of adaptive external beam rt and brachytherapy in cervical cancer. *Journal of contemporary brachytherapy.*, 10(6), 2018.

[19] G. E. Christensen et al. Image-based dose planning of intracavitary brachytherapy: registration of serial-imaging studies using deformable anatomic templates. *Int J Radiation Oncol Biol Phys*, 51, 2001.

[20] H. Luo et al. Interfractional variation in bladder volume and its impact on cervical cancer radiotherapy: Clinical significance of portable bladder scanner. *Med Phys*, 43(7), 2016.

[21] H. Zhong et al. Analysis of deformable image registration accuracy using computational modelling. *Med Phys*, 37, 2010.

[22] I. Fotina et al. Feasibility of cbct-based dose calculation: comparative analysis of hu adjustment techniques. *Radiother Oncol.*, 104(2), 2012.

[23] J. Indrin et al. Deformable registration for dose accumulation. *Semin Radiat Oncol.*, 29, 2019.

[24] J. Kim et al. A novel approach for establishing cbct/ct deformable image registration in prostate cancer radiotherapy. *Phys Med Biol*, 58, 2013.

[25] J. Mayer et al. Imrt, igrt, sbrt - advances in the treatment planning and delivery of radiotherapy. *KARGER*, 2007.

[26] J. Pouliot et al. Low-dose megavoltage cone-beam ct for radiation therapy. *Int J Radial Oncol Biol Phys.*, 61(2), 2005.

[27] J. Stewart et al. Automated weekly replanning for intensity modulated radiotherapy of cervical cancer. *Int. J. Radiation Oncology Biol. Phys*, 78(2), 2010.

[28] J. Zeng et al. Assessing cumulative dose distributions in combined external beam radiotherapy and intracavitary brachytherapy for cervical cancer by treatment planning based on deformable image registration. *Transl Cancer Res*, 9(10), 2020.

[29] J.J. Lagendijk et al. Mri/linac integration. *Radiother Oncol.*, 86(1), 2008.

[30] K. Brock et. al. Use of image registration and fusion algorithms and techniques in radiotherapy: Report of the aapm radiation therapy committee task group no. 132. *Medical Physics*, 44(7), 2017.

[31] K. Lim et al. Pelvic imrt for cervix cancer: Is what you plan actually what you deliver? *Int J Radiation Oncl. Biol. Phys.*, 74(1), 2009.

[32] K. Lim et al. Pelvic radiotherapy for cancer of cervix: is what you plan actually what you delivered? *Int. J. Radiat. Oncol. Biol. Phys.*, 704, 2009.

[33] K. Motegi et al. Usefulness of hybrid deformable image registration algorithms in prostate radiation therapy. *J Appl Clin Med Phys*, 20:1, 2019.

[34] K. S. H. Lim et al. Whole pelvis imrt for cervix cancer. what gets missed and why? *Int J Ratdiat Oncol Biol Phys*, 72: S112, 2008.

[35] K. Tanderup et al. Embrace 2. image guided intensity modulated external beam radiochemotherapy and mri based adaptive bracytherapy in locally advanced cervical cancer. *EMBRACE study protocol v. 1.0*.

[36] K. Yoo Kang et al. Intensity-modulated radiotherapy reduces gastrointestinal toxicity in pelvic radiation therapy with moderate dose. *PLoS One.*, 12(8), 2017.

[37] L. Van de Bunt et al. Motion and deformation of target volumes during imrt for cervical cancer: What margins do we need? *Raiother Oncol*, 88, 2008.

[38] L. Ye et al. Effects of bladder status on cervical cancer treatment with intensity-modulated radiation therapy plans. *Prec Radiat. Oncol*, 1, 2017.

[39] L.B. Harrison et al. Head and neck cancer: a multidisciplinary approach. *Lippincott William and Wilkins*, 2008.

[40] M. J. Murphy et al. A method to estimate the effect of deformable image registration uncertainties on daily dose mapping. *Med. Phys.*, 39, 2012.

[41] M. MacManus et al. Use of pet and pet/ct for radiation therapy planning: Iaea expert report 2006 - 2007. *Radiother Oncol*, 91(1), 2009.

[42] M. Rubeaux et al. Numerical phantom generation to evaluate non-rigid ct/cbct registration algorithms for prostate cancer radiotherapy. *Nice (France): Image-Guidance and multimodal dose planning in radiation therapy.*, 2012.

[43] M. Thor et al. Deformable image registration for contour propagation from ct to cbct scans in rt of prostate cancer. *Acta. Oncol*, 50, 2011.

[44] Marcel van Herk et al. The probability of correct target dosage: dose-population histograms for deriving treatment margins in radiotherapy. *Internaltional Journal of Radiattion Oncology, Biology, and Physics*, (Vol 47, Issue 4), July 2000.

[45] Marcel van Herk et al. Errors and margins in radiotherapy. *Seminars in Radiation Oncology*, (Vol 14, No 1), January 2004.

[46] M.D. Bethesda et al. Report icru 50. prescribing, recording and reporting photon beam therapy. international commission on radiation units and measurements. 1993.

[47] M.D. Bethesda et al. Report icru 62. prescribing, recording and reporting photon beam therapy (supplement to icru report. 50). international commission on radiation units and measurements. 1999.

[48] M.D. Randall et al. Intensity-modulated radiation therapy for gynecologic cancers: Pitfalls, hazards, and cautions to be considered. *Semin Radiat Oncol*, 16, 2006.

[49] N. B. K. Jensen et al. Cone beam computed tomography-based monitoring and management of target and organ motion during external beam radiotherapy in cervical cancer. *Physics and Imaging in Radiation Oncology*, 9, 2019.

[50] N. Bhatla et al. Revised figo staging for carcinoma of the cervix uteri. *J Gyn Obst*, 145(1), 2019.

[51] N. Cihoric et al. Dose escalated intensity modulated radiotherapy in the treatment of cervical cancer. *Radiat Oncol*, 10, 2015.

[52] N. Kadoya et al. Multi-institutional validation study of commercially available deformable image registration in rt. *Med Phys*, 42, 2015.

[53] N. Suntharalingam et al. Radiation oncology physics: A handbook for teachers and students. *IAEA publication*, (ISBN 92-0-107304-6), 2006.

[54] P. Buranaporn et al. Relation between dir recalculated dose based cbct and gi and gu toxicity in postoperative prostate cancer patients treated with vmat. *Radiotherapy and Oncology*, 2020.

[55] P. Cadman et al. Dosimetric consideration for validation of a sequential imrt process with a commercial treatment planning system. *Physics in Medicine and Biology*, (47(16): 3001-10), 2002.

[56] P. Chan et al. Inter- and intrafractional tumour and organ movement in patients with cervical cancer undergoing rt: A cinematic mri point-of-interest study. *Int J Radiat Oncol Bio Phys*, 70, 2008.

[57] R. Ahmad et al. Interfraction bladder filling variations and time trends for cervical cancer patients assessed with portable 3-dimensional ultrasound bladder scanner. *Radiother Oncol*, 89, 2008.

[58] R. Ahmad et al. A margin-of-the-day online adaptive intensitive-modulated radiotherapy strategy for cervical cancer provides superior treatment accuracy compared to clinically recommended margins: a dosimetric evaluation. *Acta Oncol.*, 52, 2013.

[59] R. Bastien et al. Deformable image registration for rt: principle, methods, applications and evaluation. *Acta oncologica.*, 58(9), 2019.

[60] R. Jadon et al. A systematic review of organ motion and image-guided strategies in external beam radiotherapy for cervical cancer. *Clin Oncol*, 26(4), 2014.

[61] R. Pötter et al. Recommendations from gynaecological (gyn) gec estro working group (ii): concepts and terms in 3d image-based treatment planning in cervix cancer brachytherapy-3d dose volume parameters and aspects of 3d image-based anatomy, radiation physics, radiobiology. *Radiother Oncol*, 78(1), 2006.

[62] R. Pötter et al. The emvrace ii study: the outcome and prospect of two decades evolution within the gec-estro gyn working group and the embrace studies. *Clin Transl Radiat Oncol*, 9, 2018.

[63] R. Zakariaee et al. Validation of non-rigid pointset registration methods using a porcine bladder pelvic phantom. *Phys Med Biol.*, 61, 2016.

[64] S. J. Huh et al. Interfractional variation in position of the uterus during radical radiotherapy for cervical cancer. *Radiother Oncol*, 71, 2004.

[65] S. Oh et al. Hybrid adaptive rdiotherapy with online-mri in cervix cancer imrt. *Radiother Oncol*, 110, 2014.

[66] S. Sehgal et al. Impact of volumetric imaging cbct in defining ptv margins in the treatment of carcinoma cervix. *Journal of Cancer Prevention and Current Research*, 10, 2019.

[67] S. V. Jamema et al. Inter-application variation of dose and spatial location of d2cc volumes of oars during mr image based cervix brachytherapy. *Radiother Oncol*, 107, 2013.

[68] Schneider Ω et al. Correlation between ct numbers and tissue parameters needed for monte carlo simulations of clinical dose distributions. *Phys Med Biol.*, 45(2), 2000.

[69] Suk Lee et al. Physical and radiobiological evaluation of radiotherapy treatment plan. 2014.

[70] T. Abe et al. Assessing cumulative dose distributions in combined radiotherapy for cervical cancer using deformable image registration with pre-imaging preparations. *Radiation Oncology*, 9, 2014.

[71] T. C. Huang et al. Fractionated changes in prostate cancer radiotherapy using cone-beam computed tomography. *Medical Dosimetry*, 40(3), 2015.

[72] T. E. Schultheiss et al. Point/counterpoint: It is not appropriate to "deform" dose along with dir in adaptive radiotherapy. *Med Phys*, 39, 2012.

[73] V. Giacometti et al. An evaluation of techniques for dose calculation on cone-beam ct. *The British Journal of Radiology*, 92(1096), 2019.

[74] V. Grégoire et al. Report icru 83. the icru report 83: prescribing, recording and reporting photon-beam intensity-modulated radiation therapy (imrt). *Oxford university press*, (10(1)), 2010.

[75] W. A. Tome et al. Toward adaptive radiotherapy for head and neck patients; uncertainties in dose warping due to the choice of deformable image registration algorithm. *Med. Phys.*, 42, 2015.

[76] W. Nobnop et al. Evaluation of deformable image registration methods for dose accumulation in nasopharyngeal cancer patients during radiotherapy. *Radiol Oncol*, 51(4), 2017.

[77] W. Thongsuk et al. Dose accumulation with deformable image registration method using helical tomotherapy images for prostate cancer. *Journal of Radiotherapy in Practice*, 19, 2020.

[78] X. Wang et al. An assessment of interfractional bladder, rectum and vagina motion in postoperative cervical cancer based on daily cone-beam computed tomography. *Mol Clin Oncol*, 4(2), 2016.

[79] X. Wang et al. An assessment of interfractional bladder, rectum and vagina motion postoperative cervical cancer based on daily cbct. *Molecular and clinical oncology*, 4, 2016.

[80] X.L. Du et al. Intensity-modulated radiation therapy for advanced cervical cancer: a comparison of dosimetric and clinical outcomes with conventional radiotherapy. *Gynecol Oncol.*, 125(1), 2012.

[81] Y. M. Tsang et al. The impact of bladder preparation protocols on post treatment toxicity in radiotherapy for localised prostate cancer patients. *Tech Innov Patient Support Radiat Oncol*, 3, 2017.

[82] Y. Yang et al. Evaluation of onboard kv cone-beam ct (cbct)-based dose calculation. *Physics in Medicine and Biology*, 52(3), 2007.

[83] Ye. Lan et al. Effects of bladder status on cervical cancer treatment with imrt plans. *Prec. Radiat. Oncol.*, 1, 2017.

[84] Z. Jing et al. Assessing cumulative dose distributions in combined external beam rt and intracavitary for cervical cancer by treatment planning based on deformable image registration. *Transl Cancer Res.*, 9(10), 2020.

[85] B. Jane. On target ensuring geometric accuracy in radiotherapy. *The Royal College of Radiologists*, (ISBN: 978-1-905034-33-8), 2008.

[86] F. M. Khan. *Treatment planning in Radiation Therapy.* 2016.

[87] T. Krieger and O.A. Sauer. Monte carlo - versus pencil beam/collapsed cone dose calculation in a heterogeneous multi-layer phantom. *Phys. Med. Biol.*, (50: 859 - 868), 2005.

[88] S. G. Levernes. Volum og doser ved strålebehandling definisjoner, retningslinjer for bruk, dokumentasjon og rapportering. *Strålevern rapport*, 12, 2003.

[89] X. Allen Li. *Adaptive Radiation Therapy.* 2011.

[90] C. Paganelli and Giorgia Meschini. Patient-specific valiadation of deformable image registration in radiation therapy: Overview and caveates. *Med. Phys.*, 45(10), 2018.

[91] W. Parker and H. Patrocinio. Clinical treatment planning in external photon beam radiotherapy. *IAEA publication*, (ISBN 92-0-107304-6), 2012.

[92] W. Svensson. The anaconda algorithm for deformable image registration in radiotherapy. *Medical Physics*, 42(1), 2015.

[93] M.M.G. Videtic and M. Neil Woody. *Handbook of treatment planning in radiation oncology.* 2 edition.